

# Digital Cellular Solids: reconfigurable composite materials

by

Kenneth C. Cheung

B.Arch., Cornell University, 2005  
S.M., Massachusetts Institute of Technology, 2007

Submitted to the Program in Media Arts and Sciences, School of Architecture and Planning  
in partial fulfillment of the requirements for the degree of

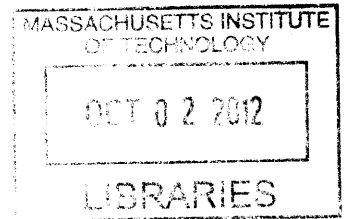
Doctor of Philosophy

at the

MASSACHUSETTS INSTITUTE OF TECHNOLOGY

September 2012

ARCHIVED



© 2012 Massachusetts Institute of Technology. all rights reserved

Signature of Author:

Handwritten signature of Kenneth C. Cheung in black ink.

Program in Media Arts and Sciences  
August 7, 2012

Certified by:

Handwritten signature of Prof. Neil Gershenfeld in black ink.

Prof. Neil Gershenfeld  
Director, Center for Bits and Atoms (CBA)  
Program in Media Arts and Sciences

Accepted by:

Handwritten signature of Prof. Patricia Maes in black ink.

Prof. Patricia Maes  
Associate Academic Head  
Program in Media Arts and Sciences

(This page intentionally left blank)

# Digital Cellular Solids: reconfigurable composite materials

by

Kenneth C. Cheung

Submitted to the Program in Media Arts and Sciences, School of Architecture and Planning  
on August 7, 2012 in partial fulfillment of the  
requirements for the degree of Doctor of Philosophy

## Abstract

Digital materials are comprised of a small number of types of discrete physical building blocks, which assemble to form constructions that meet the versatility and scalability of digital computation and communication systems. This work seeks to demonstrate the applicability of a digital material approach in designing new cellular materials and methods for assembly of structures with static reconfigurability. The science of cellular solids has enabled the widespread use of lightweight materials to meet important engineering needs, such as passive energy absorption, but they are not in widespread use for structural applications, perhaps due to a large gap between the strength and stiffness to weight ratios of popular classical solids, and the performance of known lightweight cellular materials that are produced from the same constituent material. The engineering of fiber reinforced composite materials has enabled structures with large reductions in weight for given strength and stiffness targets, but at very high design and processing costs, and many challenges producing mechanical interfaces (joints). Digital materials promise scalable methods of producing functional things with reconfigurable sets of discrete and compatible parts, but the presence of many reversible connections raises questions about the performance of the end result. Digital Cellular Solids are cellular solids that exhibit improvements in relative stiffness and strength compared to relative density, over current practices for producing lightweight materials. This is accomplished by assembling lattice geometries that perform better than any that we know how to make with traditional methods. When implemented with fiber composites, the result is not only stiffer and stronger than any previously known ultra-light material, but it presents a new scalable and flexible workflow for applying fiber composites to engineering problems.

Thesis Supervisor:

Prof. Neil Gershenfeld

Director, Center for Bits and Atoms (CBA)

Program in Media Arts and Sciences

(This page intentionally left blank)

# Digital Cellular Solids: reconfigurable composite materials

by  
Kenneth C. Cheung

Thesis Reader:

---

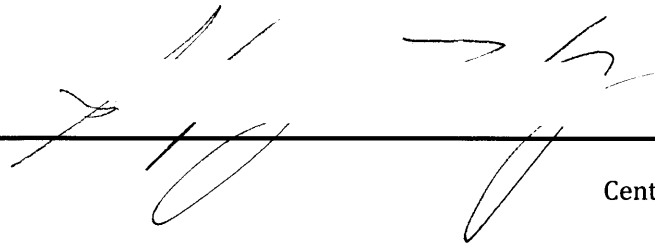
  
Erik Demaine, Ph.D.  
Professor of Electrical Engineering and Computer Science (EECS)  
Computer Science and Artificial Intelligence Lab

(This page intentionally left blank)

# Digital Cellular Solids: reconfigurable composite materials

by  
Kenneth C. Cheung

Thesis Reader:

Handwritten signatures of the thesis readers, including a large signature on the left and another on the right.

---

Shuguang Zhang, Ph.D.  
Center for Bits and Atoms (CBA)

(This page intentionally left blank)

## Acknowledgements

I thank Neil Gershenfeld and the Center for Bits and Atoms for the vision and environment to support this work. The diversity of perspective amongst the faculty and students of CBA makes for a wonderful place to do research.

The fab labs have allowed me to develop a perspective of technology and society that will always frame my work. Thank you, to Sherry Lassiter, for your tireless work in support of the entire fab lab network.

Sometimes, I'm asked: what makes MIT work? I answer – it's the community of interested people who always seem to be able to dispense with the old and discover new and more beautiful ways of seeing the world. Of these, I must in particular thank Erik Demaine and Shuguang Zhang for being my committee members, and for being good friends and offering sage advice.

The work presented here, is about making things, and how we might be able to make things in better ways. In order to try and show this, I spent a lot of time making things. This often meant using facilities and equipment in ways that are not described in the manuals. Thank you, John D, for making these accessible while keeping us safe. I must also thank the many helping hands that I had during the course of this project, including Joseph K, Stevie B, Matt K, and Sarah H.

To the individuals who helped to fuel the discussions that resulted in this work, I thank you. Chris W; working with you and everyone at the Spirit Aerosystems Composite Development Center has been a pleasure. Mitch Z and Gill P, the groups of researchers that you pull together are inspiring.

To Michael K, thank you for your care.

To my family, and in particular my mother and father, Christine and Moses, thank you for all of the opportunity that one could hope for.

To Laura, thank you for appreciating me for who I am.

(This page intentionally left blank)

## Table of Contents

Introduction.....	17
Digital Materials .....	17
Background.....	19
Natural Fabrication .....	19
Natural Materials.....	20
Engineered Fabrication.....	21
Engineered Materials .....	23
Design and Analysis .....	25
Geometry.....	28
Mechanics.....	40
Case Study Digital Material Design – The Cuboct Truss.....	47
Method .....	52
Workflow .....	52
Part Fabrication Method.....	54
Physical Testing Method.....	61
Results .....	69
Density .....	69
Mechanical Performance .....	69
Failure Modes .....	79
Applications .....	83
Reconfigurability.....	83
Interfaces .....	92
Skins (two-dimensional digital cellular materials).....	93
Self Assembly.....	97
Conclusions .....	99
Grand Challenges.....	107
#1 – Engineered Molecular Digital Composites.....	107
#2 Digital Composite Electronics Reconfigurator .....	108
#3 – Digital Flexural Mechanisms.....	109
#4 Passive Shape Optimization and Resonant Aerodynamic Propulsion.....	110

#5 Rapidly Deployable Infrastructure.....	111
#6 Three Dimensional Villages .....	112
References.....	115
Appendices.....	120

Table of Figures

FIGURE 1 EXAMPLE DIGITAL MATERIALS _____	18
FIGURE 2 CT SCAN OF WILD PHEASANT BONE, PICTURE OF EUPLECTELLA SP. AND CT SCAN _____	20
FIGURE 3 THE BOEING DREAMLIFTER: AN EXAMPLE OF THE LENGTHS (AND WIDTHS) THAT ARE GONE TO, IN TODAY'S LEADING EDGE COMPOSITE PRODUCTION. THIS AIRCRAFT WAS DESIGNED AND MANUFACTURED SPECIFICALLY AS PART OF THE PRODUCTION PROCESS FOR THE BOEING 787 PASSENGER AIRCRAFT, WHICH IS COMPRISED OF LARGE MONOLITHIC COMPOSITE COMPONENTS. _____	22
FIGURE 4 AIRCRAFT OF CONVENTIONAL RECONFIGURABLE MATTER _____	23
FIGURE 5 CONCEPT DIAGRAM FOR DIGITAL COMPOSITES – CHAINED CONTINUOUS FIBER LOOPS _____	25
FIGURE 6 PART SIZE HIERARCHY, CORE STRUCTURAL VARIATION, INTRODUCTION OF VOIDS AS METHODS OF STRUCTURAL TUNING _____	26
FIGURE 7 SNAP FIT FLEXURAL LATTICE STUDIES: LEFT, MIDDLE, TENSEGRITY CRYSTAL; RIGHT, HYPERBOLIC/GEODESIC SURFACE KIT _____	27
FIGURE 8 SNAP FIT FLEXURAL LATTICE STUDIES: LEFT, SIMPLE CUBIC LATTICE WITH TWO PART SCHEME; RIGHT, 12 CONNECTED OCTET TRUSS WITH THREE PART SCHEME _____	28
FIGURE 9 TWO PART SCHEME FOR CUBOCT TRUSS _____	29
FIGURE 10 RELATIVE DENSITY VS MODULUS SCALING CURVES _____	44
FIGURE 11 HYPOTHETICAL DESIGNED DIGITAL MATERIAL STRESS STRAIN CURVES _____	45
FIGURE 12 CUBOCT TRUSS GEOMETRY _____	48
FIGURE 13 CASE STUDY DESIGN ASSEMBLY _____	49
FIGURE 14 CASE STUDY DESIGN LOAD RESPONSE DIAGRAM _____	50
FIGURE 15 CASE STUDY DESIGN FIBER ORIENTATION LAYOUT _____	50
FIGURE 16 CASE STUDY DESIGN ASSEMBLIES _____	51
FIGURE 17 DESIGN WORKFLOW _____	52
FIGURE 18 PARAMETRIC DESIGN TOOLS EMPLOYED FOR DIGITAL COMPOSITES EXPERIMENTS; RHINOCEROS API AND GRASSHOPPER _____	53
FIGURE 19 OPTIMIZED PART MULTIPLEXED WINDING MOLD DESIGN _____	54
FIGURE 20 OPTIMIZED PART MULTIPLEXED WINDING MOLD ASSEMBLY _____	55
FIGURE 21 OPTIMIZED PART MULTIPLEXED WINDING PROCESS _____	55
FIGURE 22 OPTIMIZED PART MULTIPLEXED WINDING SLICING _____	56
FIGURE 23 CLOSE-UP VIEW OF PART PRODUCED BY MULTIPLEXED WINDING. GRADATIONS ON SCALE ARE 100THS OF AN INCH. _____	57
FIGURE 24 COMPARISON CNC MILLING OF QUASI-ISOTROPIC LAMINATE PROCESS – VORTEX TUBE COOLING, DIAMOND COATED TOOLING _____	58
FIGURE 25 PHOTOGRAPHS OF DIGITAL COMPOSITE TEST SPECIMEN _____	59
FIGURE 26 PRELIMINARY CONNECTION TESTING (INSTRON 4411) _____	60
FIGURE 27 PHYSICAL TESTING OF AN EARLY DIGITAL COMPOSITE SAMPLE _____	61
FIGURE 28 INITIAL PART CONSTRAINT TESTING; SETUP, LOAD TESTING WITH SLIDING CONSTRAINT, LOAD TESTING WITH FIXED CONSTRAINT _____	62
FIGURE 29 INITIAL RESULTS CONSTRAINT TESTING, PROVIDING UPPER BOUND _____	63
FIGURE 30 CONNECTION TESTING _____	63
FIGURE 31 DIMENSIONAL TOLERANCE EVALUATION, ISOTROPY MEASUREMENT SAMPLES _____	64
FIGURE 32 2x2x2, OPTIMIZED PARTS _____	64
FIGURE 33 FIXTURING AND FINAL TESTING _____	65
FIGURE 34 FIXTURE COMPLIANCE TESTING WITH SOLID ALUMINUM BLOCK _____	66

FIGURE 35 RAW DATA, WITHOUT COMPLIANCE CORRECTION _____	67
FIGURE 36 COMPLIANCE CORRECTED DATA _____	67
FIGURE 37 OPTIMIZED PARTS AND CONVENTIONAL PARTS, _____	69
FIGURE 38 TENSION AND COMPRESSION CYCLING SHOWING TRANSITION FROM LINEAR TO NON-LINEAR ELASTICITY WITH LOW HYSTERESIS _____	70
FIGURE 39 STRESS STRAIN CHART FOR THE SAMPLES SHOWN IN THE PHOTOGRAPHS BELOW. _____	71
FIGURE 40 SINGLE UNIT (UNCONSTRAINED ON EDGES) RESPONSE TO TENSION (LEFT) AND COMPRESSION (RIGHT) SHOWING COORDINATED BUCKLING. _____	71
FIGURE 41 ANSYS SIMULATION WITH DEFLECTION MULTIPLIER SHOWING COORDINATED BUCKLING MODE _____	72
FIGURE 42 MODULUS PLOTTED AGAINST NORMALIZED SIZE (# CELLS), ANSYS SIMULATION _____	72
FIGURE 43 RELATIVE STRENGTH AND MODULUS OF DIGITAL COMPOSITES _____	73
FIGURE 44 DIGITAL COMPOSITE MODULUS SCALING WITH DENSITY _____	74
FIGURE 45 PREVIOUSLY KNOWN ULTRA-LIGHT MATERIALS _____	77
FIGURE 46 PREVIOUSLY KNOWN CELLULAR MATERIALS WITH BETTER THAN QUADRATIC DENSITY MODULUS SCALING PROPERTIES _____	78
FIGURE 47 DIGITAL CELLULAR COMPOSITE MATERIAL PERFORMANCE – THE LINE REPRESENTS QUADRATIC SCALING FROM THE IDEAL AXIALLY ALIGNED CARBON FIBER COMPOSITE SOLID. _____	79
FIGURE 48 SEQUENTIAL CYCLIC LOADING AFTER FAILURE EVENTS, SHOWING GRADUAL REDUCTION IN EFFECTIVE MODULUS ____	80
FIGURE 49 DESIGNER FAILURE MODES: CRACK PROPAGATION, NON-LINEAR ELASTICITY BY ELASTIC BUCKLING, BRITTLE CRUSHING _____	81
FIGURE 50 IMPERIAL PROBE DROID _____	83
FIGURE 51 TUNABLE ELASTICITY _____	84
FIGURE 52 TEST FLEXURE TOWER SETUP _____	85
FIGURE 53 DIGITAL COMPOSITE COLUMN PROFILE, LOADING SCHEME, (PHOTOGRAPHS) _____	86
FIGURE 54 DIGITAL COMPOSITE COLUMN PROFILE, SIMULATION AND ACTUAL EXPERIMENT (PHOTOGRAPH) FOR FIRST ASSEMBLY, SHOWING PURE AXIAL COMPRESSION _____	87
FIGURE 55 SIMULATION AND ACTUAL EXPERIMENT (PHOTOGRAPHS) FOR SIMPLE SINGLE AXIS BUCKLING ASSEMBLY _____	88
FIGURE 56 SIMULATION AND ACTUAL EXPERIMENT (PHOTOGRAPHS) FOR COMPLEX BUCKLING ASSEMBLY _____	89
FIGURE 57 WING SHAPE MORPHING SCHEMES (HIGH LIFT, CRUISE, CONTROL/FLAP); AIRFOIL SHAPES FOR DIFFERENT AERODYNAMIC REGIMES _____	90
FIGURE 58 DIGITAL AIRFOIL SHAPE MORPHING SCHEME, PARTS _____	91
FIGURE 59 DIGITAL CELLULAR AIRFOIL _____	92
FIGURE 60 DIGITAL CELLULAR AIRFOIL: INTERFACE BETWEEN STRUCTURE AND AIRSTREAM PROVIDED BY CELLULAR SKIN ____	93
FIGURE 61 DIGITAL CELLULAR AIRFOIL _____	94
FIGURE 62 DIGITAL CELLULAR AIRFOIL IN THE MIT WRIGHT BROTHERS WIND TUNNEL _____	95
FIGURE 63 1D → 3D WORKFLOW WITH POTENTIAL APPLICATIONS TO DIGITAL COMPOSITE ASSEMBLY (CHEUNG, ET AL 2011) _____	97
FIGURE 64 ONE DIMENSIONAL WORKFLOW FOR FRAMEWORK CONSTRUCTION _____	98
FIGURE 65 DIGITAL COMPOSITE WING WEDGE, SIZED TO REPLACE EXISTING COMPONENT ON COMMERCIAL JET PRODUCED BY SPIRITAERO _____	102
FIGURE 66 BEAM PERFORMANCE INDEX FOR VARIOUS MATERIALS _____	104
FIGURE 67 ANDEAN CONDOR _____	105
FIGURE 68 ENGINEERED MOLECULAR DIGITAL COMPOSITES _____	107
FIGURE 69 CONDUCTIVE AND INSULATING DIGITAL COMPOSITE PARTS _____	108
FIGURE 70 DIGITAL COMPOSITE ORTHOSES AND PROSTHESES _____	109
FIGURE 71 DIGITAL COMPOSITE SHAPE MORPHING WINGS _____	110

FIGURE 72	RESONANT AERODYNAMIC PROPULSION	110
FIGURE 73	DISASTER RELIEF WITH RAPIDLY DEPLOYABLE DIGITAL COMPOSITE INFRASTRUCTURE	111
FIGURE 74	AERIAL CONCEPT VIEW	112
FIGURE 75	MIT CAMPUS, CONSOLIDATED.	113
FIGURE 76	THREE DIMENSIONAL VILLAGE FLOOR PLAN (ABOVE), SECTION (BELOW)	114
FIGURE 77	PRELIMINARY CHAIN TESTING	121
FIGURE 78	PROCESS DEVELOPMENT TESTING	123
FIGURE 79	3D PRINTED (X10 SCALE) CT SCAN DATA FROM BONES	129
FIGURE 80	CUSTOM CT DATA PROCESSING SOFTWARE	130
FIGURE 81	CT DATA RENDERINGS	131
FIGURE 82	CURVATURE BASED CREASE FINDING ON STANFORD BUNNY MODEL	131
FIGURE 83	PRELIMINARY MATERIAL DISTRIBUTION CHARACTERIZATION METHOD	132
FIGURE 84	STRUCTURAL WEDGE COMPARISON MODEL	133
FIGURE 85	GENERIC WING BOX RELATIVE PRESSURE MAP	134
FIGURE 86	MULTIPLEXED WINDING MOLD DIAGRAM	135
FIGURE 87	ASSEMBLY PROCESS	138
FIGURE 88	FIBER LAYUP WITHIN COMPONENTS	139
FIGURE 89	SLICED PULTRUSION / BONDED PARTS	140
FIGURE 90	FIBER LAYUP WITHIN PRE-FORMED LAMINATE	140
FIGURE 91	– GENERALIZED INTERACTION POTENTIAL DIAGRAMS	143
FIGURE 92	A SCHEME WITH ONLY ONE PART TYPE (PINS INCORPORATED)	144
FIGURE 93	ROLL TO ROLL MANUFACTURING OF POP-UP CELLS	145
FIGURE 94	KELVIN STRUCTURE	145
FIGURE 95	TODAY’S ASSEMBLERS	145
FIGURE 96	DIRECTIONAL CONNECTION STRUCTURES (RIGHT)	146
FIGURE 97	DIRECTIONAL CONNECTION SCHEMATIC	147
FIGURE 98	DIRECTIONAL CONNECTION CELL TYPES (TENSION, LEFT; COMPRESSION, RIGHT)	147

(This page intentionally left blank)

## Introduction

### Digital Materials

The digital revolutions in communication and computation have enabled engineered systems that functionally scale to Avogadro numbers of their functional units. This is largely achieved through error reduction and correction strategies that rely on stochastic near-certainties that are driven by the physics of the system. Biology shows us that these goals can be satisfied in a system for fabricating things, or “programming matter,” through the encoding of structural and functional information, with a small and discrete set of parts. We refer to materials that follow these principles as digital materials, and the methods of organizing these materials into functional assemblies as digital fabrication.

To realize designed and engineered digital materials and fabrication processes, I look to develop low cost and reversible material systems that can form mechanically useful assemblies and require low precision assembly methods. While determining exactly how biological fabrication works is an unsolved problem, the complex structural requirements that are satisfied in natural systems provide proof of their possibility. Much progress is being made on determining the exact schemas of construction (i.e. protein folding, growth regulation) in biological systems, as well. In any case, the potential complexity and diversity of assemblies that are accessible by this digital fabrication approach has long been appreciated (e.g. Mayer 2005).

Conventional designed and engineered fabrication methods employ digital computation and communication algorithms to control analog mechanical equipment that additively or subtractively forms shapes from masses of bulk material. Digital material systems propose a method for fabrication from discrete parts with discrete relative local positioning, instead of continuous variation of composition and location of material, as in an analog fabrication system. This may be thought of as printing, noting that an important distinction between digital material printing and conventional commercially available three dimensional printing processes is that digital material printing is reversible, and the information regarding the shape, assembly, and function of a finished product is intrinsic to the material that it is composed of (“...can you tell the shape and fabrication method of a part by its function?...”).

The process of printing ink on pages changed fundamentally with the introduction of the page description language, which enabled the “desktop publishing” revolution of the 1980s by

packaging the information describing printed material as executable programs. Similarly, a “desktop fabrication” revolution will rely on the transfer of information to fabrication systems, as part specific executable programs, instead of machine specific control instructions (Gershenfeld 2005). This is enabled by embedding metrology and positioning constraints within the design of material building blocks.

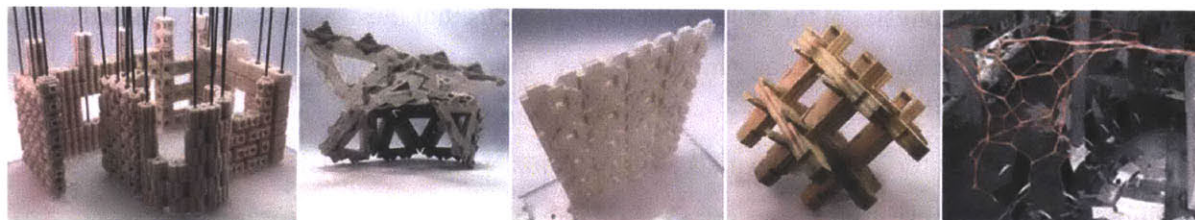


Figure 1 Example Digital Materials

There are various ways to envision architectures for such a programmable matter system. The biological analogy leads us towards self-assembling and self-reconfigurable systems with both extrinsically functional products and intrinsically functional machinery (for operating on the system itself) being made of the same fundamental set of units. A considerably simpler model allows for an external operator (“hand-of-[your preferred deity],” if you will) to perform assembly and reconfiguration steps on mechanically passive parts. It is this latter model that we propose for the subject of this work.

A primary proposition of this work is that properly engineered kits-of-parts (with many fewer primitives than your average reconfigurable toy construction set) with automated assembly and disassembly (hence static reconfigurability) can produce functionally useful parts (not just toys, although this is also acceptable use!) that have life cycle efficiencies exceeding that of conventional engineered fabrication methods. The included case study addresses the mechanical digital material design problem, from the perspective of analysis and testing of an example called digital composites.

## Background

### Natural Fabrication

Imagine a structural building kit for building high performance structures ranging from centimeters to tens of meters. In this kit, there is a small and finite set of types of building blocks. Some of these types are very strong, and others are very tough. For structural purposes, it is typical to assemble these units in different ways – for example, very dense or very sparse. Different structural types can also be combined to strategically manage a wide variety of loading conditions. From the point of view of composition, the dense assemblies resemble structures formed from bricks, as they are composed of regular units at regular spacing, and the sparse assemblies resemble flexible space frames, with regular units that are compliant enough to permit a wider (yet still finite) set of valid connections.

Structures that are built with this kit may be well tuned to support a wide range of static and dynamic loads. Further, the system has the ability to gradually adapt to new load patterns, with mobile units that travel over the structure and delete portions of its own structure, as well as other units that are capable of adding new material. Even in its densest form, these structures maintain an integral set of communication channels that allow for the diffusion of information, such as signaling the need to adapt the structure.

The smallest birds and the largest whales share a system that fits this description, in their bones. Building block types include cortical plexiform bone, with its dense brick-like assemblies. Cells that resorb or delete existing bone are known as osteoclasts, and osteoblasts add new structural material. These cells are set into coordinated action with the help of communication channels known as inter-lacunar canaliculi. The efficiency with which this system maintains itself and adapts to new loading patterns – or even failures – far outperforms conventional engineered structural systems, and provides real inspiration for our research on Digital Materials, which seeks to design and engineer artificial systems with some of the qualities described above.



Figure 2 CT scan of wild pheasant bone, picture of Euplectella sp. and CT scan

### Natural Materials

Material science has made much progress in the description of natural cellular solids, such as wood and bone (Gibson 2005). We may consider such biological cellular solids to be a prime example of natural structural fabrication that is high performing with complex constraints. For analysis, it is now typical to treat cellular materials as classical solids. The properties of the cellular solid are therefore defined by the properties of the solid material that it is made from (the “constituent solid”), and its spatial configuration (Gibson & Ashby 1988).

Much of the art – of continuum mechanics of cellular solids – lies in developing a classically analyzed cell model that is an effective representation of the stochastically varying nature of the actual material. The field has done quite well to characterize readily available natural cellular solids in this manner. Natural scaling laws are well known (Gibson & Ashby 1988), and relate the mechanical properties of the cellular solid to those of the constituent solid material (that which comprises cell edges and/or walls), via the relative density of the former to the latter.

A large variety of applications have developed around the science of cellular solids, evidenced by the widespread use of these materials for passive energy absorption, thermal insulation, and fluid filtering (Maiti et al 1984). However, despite their low density, they are largely limited in their use for structural applications, because for the weight of popular and inexpensive cellular solids, they are not particularly strong. The conventional model typically considers the geometry of stochastic foams to be such that transverse beam bending dominates the behavior of the material (Gibson & Ashby 1988). This results in an overall relative modulus that is expected to be proportional to the square of the relative density, for natural foams.

$$\frac{E^*}{E_s} \propto \frac{\rho^2}{\rho_s^2}$$

Equation 1

In addition to biological cellular solids, this scaling law is useful for analyzing and predicting the properties of non-biological natural foams (e.g. pumice) and engineered foams (e.g. polymer foams, metal foams), whether chemically or mechanically produced. Further analogies to natural cellular structures exist in conventional engineered structures (Aizenberg et al 2005). Depending on the relative scale desired for analysis, one might look towards the aforementioned engineered foams, or space frame trusses and aero-structures.

### Engineered Fabrication

Architecture and civil engineering have employed space frame truss structures for many years. These have not previously been scaled volumetrically, as a perfect lattice, to the orders of units that make it practical to consider the bulk assemblies as a continuum, as would be beneficial for engineering and design purposes. Further, it is well known that space frames with many elements sharing structural duty possess highly desirable characteristics in terms of failure modes and damage tolerance (Lakes 1993; Huybrechts & Tsai 1996). This is evident in “geodetic” airframe designs (Paul et al 2002).<sup>1</sup> The current state of robotic manufacturing technology makes it easy to see how we can implement massively parallel assembly of digital materials, including the assembly of structures that are larger than the assembly machinery.

The commercial aerospace industry has been moving towards aircraft designs that have fewer but larger monolithic fiber composite parts, in order to produce highly tuned and lightweight structural systems that meet extreme service, monitoring, and general environmental requirements. Conventional wisdom is that larger monolithic parts are better than an assembly of smaller parts because producing effective joints between parts is highly problematic in practice. Conventional manufacturing processes have scaled up, accordingly, which requires tools (e.g., molds for defining the shape of the part), and ovens (e.g., autoclaves for polymer matrix curing)

---

<sup>1</sup> These were last seen in large scale production in the 1960s. There are a number of theories published, attempting to explain the recent unpopularity of the design. Some argue that this is because of the labor intensive nature of production processes of the time. Others argue that it is merely a result of necessarily aggressive regulation of the aircraft industry, coupled with the business success of the DC-4, which while not necessarily owed to its strategy of construction in particular, nonetheless cemented the alloy spar-rib-skin design into modern aviation qualifications (Paul 2002).

that are large enough to influence the size of the buildings that must contain them. Some may consider that the expense involved with these manufacturing methods limits the industry altogether; there is no question that it limits prototyping capabilities. Further, the per-part investment is high enough to warrant complex repair processes as defects of small relative size arise, to say nothing of their contribution to resource intensive qualification procedures (USDOD 2002).



Figure 3 The Boeing Dreamlifter: an example of the lengths (and widths) that are gone to, in today's leading edge composite production. This aircraft was designed and manufactured specifically as part of the production process for the Boeing 787 passenger aircraft, which is comprised of large monolithic composite components.

These relatively recent methods also rely on a basis set of conventional manufacturing and fabrication tools and processes. Conventional subtractive manufacturing techniques (i.e. milling,

water-jet cutting) work poorly with fiber reinforced polymer materials (i.e. requiring diamond tipped bits for carbon fiber composites, subject to wetting and de-lamination during abrasive water-jet cutting). Conventional additive fiber reinforced polymer manufacturing techniques involve dynamic weaving and robotic layup about formwork that is the size of a part (or larger), requiring very large investments in tooling. Other conventional rapid prototyping technologies such as additive computer controlled three dimensional material printing processes do not produce structurally tuned fiber reinforced composite parts. Digital composites would allow for rapid prototyping of fiber composite parts with high throughput robotic digital assemblers. The individual components are may be produced through conventional means, as suited for mass production of identical parts. With digital assembly of sparse volumes composed of many smaller components, all of the tooling required may be significantly smaller than the finished assemblies.

This work addresses volume filling reconfigurable digital material systems with press-fit or snap-fit connections. Current commercially available systems, which meet these criteria and are designed as shape universal systems, are mostly designed as children’s toys. This work will consider assemblies of these systems from a continuous bulk material perspective.

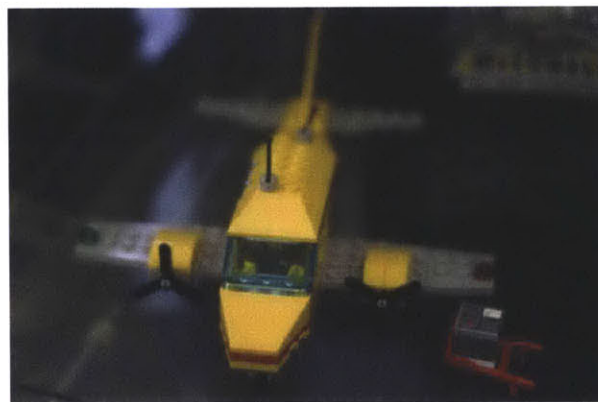


Figure 4 Aircraft of Conventional Reconfigurable Matter

### **Engineered Materials**

The aforementioned advances of material science in engineering of cellular solids, such as honeycomb core materials and foams, have resulted in our ability to design with lighter, more elastic, more insulating, and more energy absorptive materials. The practice of treating cellular

solids as conventional continuous solids allows for simple application with conventional engineering and design methods.

In the context of cellular materials, it has been noted that “constructed” (Sypeck et al 2001) periodic metal lattices allow for much larger cell size, and therefore lower relative density, compared to other methods of producing cellular metals (Wadley 2002).<sup>2</sup>

A natural result – of the understanding and application of cellular material property scaling laws – has been an interest in ultra-light materials.<sup>3</sup> We may consider ultra-light materials to include any material that is less than 0.1 grams per cubic centimeter. These materials are generally known to obey a less desirable scaling than the denser stochastic cellular materials (Schaedler et al 2011), as in Equation 1.

$$\frac{E^*}{E_s} \propto \frac{\rho^3}{\rho_s^3} \quad \text{Equation 2}$$

While this generally applies to aerogels, recent results have shown processes that achieve the quadratic scaling of denser stochastic cellular materials (Schaedler et al 2011; Mecklenburg et al 2012). I will show improvements upon this, with digital composites.

---

<sup>2</sup> Templated truss topologies have proven to be too expensive (Wadley 2002). Other methods using folded and sintered/brazed sheets/textiles (Sypeck & Wadley 2001) are in development.

<sup>3</sup> Prior digital material systems have generally addressed dense assemblies of units made from isotropic materials.

## Design and Analysis

Digital Composites can be viewed as engineered cellular solids with many reconfigurable connections. This method of production confines the stochasticity of the material to the production of each part, and allows for highly porous large scale volumetric assemblies. In the case of digital materials, conventional cellular solid analyses are therefore simplified, since we can design the geometry of the cellular structure as an assembly of digital components. The difficult task – of developing a classically analyzed cell model that is an effective representation of the stochastically varying nature of the actual material – is not necessary, here. Some variation is introduced through part production and assembly processes, but these can be taken as micro-level stochastic processes that are simple to analyze and characterize.

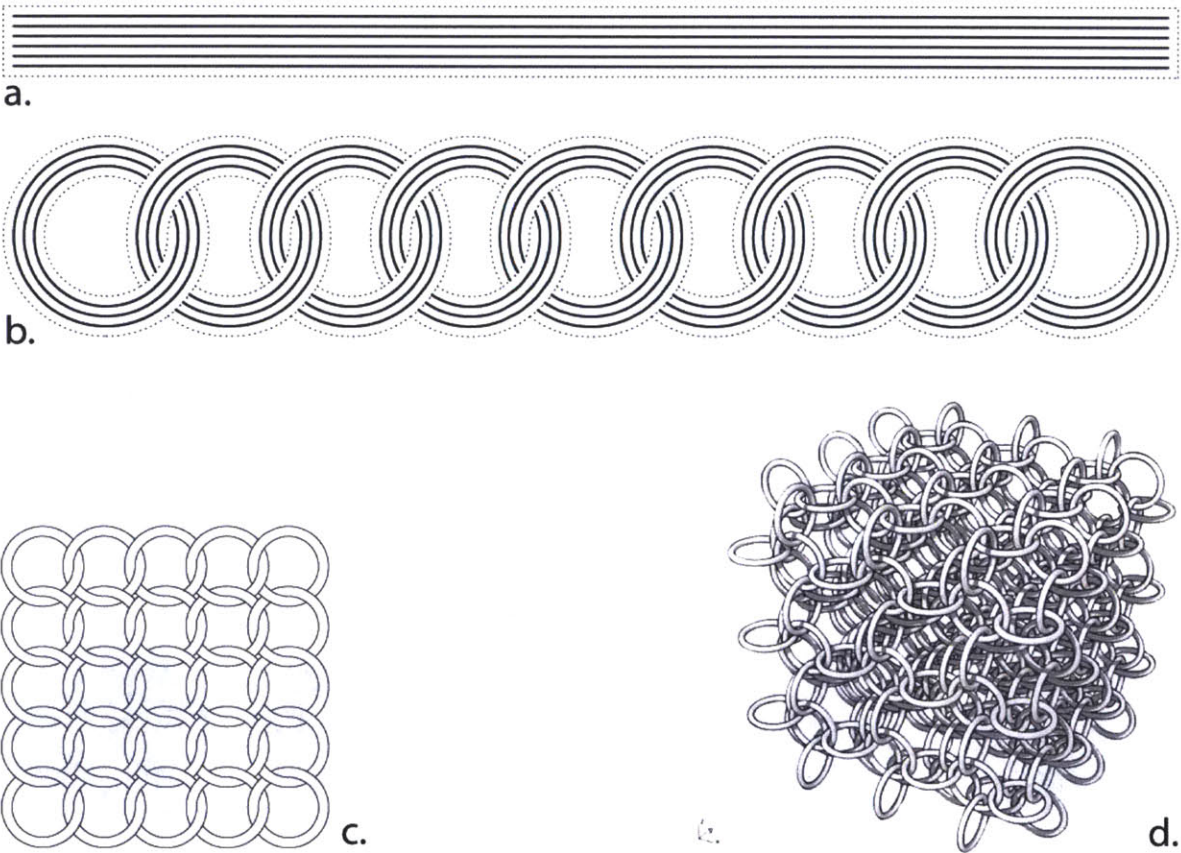


Figure 5 Concept Diagram for Digital Composites – chained continuous fiber loops

As an application of fiber composites, the core concept is that a chain of discrete fiber composite parts can be close to the strength of a monolithic part, and would have advantages with manufacturing processes, serviceability, and reusability, in addition to the tunability and extensibility that are general goals of digital materials.

The structure can therefore be thought of as a chain of parts, each transferring load through load bearing holes with continuous circuits of fiber around their perimeter. This way, the structure is an assembly of linked tiles that are individually tuned through their fiber layup, so that forces are transferred between the tiles, rather than having continuous fibers span entire macro-structures.

A major difference between conventional cellular solids and digital cellular solids is the presence of many reversible connections, the behavior of which will be accounted for in later chapters. The primary benefit is the manufacturability of complex geometries that result in mechanical property scaling laws that are quite different to those of both stochastic foams and previously reported non stochastic ultra-light materials. While these connections can also be used to design novel structural behavior, they do come at an overall density cost. I will show, here, that this density cost is minimal when employing this strategy for ultra-light materials.

Digital Materials, in general, employ a finite number of types of simple discrete components which can be assembled to large structures according to local-only rules, which makes them good candidates for trivial adaptation to various shapes at a large scale. In addition to simple spatial distribution of regular lattices, precise distribution of parts for a given structural function may also be automatically accomplished through algorithmic distribution throughout a prescribed volume, according to external constraints (Hiller & Lipson 2012). Other strategies for tuning of mechanical properties include introducing voids, varying part ratios, varying core geometry, and introducing kinematically indeterminate lattice states (Guest & Hutchinson 2003).



Figure 6 part size hierarchy, core structural variation, introduction of voids as methods of structural tuning

For complex shapes, Digital Materials provide a potential "tool-less" (or "less-tool") assembly process, where the geometry of the parts being assembled provides the dimensional constraints required to precisely achieve complex forms. This does not rely on each part being very precise, but instead relies on specific knowledge of the nature of the errors that do occur (part production must be a stochastic process). For instance, a system whose assembly over-constrains elastic components can provide positioning with much higher precision than that which is contained within the shape of any single component.

Reversible interlocking assembly allows deconstruction and reuse of individual components. In addition, service life of larger assemblies can be greatly increased by the ability to selectively replace small portions of a structure. While the assemblies in this study have been assembled by hand, a digital assembler may be considered critical to the viability of digital fabrication, in order to have practical advantages over existing manufacturing technologies – with regard to factors such as cost and time, given the increased resolution. The suggestion here is that assemblies should be produced from orders of magnitude more individual parts than are typically used in manufacturing, today. The key to making this plausible might be robotic digital assemblers that can build structures much larger than themselves, and that work in parallel. An important attribute of digital materials that makes this possible is the finite and low number of part types and connection schemes. This chapter addresses the design of Digital Composites, in terms of Geometry and Mechanics.



Figure 7 snap fit flexural lattice studies: left, middle, tensegrity crystal; right, hyperbolic/geodesic surface kit

## Geometry

The goal of this section is to present geometric theory for digital material assemblies as cellular solids. The primary questions surround the effect of geometric design on the relative density of the final structure. Purely geometric effects on mechanical behavior will be introduced, but addressed in more detail in the following section. Here, I look to determine global characteristics in structures as defined by local geometry.

The versatility of the digital material approach, in terms of lattice geometry, is loosely illustrated by the scope of designs apparent in Figure 1 and Figure 8. The former two figures show a variety of four-connected units in orthotropic arrangements, topologically similar to the design that is shown in the left side of Figure 8. The designs in the latter figure are snap-fit structures that utilize flanged members to increase torsional rigidity. An idealized isotropic lattice structure is shown on the middle and right side of Figure 8, with regular twelve-connected nodes forming a hexagonally close packed (HCP) structure.

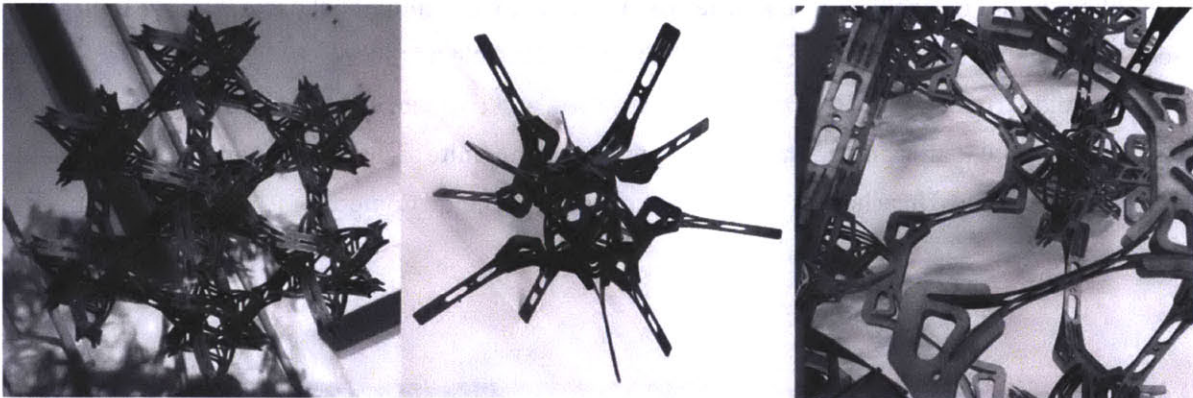


Figure 8 snap fit flexural lattice studies: left, simple cubic lattice with two part scheme; right, 12 connected octet truss with three part scheme

While the parts for the schemes above are fabricated as two dimensional shapes, and there are relatively few different shapes per scheme (two for the orthotropic scheme, three for the HCP scheme), there are many parts per spatial unit (twelve for the orthotropic scheme, thirty for the HCP scheme). Given that iterative quantity is required for bulk characterization as a cellular solid, and considering that every connection incurs assembly cost (structural cost/benefit depends on

structural objective), the case study that I address in most detail is a simpler design, such as the one shown in Figure 9.

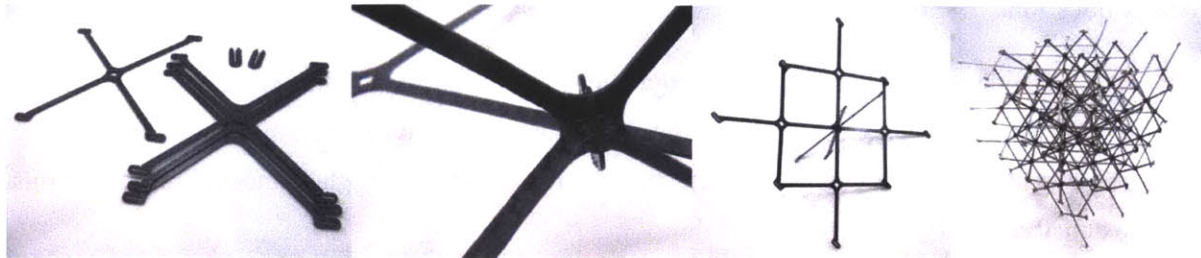


Figure 9 two part scheme for cuboct truss

At the heart of the original design problem is the decomposition of a regular lattice into self similar units that tessellate throughout space. The most basic decomposition separates every node and strut member in the lattice into individual units, requiring two connections per strut member and  $m$  connections per node, for a lattice with  $m$ -connected nodes. When designing a scheme for digital materials, it is advantageous to find ways to partition this lattice into tessellating units that contain multiple strut members each, for practical reasons as well as mechanical reasons that will be discussed in the next section. Considering that the space of all reversible connections used in engineering are fair game for adoption as connection strategies, we may see this as a very high dimensional problem, wherein certain types of solutions for one factor may constrain the possible solutions for another. This does not stop us from examining the relative importance of a few of the high level geometric decisions that need to be made when embarking on the design process. In particular, I will look at density in relationship to connectedness, starting with two dimensional systems and then expanding to three dimensional systems, for clarity.

Our oldest record of the two dimensional minimal edge packing problem dates back to 36BC, from Marcus Terentius Varro (Hales 2001), and is commonly referred to as the Hexagonal Honeycomb Conjecture. While it has been widely assumed to be true for lack of a counter example, this goal – of proving the most efficient division of a plane into similar units – stood unsolved until 1999 (a proof by Thomas Hales). There are three obvious regular polygonal area filling tilings of a plane – triangles, squares, and hexagons. However, as long as a pattern is repeating so that a small family of parts can be assembled to produce the final pattern, such as a kagome lattice constructed

from triangles (Connelly et al 2008), the geometry is fair game for digital materials. After the proof of Hales, we have reason to believe that hexagonal tiling provides the most space per unit edge, whether produced by regular tiling or not, and therefore the lowest density. Before considering the relationship of density to mechanical attributes, I will proceed with a short exploration of this density question.

Given a polygonal lattice of  $z$ -connected nodes and the corresponding strut members of equal length, what is the effect of connectedness on density? Intuitively, we can assume that low connectivity will give us low relative density, but just how much does high connectedness affect this relative density?

## An Estimation of an Upper Bound on the Perimeter to Area Ratio of Not-Necessarily-Space-Filling Two-Dimensional Grids Composed of Polygons

Consider a tiling on a Euclidean plane, which consists of straight strut members of length (l), connected at each end with nodes of arbitrary connectedness (z). Assume that the angles ( $\alpha$ ) between strut members at each node are equal, so that:

$$\alpha = \frac{2\pi}{z} \quad \text{Equation 3}$$

Further, to enclose maximum volume per polygon, assume that the tiling consists of convex regular polygons with a number of sides (n), which can be determined from the strut member angle:

$$n = \frac{2\pi}{\frac{2\pi}{2} - \alpha} \quad (\text{for Euclidean plane, } n = 2\pi / (\pi - \alpha)) \quad \text{Equation 4}$$

which can be expressed in terms of connectedness (z):

$$n = \frac{2\pi}{\frac{2\pi}{2} - \frac{2\pi}{z}} = \frac{1}{\frac{1}{2} - \frac{1}{z}} = \frac{nz}{2} - z \quad \text{Equation 5}$$

which describes the identity relationship between sidedness and connectedness of this model: the higher the connectivity, the lower the sidedness of the constituent polygons, and vice versa:

$$n = \frac{2z}{z-2} \quad \text{and} \quad z = \frac{2n}{n-2} \quad \text{Equation 6}$$

In order to estimate the density of a grid composed of these polygons, we need to estimate the area that each polygon might represent in a given tiling. I'm looking to make a scaling argument that addresses the general sensitivity of the perimeter to area ratio to changes in constituent variables. For this, we may start by determining their characteristic length. Given the number of sides ( $n$ ), we can determine the largest characteristic dimension (a line,  $d$ , through the middle of the polygon), by starting from one side of this line and summing the components ( $\delta$ ) of each polygon side (of length  $l$ ) that are parallel to the line, considering the progression of the angle ( $\beta$ ) relative to the line, for half of the sides ( $n / 2$ ):

$$d = \sum_{i=1}^{n/2} (\delta_i) \quad \text{Equation 7}$$

Where

$$\delta_i = l \cos \beta_i \quad \text{Equation 8}$$

And

$$\beta_i = \frac{1}{2} 2\pi(i - 1) - \frac{1}{2} (2i - 1)\alpha = \frac{1}{2} 2\pi(1 + i(m - 2) - m)m = \frac{2\pi(4i - 2 - n)}{4n} \quad \text{Equation 9}$$

such that:

$$d = \sum_{i=1}^{n/2} \left( l \cos \frac{\pi(4i - n - 2)}{2n} \right) \quad \text{Equation 10}$$

which converges to  $(nl / \pi)$  for very large numbers of sides ( $n$ ). We also see that this convergence relates to the classical formula for the circumference of a circle:

$$nl = \pi d$$

Equation 11

Since we know that perimeter length is proportional to  $nl$ , and area is proportional to  $d^2$ , then minimization of perimeter to area goes by  $n/d^2$ . Looking at  $n/d^2$  per  $n$ , for unit edge length ( $l = 1$ ), clearly shows that the effect of connectedness (and sidedness) on perimeter to area – is within an order of magnitude, and insignificant if relative edge length ( $l$ ) can be varied across orders of magnitude.

These results are applicable to the design of two dimensional cellular materials (i.e. digital cellular skins), when considering load transfer across a surface (e.g. hoop stress). For now, I will move on to the three dimensional case.

Extension of these methods to examine our three dimensional problem (confined to the examination of the effect of connectedness on density) is fairly easy, if somewhat less precise (due to the addition of geometric assumptions about distribution of strut members in the third dimension). Our oldest record of the three dimensional minimal packing problem is considerably more recent than the two dimensional honeycomb problem, dating back a little over a century (Kelvin 1887). The Kelvin Conjecture addresses maximally space efficient bubble packing, with tetrakaidecahedrons arranged in a body centered cubic packing. Very recently, the Weaire-Phelan structure (Weaire & Phelan 1993) was presented as a counter-example, with two types of cells and an area to unit volume that is more efficient than that of the Kelvin structure, by a very small amount (0.3%). The problem of what is the most efficient structure remains unsolved.

While there are only a few regular polyhedral space-filling tilings, we may consider our three dimensional problem as being analogous to the two dimensional one. As in two dimensions, as long as a pattern is repeating so that a small family of parts can be assembled to produce the final pattern, the geometry is fair game for digital materials. With the efficacy of its use in modeling stochastic foams, and a belief in energy minimization in nature, we might believe that four connected (e.g. the Kelvin structure) tiling provides the most space per unit edge, and therefore the lowest density for structures consisting of all equal length strut members. Once again, before

considering the relationship of density to mechanical attributes, I will proceed with a short exploration of this density question, this time in three dimensions.

Given a polyhedral lattice of  $z$ -connected nodes and the corresponding strut members of equal length, what is the effect of connectedness on density? Intuitively, we can assume that low connectivity will give us low relative density, but just how much does high connectedness affect this relative density?

## An Estimation of an Upper Bound on the Total Edge Length to Volume Ratio of Three-Dimensional Lattices Composed of Polyhedrons

Consider a tiling in space, which consists of straight strut members of length (l), connected at each end with nodes of arbitrary connectedness (z). Take the simplification that the strut members are distributed throughout at least two discrete planes intersecting each node, so that the angles ( $\alpha$ ) between strut members are at least:

$$\alpha = 2\pi / (z / 2) = \frac{4\pi}{z} \quad \text{Equation 12}$$

To enclose maximum volume per polyhedron, assume that the tiling consists of convex regular polyhedrons with maximum possible characteristic dimensions defined by a polygon with a number of sides (n), which can be determined from the strut member angle:

$$n = 2\pi / ((2\pi / 2) - \alpha) = n = \frac{2\pi}{\pi - \alpha} \quad \text{Equation 13}$$

which can be expressed in terms of connectedness (z):

$$n = \frac{2\pi}{\pi - \frac{4\pi}{z}} = \frac{2}{1 - \frac{4}{z}} = \frac{nz}{4} - \frac{z}{2} \quad \text{Equation 14}$$

which describes the relationship between sidedness and connectedness of this model: the higher the connectivity, the lower the sidedness of the constituent polygons, and vice versa:

$$n = \frac{2z}{z-4} \text{ and } m = \frac{4z}{z-2} \quad \text{Equation 15}$$

In order to estimate the total strut member length to volume ratio of a lattice composed of polyhedra whose characteristic length is described by these polygons, we may estimate the total number of strut members as the square of the number of sides in one of these theoretical constituent polygons, and the volume as the cube of this characteristic length that is calculated from this polygon. Given the number of sides ( $n$ ) for each polygon, we can determine the largest characteristic dimension (a line,  $d$ , through the middle of the polygon), by starting from one side of this line and summing the components ( $\delta$ ) of each polygon side (of length  $l$ ) that are parallel to the line, considering the progression of the angle ( $\beta$ ) relative to the line, for half of the sides ( $n / 2$ ):

$$d = \sum_{i=1}^{n/2} (\delta_i) \quad \text{where } \delta_i = l \cos \beta_i \quad \text{Equation 16}$$

And

$$\beta_i = (-1 + i)\pi - \frac{1}{2}(2i - 1) \frac{4\pi}{z} = \frac{(2+i(z-4)-z)\pi}{z} = \frac{1}{2}(4i - 2 - n)n\pi \quad \text{Equation 17}$$

such that:

$$d = \sum_{i=1}^{n/2} \left( l \cos \frac{\pi(4i-n-2)}{2n} \right) \quad \text{Equation 18}$$

which is identical to the 2d case, since this expression only compares  $d$  and  $n$ . Given the assumption that total perimeter strut member length is proportional to  $n^2$ , and volume is proportional to  $d^3$ , then minimization of total strut member length to volume is proportional to  $n^2/d^3$ .

$$\left(\frac{2z}{-4+z}\right)^2 / \left(\sum_{i=1}^{\frac{\frac{2z}{-4+z}}{2}} \cos\left[\frac{(\pi)(-2+4i-\frac{2z}{-4+z})}{2(\frac{2z}{-4+z})}\right]\right)^3 \quad \text{Equation 19}$$

The contour of  $n^2/d^3$  per node connectedness ( $z$ ), for unit edge length ( $l = 1$ ), suggests that like the 2d case, the effect of connectedness on the total strut member length to volume ratio – is also within an order of magnitude, and therefore also insignificant if relative edge length ( $l$ ) can be varied across orders of magnitude.

These estimation results give us some confidence in retaining the design freedom to choose lattice geometries without straying into an area of the design space where obtaining desirable relative density is unlikely. Focusing further on actual design parameters, I next look towards a general scaling law that now takes into account dimensions such as strut member length ( $l$ ) and thickness ( $t$ ). This will be an expansion of known scaling laws for analytical modeling of cellular solids, with the addition of terms to account for the connections in a digital material, which we may assume to occur at the nodes in the lattice. We also consider aspect ratio as  $\varphi = t/l$ . Relative density is conventionally defined as  $(\rho^*/\rho_s)$ , where  $\rho^*$  is the mass of the lattice divided by the total bounding volume ( $v^*$ ), and  $\rho_s$  is the density of the constituent solid material (i.e. the mass of the lattice divided by only the volume of the constituent solid material  $v_s$ ):

$$\begin{aligned} \varphi &= t/l \text{ (aspect ratio, } t=\text{thickness, } l=\text{length).} \\ d &= k_p l \text{ (pitch, } k_p = \text{length constant)} \\ \rho^*/\rho_s &= (m/v^*)/(m/v_s) = v_s / v^* \text{ (Relative density)} \end{aligned}$$

Equations 20

We may also define the characteristic dimension of the repeating cell as pitch,  $d$ , which is proportional to the length of each strut member according to the lattice geometry. As such, the bounding volume  $v^*$  is proportional to  $d^3$ . The volume of the solid material per cell is composed of the sum of the volumes of the strut members and connections, which for square prism strut members may be defined as  $t^2l$  and  $k_c t^3$ , respectively (note that the size of the connection does not

depend on  $l$ , as the governing factor in connection design is stress, and therefore maximally scales with the cross sectional area of the strut member).

$$v^* \propto d^3$$

$$v_s = n_l V_{\text{strut member}} + n_c V_{\text{connection}}$$

( $n_l$  = number of strut members per unit cell,  $n_c$  = number of connections per unit cell)

$$V_{\text{strut member}} = t^2 l$$

$$V_{\text{connection}} = k_c t^3 \text{ (no dependence on } l)$$

$$v_s = n_l t^2 l + n_c k_c t^3$$

$$v_s / v^* \propto (n_l t^2 l) / d^3 + (n_c k_c t^3) / d^3 = (n_l t^2 l) / (k_p l)^3 + (n_c k_c t^3) / (k_p l)^3$$

Equations 21

This gives us the relationship of relative density to various factors:

$$\rho^* / \rho_s = (n_l / k_p^3) \varphi^2 + (n_c k_c / k_p^3) \varphi^3$$

$$\rho^* / \rho_s \propto \varphi^2$$

Equations 22

We see here, that relative density scales linearly with the number of strut members per cell, number of connections per cell, and the connection size factor. The contribution of the connection distribution, as defined by a given geometry, to relative density, scales with the cube of the aspect ratio of the strut members, and is therefore relatively unimportant. The governing side of the equation comes from the strut member contribution constants, but these scale with the square of the aspect ratio of the strut members. This suggests that the most effective geometric strategy for reducing the relative density is to reduce the ratio of strut member thickness to length. Pitch factor  $k_c$  can be understood to encapsulate the total strut member length per volume, which we expect from the previous estimation to not vary by very much between lattice geometries. To validate this understanding of the design space (that strut member aspect ratio is the most important factor in obtaining lattices with low relative density), we proceed with precise calculations of the relative density of four candidate lattices, of varying connectedness. These are, in increasing order of connectedness: the Kelvin structure with four connected nodes, a simple cubic lattice with six connected nodes, a simple cubic packing octahedral/cuboctahedral lattice (henceforth referred to

as a “cuboct” truss) with eight connected nodes, and a simple rhombic packing 2 tetrahedron 1 octahedron lattice, known as an “octet” truss (Fuller 1961), with twelve connected nodes. Given  $\rho^*/\rho_s \propto C_1\varphi^2 + C_2\varphi^3$ , we find the constants  $C_1$  and  $C_2$ , shown in the table below.

Table 1 Properties of Candidate Lattice Geometries

	connectedness	cell volume	connections per cell	strut members per cell	strut member scaling constant	connection scaling constant
	m	$v^*$	$n_c$	$n_l$	$C_1$	$C_2$
Kelvin Structure	4	$(16\sqrt{2})l^3$	12	24	$(3\sqrt{2})/4$	$3/(4\sqrt{2})$
Simple Cubic	6	$l^3$	1	3	3	1
Cuboct	8	$(2\sqrt{2})l^3$	3	12	$3\sqrt{2}$	$3/(2\sqrt{2})$
Octet	12	$(\sqrt{2}/2)l^3$	1	6	$6\sqrt{2}$	$\sqrt{2}$

Given that the connection scaling constant,  $C_2$  is not significant, since it scales with the cube of the strut member aspect ratio, examining the strut member scaling constant,  $C_1$ , should give us some indication of the relative impact of strut member length and width for these actual lattice designs. This constant essentially gives us a measure of the volume contribution of the strut members, to the overall volume. In this version of the model, it also can be taken to account for some of the “double-counted” material that is a result of the method of counting total strut member volume (Gibson & Ashby 1988). It does not take into account the increasing spatial complexity of the problem of designing reversible connections, with increasing node connectedness. This is a somewhat different type of problem, which will be left to future work.

It is hoped that these results provide a useful description of the problem space of designing lattices with relative density as a figure of merit. Characteristics such as lattice type, connectivity, and connection size all contribute to the final relative density, with proportional scaling that is within an order of magnitude. In particular for ultra-light materials, the most significant changes in relative density are made by changing the aspect ratio of the strut members.

## Mechanics

In stochastic foams, conventional models typically consider the average connectedness to be four, and strut members effectively meeting at midpoints of other strut members, resulting in characteristic behavior that is dominated by transverse beam bending (Gibson & Ashby 1988). This results in an overall relative modulus that is expected to be proportional to the square of the relative density, for open cell foams:

$$\frac{E^*}{E_s} \propto \frac{\rho^2}{\rho_s^2} \quad \text{Equation 23}$$

It is known that it is possible to improve upon this, with non stochastic geometry (Deshpande et al 2001), and we expect to do better, accordingly. In an ideal sparse structure,  $E/E_s \propto (\rho/\rho_s)$ , when loads are perfectly distributed so as to be purely axial on all elements in the structure. In compression, this is limited by member buckling, beyond the point at which infinitesimal offsets in the loading of an element will produce a bending moment that will receive further contribution from the axial load. In tension, such a proportional relationship is geometry dependent, and relies on the degree of mechanical constraint of each element, as afforded by the lattice geometry (Maxwell 1864; Calladine 1978), as well as the ability to efficiently transmit bending moments between elements (Broedersz 2011).

A key point here is a small departure from the bulk of the cellular solids literature, which has mostly considered two states of structures: those whose elements are maintained in pure axial loading (therefore dominated by stretching behavior), and those which fall into bending dominated behavior (and therefore consider negligible stretching contribution). A clue as to the practical existence of a third state comes from the statistical mechanics literature, as pertains to the mechanical behavior of interconnected networks of proteins. This class of materials, such as actin meshworks, microtubules, and fibrin and collagen matrices, is known to display higher strength and stiffness than their structural connectivity predicts with traditional framework rigidity criteria. While the exact phenomena that explain this are still under debate, pure mechanical models that show the ability of stretch-bend coupled systems to display proper behavior seem promising (Broedersz 2011). This relies to some degree on the relative strength and elasticity scaling of microscopic interactions for these materials (e.g. proteins), which form networks with a large

disparity in bond strengths (Jacobs et al 2001). In any case, if this intermediate phase of mechanical structure exists, then we should be able to show similar behavior at the macro scale.

There are two main reasons to choose a stretch-bend coupled material over a stretch dominated material. The first is versatility – if we can show this intermediate mechanical mode, then tuning parts to the better characterized bending and stretching dominated modes should be relatively easy. The second reason is failure mode – we expect that a stretch dominated fiber composite cellular solid would fail in a brittle fashion, and we are interested in knowing what the macro-scale failure mode of a stretch-bend coupled material looks like. A possible third reason has to do with the connections – when not building parts from a material such as carbon fiber, it may be helpful for the design and relative density to avoid pure axial loading of the joints, assuming that strength and stiffness requirements can be met without this.

Consider a model of a sparse digital material lattice as its true geometry, composed of members of length  $l$  and square cross section of side  $t$ . The relative density  $\rho/\rho_s$ , and the second moment of area of a member,  $I$ , are related to the dimensions  $t$  and  $l$  by:

$$\frac{\rho}{\rho_s} = \frac{\rho_c}{\rho_s}(\text{connection contribution}) + \frac{\rho_l}{\rho_s}(\text{ligament contribution})$$

$$\frac{\rho}{\rho_s} = C_c \frac{t^3}{l^3} + C_l \frac{t^2}{l^2} \propto \frac{t^2}{l^2}$$

$$I = t^4/12 \text{ for square cross section; } I \propto t^4$$

Equations 24

where

$\rho$  = mass density of structure

$\rho_s$  = mass density of constituent solid

$t$  = strut member thickness

$l$  = strut member length

for a Kelvin structure,  $C_c = 3\sqrt{2}/4$ , and  $C_l = 3/(4\sqrt{2})$  (Gibson & Ashby 1988)

for a cuboct structure,  $C_c = 3\sqrt{2}$ , and  $C_l = 3/(2\sqrt{2})$

Equations 25

For conventional foams and flexural functional composite part types, transverse beam bending deflection describes the primary response mechanism, modeled as beams that are simply supported at both ends and loaded in the middle (Gibson & Ashby 1988).

$$\delta \propto \frac{Fl^3}{E_s I}$$

$$\delta = \delta_{\text{bending}} \propto Fl^2/E_s I \text{ (for low } \rho/\rho_s\text{)}$$

Equations 26

Where

$\delta$  = change in length

$E$  = modulus of elasticity of structure

$E_s$  = modulus of elasticity of constituent solid

$\sigma = F/A_c$

$\varepsilon = \delta/L_c$

for a Kelvin structure,  $A_c = l^2/2$ , and  $L_c = l\sqrt{2}/2$  for single beam ( $A_c = 2l^2$ , and  $L_c = l\sqrt{2}$  for entire cell)

for a cuboct structure,  $A_c = 8l^2$ , and  $L_c = l\sqrt{2}/2$  for single beam ( $A_c = 32l^2$ , and  $L_c = 4l\sqrt{2}$  for entire cell)

Equations 27

from which  $E = \sigma/\varepsilon$  gives an expected relative modulus of:

$$E/E_s = (FL_c/A_c\delta)/E_s$$

$$\text{for a Kelvin structure, } E/E_s = (\sqrt{2})((F/l\delta)/E_s)$$

$$\text{for a cuboct structure, } E/E_s = (1/(8\sqrt{2}))((F/l\delta)/E_s)$$

$$\text{thus, we may assume } E/E_s = C_g((F/l\delta)/E_s)$$

Equations 28

And

$$E/E_s = C_g((F/l\delta)/E_s) \propto C_g \frac{F}{l(FI^2/E_s I)E_s} \propto C_g \left(\frac{t^2}{l^2}\right) \quad \text{Equation 29}$$

assuming, from above, that  $\rho/\rho_s \propto t^2/l^2$  and  $I \propto t^4$ ,

$$E/E_s \propto t^2/l^2 \propto (\rho/\rho_s)^2 \quad \text{Equation 30}$$

In contrast, the ideal loading condition for any subunit of the system is purely axial, so that  $E/E_s \propto (\rho/\rho_s)$ . It is known that this can be effected by high degrees of co-constraint, provided by lattice geometries with high connectivity (Warren & Kraynik 1988). This effect is intuitive upon examination of lattice types, as lattices with higher connectivity tend to connect strut members in such a way to produce axial loading of the individual strut members in the structure. Generally speaking, it is seen that lattices with higher connectivity at each node are better able to constrain the load paths, accordingly. In contrast, a lattice with low connectivity, such as the Kelvin structure, lacks any direct axial loading of material throughout the structure, is in some ways an effective representation for the myriad stochastic cellular solids currently used in engineering practice, and exhibits the quadratic modulus scaling law that makes engineered cellular solids more ideal for applications such as energy absorption, than those requiring high stiffness. If we can design the lattice for a cellular solid, because we are assembling it from discrete components, then we can prescribe a degree of connectivity that can result in these load pathways balancing through the

material as necessary. The important summary suggestion is that geometrically defined constraints can greatly influence the scaling relationship between mechanical material properties and relative density.

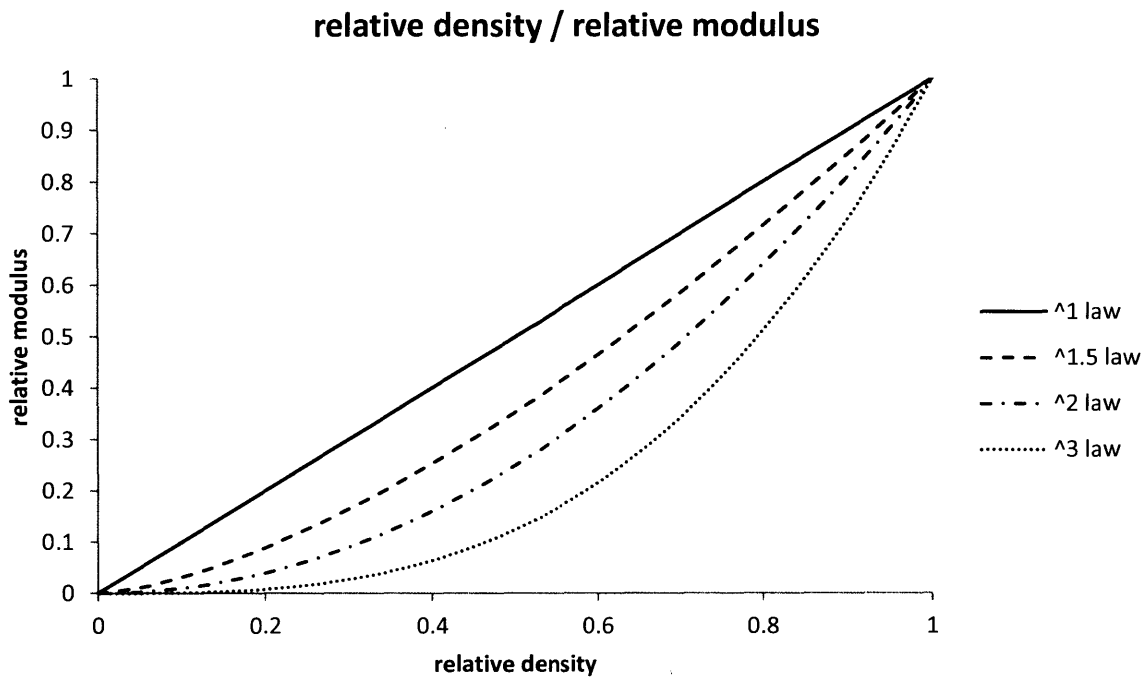


Figure 10 Relative Density vs Modulus Scaling Curves

This emphasis on end constraints for strut members leads us to another critical role of the connections. The use of many smaller parts to assemble a large part allows for the use of elastic averaging (Slocum 2003) in order to reduce error in manufacturing methods. When many parts are used to locate a single feature, with enough elastic compliance to adjust to small inconsistencies in the location of the feature, the effective location of the feature will be the average of the individual constraints provided by the surrounding parts. When this process is performed correctly, this average location can be more precise than the process used to fabricate the individual parts. The original per-part error must be within a certain threshold for a given system.

By the same rules, when forces are effectively distributed throughout an assembly of smaller parts, tolerances on strength requirements may be reduced as the observed bulk strength

of the assembly will be a result of this distribution. This is also naturally enabled by natural coupling of elasticity to strength, whereby weaker and more elastic components transfer load through stronger and stiffer components, while still contributing to overall stiffness.

The major components at hand, in a sparse digital material system as I have defined it, are the strut members and the connections. The properties of either are a question of design. When considered as a continuum, second order material properties will result from the behavior of both. Whether or not the behavior of either is responsible for the characteristic behavior of the continuum, for a given stress regime, is once again a matter of design. As such, the connections may be designed such that the  $\sigma/\epsilon$  curve of the connection ( $\sigma(\epsilon)_c$ ) has a particular relationship to the  $\sigma/\epsilon$  curve of the most elastic within-part strut member ( $\sigma(\epsilon)_p$ ).

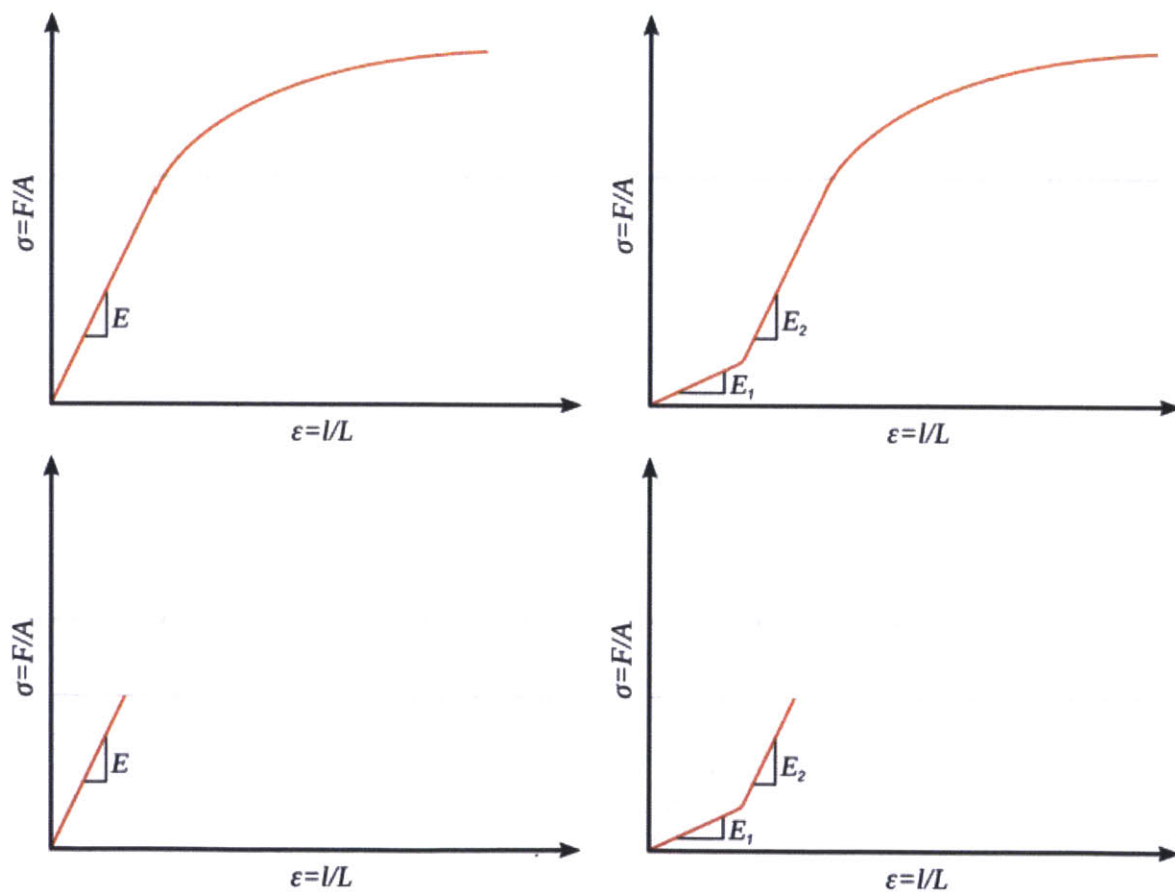


Figure 11 hypothetical designed digital material stress strain curves

For instance, if  $\sigma(\epsilon)_c$  is always greater than or less than  $\sigma(\epsilon)_p$ , then the connection either does not contribute to, or dominates, respectively, the bulk material behavior of the digital material. The  $\sigma/\epsilon$  curve of the bulk material will look typical, as in the upper left of Figure 11. On the other hand, if  $\sigma(\epsilon)_c$  intersects  $\sigma(\epsilon)_p$ , then the material will appear to have two phases of elasticity, such as in the upper right of Figure 11. The first phase of elasticity may be particularly useful to the development of morphing structures, as it allows for actuation forces that stay well within structural safety limits for the material. As previously noted, digital frangibility is a potentially useful property of digital materials. Hypothetical  $\sigma/\epsilon$  curves for such frangible digital materials are shown in the bottom of Figure 11.

This multiplexing of behaviors, in the aforementioned case including strut members and connections, can be extended to non-linear behavior within a component or connection (e.g. a flexural component that approaches a hard stop at a specified strain), or multi-part-type designs, which will be addressed in a later chapter. To bound the analytical and physical work, I have chosen to focus on regular three dimensional lattice geometry and mechanical structure as the primary dimension of merit. This includes, most notably, elasticity and strength. It is hoped that this provides a representative perspective that is generalizable to a large scope of digital materials.

## Case Study Digital Material Design – The Cuboct Truss

With the previous analyses, we might consider ourselves reasonably well equipped to design a general purpose digital material system. For such a system, a desirable attribute is isotropy. There are many perfect lattices or crystal structures with a defining characteristic of anisotropy. Relating to the previous section on mechanics of digital material lattices, this anisotropy can be viewed as asymmetry in the constraint of subsets of strut members that are aligned along specific planes throughout the material, or simply a lack of preservation of mechanical equilibrium under load. Of the four very basic lattices that I have discussed so far, the two with the lowest connectivity (the Kelvin structure, four connected, and the simple cubic lattice, six connected) are known for their lack of rigidity (Maxwell 1864).

A strategy for computer design of an isotropic cellular solid is to take one of these simple efficient anisotropic structures, such as the Kelvin structure, and to introduce random or periodic local perturbations on node locations that preserve the overall topology (Roberts & Garboczi 2002). I find this to be undesirable for our application both because this defeats the goal of maintaining strut member constraints and because this defeats a feature of digital materials that I expect to be able to use as an advantage. With regard to the former, as a result of removing all aligned load paths, we might expect mechanical performance to drop to the lowest common denominator for the geometry, which produces typical quadratic relative density scaling with relative modulus. Regarding the latter, digital materials with large overall dimension to part size ratios can be constructed such that they can be expected to behave as perfect lattices, which appeals to our sensibilities. A reason for this is that it maintains the option of introducing perturbations for functional purposes. Regardless, recent theory on the existence of strongly coupled stretch-bend modes in three dimensional lattices suggests that purely bending dominated behavior can be avoided in other ways (Broedersz et al 2011).

The lowest connectivity lattice that we find, which is composed of equal length strut members, regular polyhedra, and that satisfies Maxwell's rigidity criterion – is the cuboct truss. The structure can be seen as vertex connected regular octahedrons or square-face connected cuboctahedrons, and in this design is decomposed into elements that comprise four strut members, five parts of connections, and a shear clip to fasten the connections. When assembled, the ends of four crossbar units meet at the center and orthogonal to a fifth crossbar unit, where they are secured with a clip that is inserted orthogonally to the five crossbars.

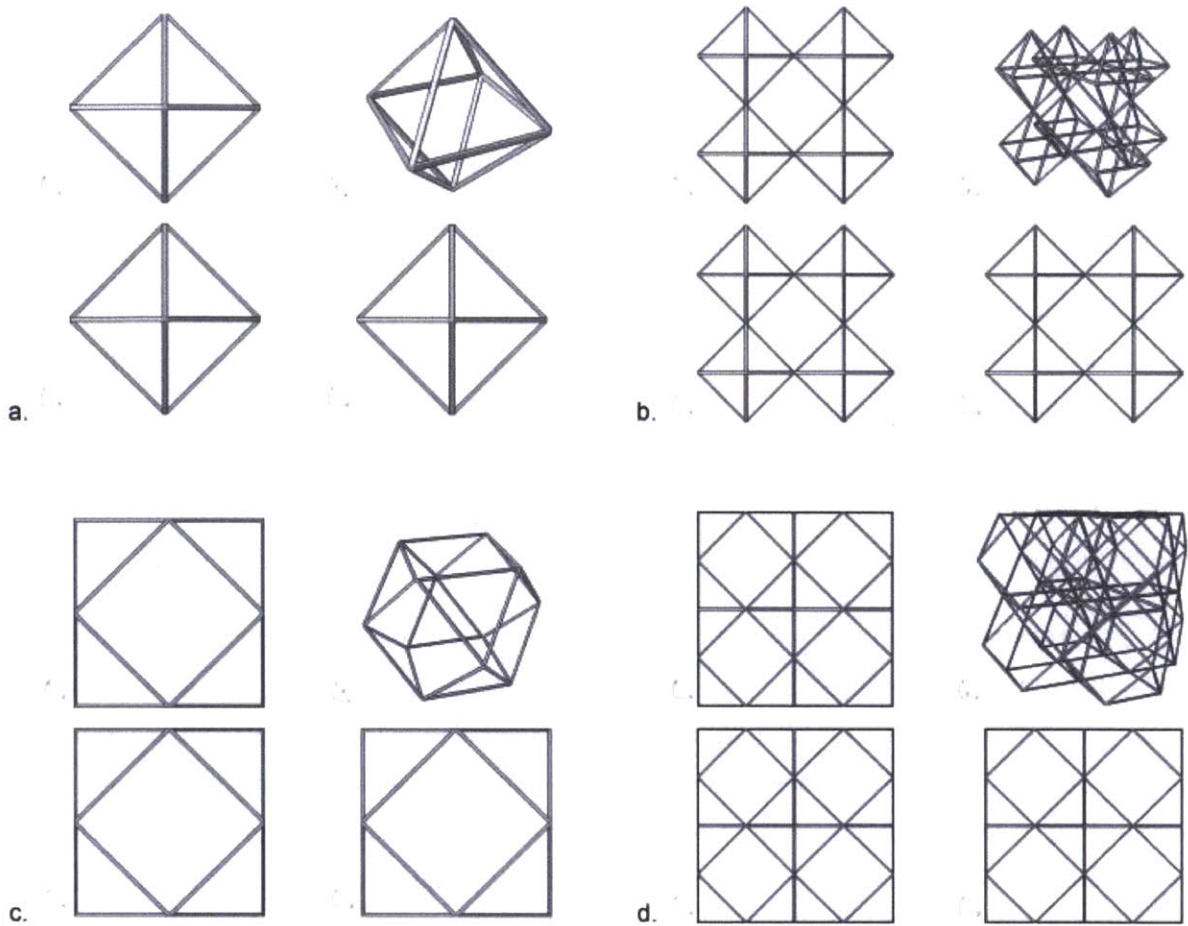


Figure 12 Cuboct Truss Geometry

The ends of the crossbar units are slotted tabs (Figure 14, c) that fit into larger slots at the center of the intersecting fifth unit, and stacked next to another three ends of three other units, sharing the center slot (keyhole) of the fifth unit (Figure 14, f). These tabs can include small snap fit tabs, but the primary fastening mechanism used in the case study is the shear pin. Included in Figure 13 are handles that aid in automated assembly as something that remains out of the way of the connection, which a machine can easily grasp (also in Figure 14, d). The central keyhole (Figure 14, f) allows four orthogonal units (two from either direction) to be simultaneously locked in. The regularity of the spatial arrangement of these four parallel tabs in the central keyhole will affect connection derived elastic properties, to a degree that depends on the aspect ratio of the parts

(thickness to strut member length). The simplest solution, used in the case study, is to use consistent and equalized placement of tabs according to global orientation.

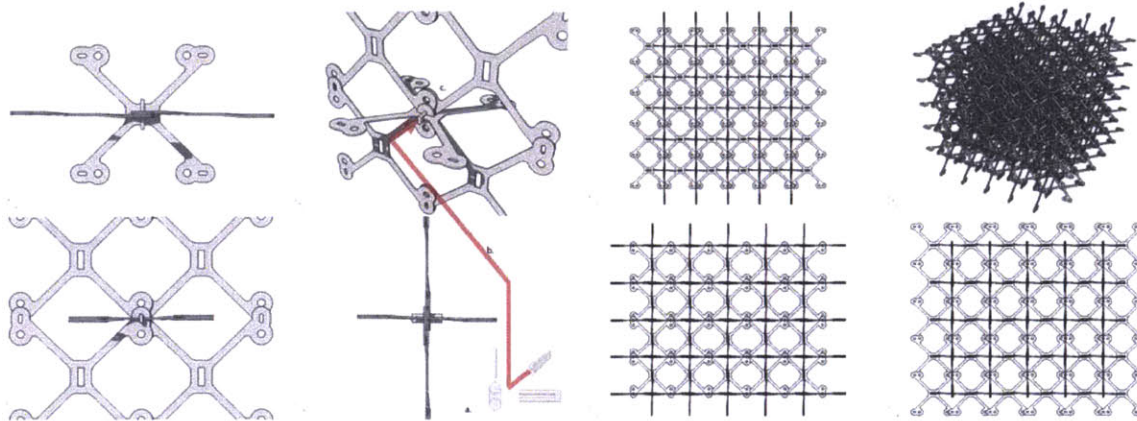


Figure 13 Case Study Design Assembly

The load transfer mechanisms simply utilize the ideal angle of the strut members in the crossbar. Loading is shown by the arrows marked 'a.' in Figure 14, with reaction deflection shown by the arrows marked 'b.' in the same Figure. The forces required to assemble these structures need to be provided by an external device that places the pins; the forces required to disassemble these structures are either simply set by the shear capacity of the pins, or need to be provided by an external device, such as a robotic digital assembler/dis-assembler. If connection based elastic properties are to be minimized in this design, then the crossbar strut members should be made slender relative to the connection details, which should provide large surface area for the pin connection. For experimental simplicity, the examples presented from here utilize this design option of having the connection stiffness exceed that of the strut members.

Since the load pattern through each part is well described, this presents a unique application for fiber reinforced composite materials. The figure below is diagram of fiber continuity and orientation for these parts. Note the loops of fibers around the holes, and the end-to-end continuity of other fibers that extend across the strut members and around the slots.

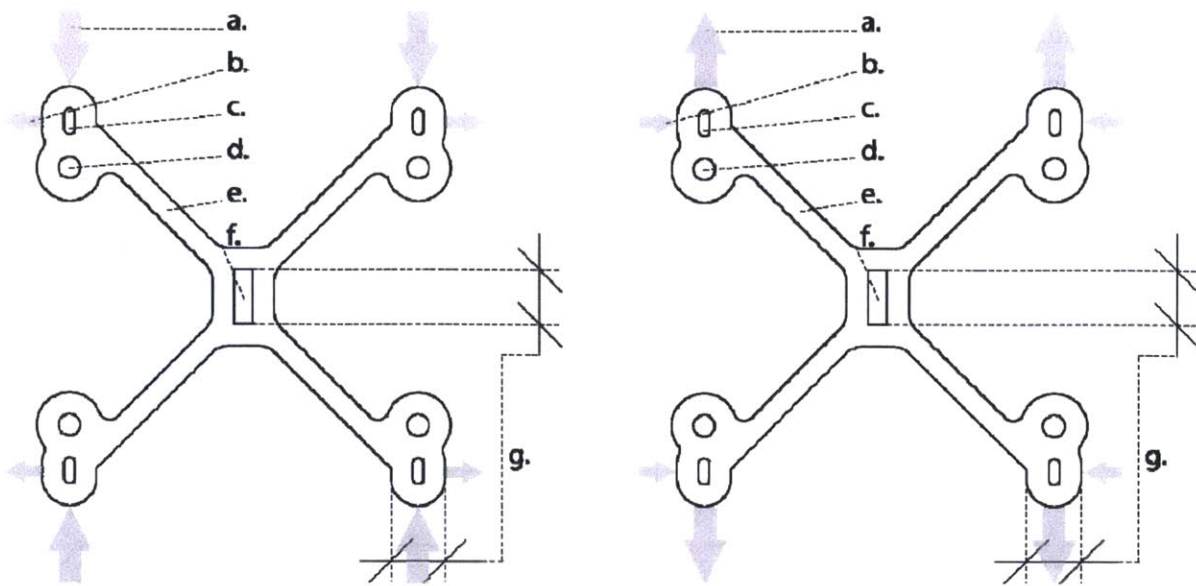


Figure 14 Case Study Design Load Response Diagram

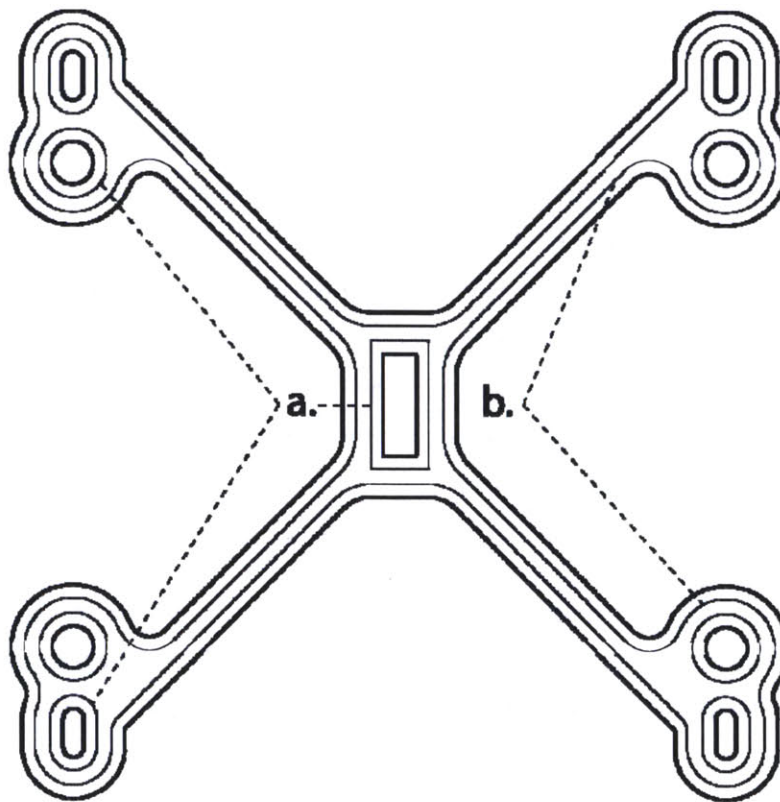


Figure 15 Case Study Design Fiber Orientation Layout

Production of the parts may be via pre-preg layup or multiplexed winding (explained in the next section) with conventional resin transfer molding, followed by slicing. Production of individual parts by conventional resin transfer molding is also a possibility, with the development of compatible fiber placement processes. Suitable prototype parts may also be made via two dimensional cutting of preformed laminates with appropriately oriented fibers, such as from quasi-isotropic laminate.

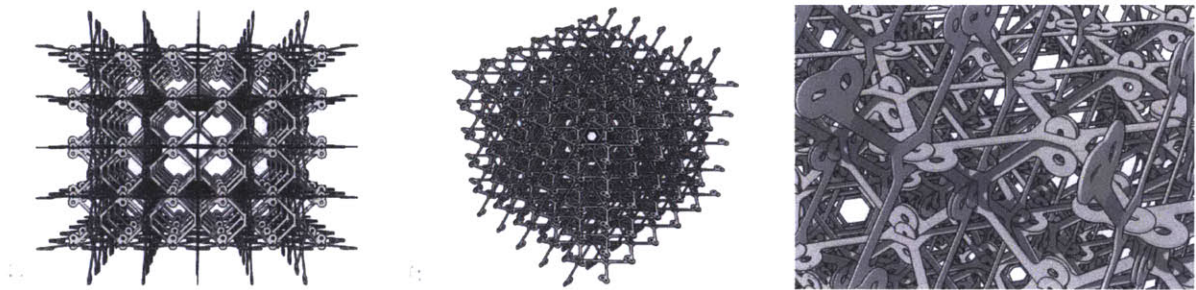


Figure 16 Case Study Design Assemblies

## Method

### Workflow

How can we get from a description of an object to the digital information needed to most efficiently fabricate the object? Much progress is being made in the areas of algorithmic descriptions and the ability to simulate functional constraints in the CAD environment. This is converging towards CAD descriptions that are functional object oriented systems.<sup>4</sup>

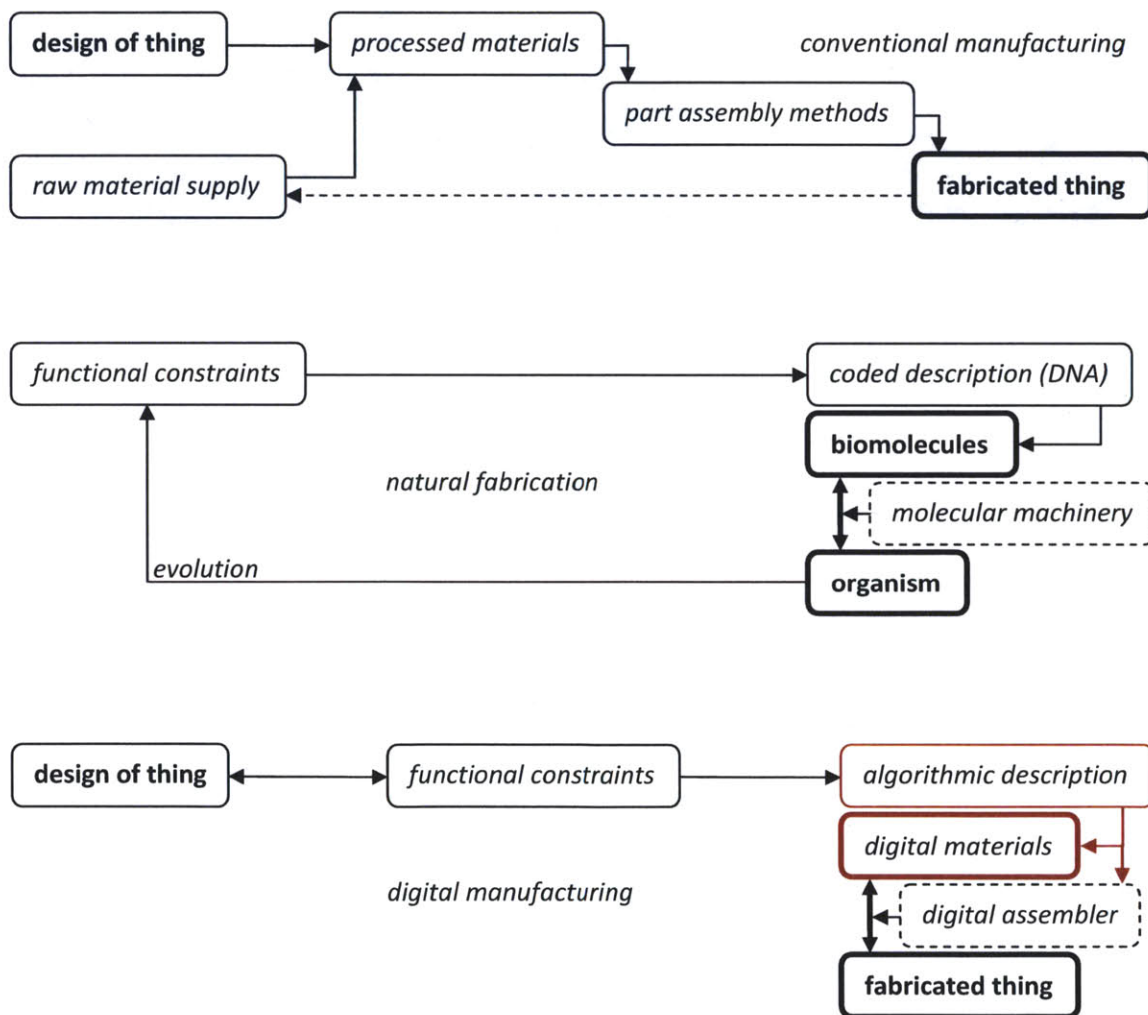


Figure 17 Design Workflow

<sup>4</sup> Such as with Peter Schmitt's "Object-Oriented Mechatronics." (2011 MAS PhD Thesis)

This may be mapped directly to digital material systems, whereby parts may be thought of as data types, physical assemblies may be thought of as classes, and robotic digital assemblers may be thought of as compilers.

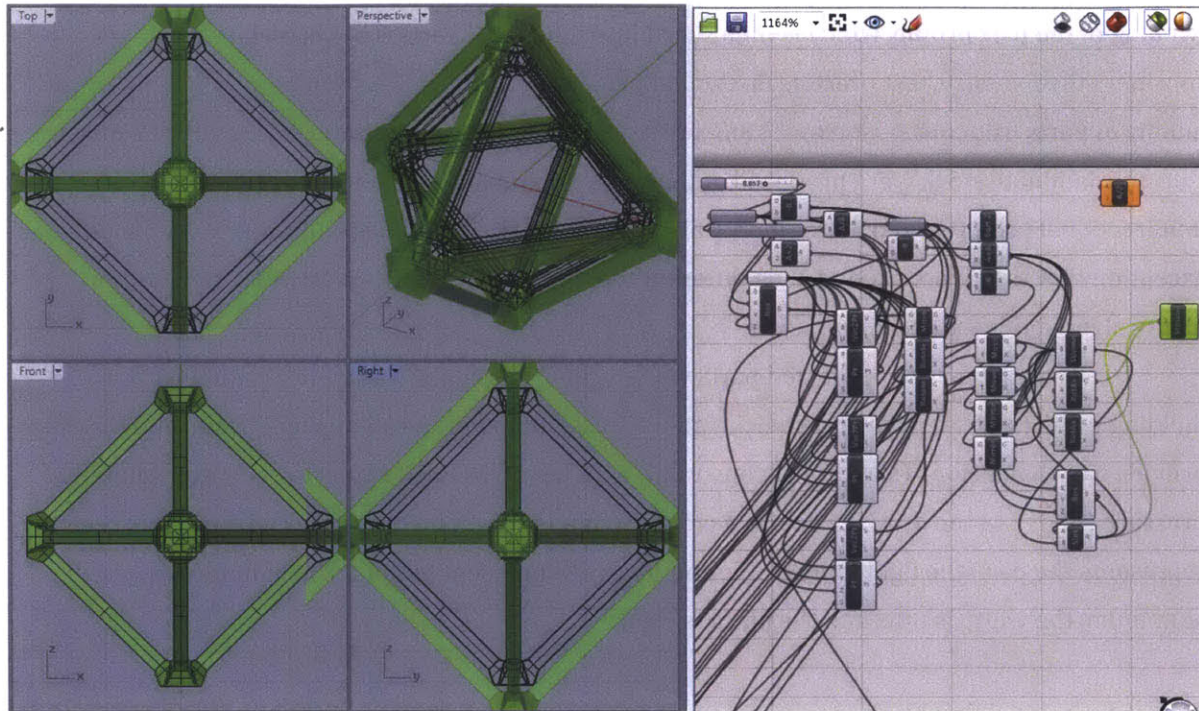


Figure 18 Parametric Design Tools Employed for Digital Composites Experiments; Rhinoceros API and Grasshopper

For this study, a rudimentary implementation of this was done, primarily driven by the convenience of free parameterization of the parts (both for analysis and fabrication). Basic C# scripts were written to interface with Rhinoceros and occasionally as Grasshopper tiles, for export as stl files which are easily processed with existing CAM interfaces. In addition our scripting methods were designed to output dxf files, only because of their standardization with existing CAM methods. The image above shows a parameterized cuboct truss cell unit with fixed connection design, and strut member aspect ratio as a user setting (slider in upper left hand corner of the graph), which results in corresponding variations to the cell pitch. Future work aims to solve the graph gui spaghetti-ball problem with real space correspondence between the graph and the

drawing product, while also addressing the CAM interface file divergence problem by interfacing directly with machine tools.

### Part Fabrication Method

Two strategies are used for part fabrication, for comparison. The primary strategy focuses on optimization of fiber placement within each part. This can be summarized as a multiplexed winding of the part profile, which is then sliced into individual parts. The secondary strategy considers the industry best practice method of producing this part. This can be summed up as cnc milling of parts from quasi-isotropic laminate stock. Both the multiplexed winding and the quasi-isotropic laminate stock were produced at the same time, using the same source batch of unidirectional pre-preg, and under identical environmental processing conditions, with the obvious exception that they were produced on different tooling (both primarily aluminum, and with identical mold release agent).

The tooling for the optimized parts was originally designed for use in a resin transfer molding press (spiritaero cdc prestwick, radius press), utilizing an existing tool frame and blanks to provide two dimensions (x and y) of constraint, with the press itself supplying vertical clamping pressure (6bar). In the drawing below, a cross section is shown on the right. The dark blue region represents the part; the light blue, white, and black all represent tooling. The light blue is aluminum, the white is ptfe, and the black is steel.

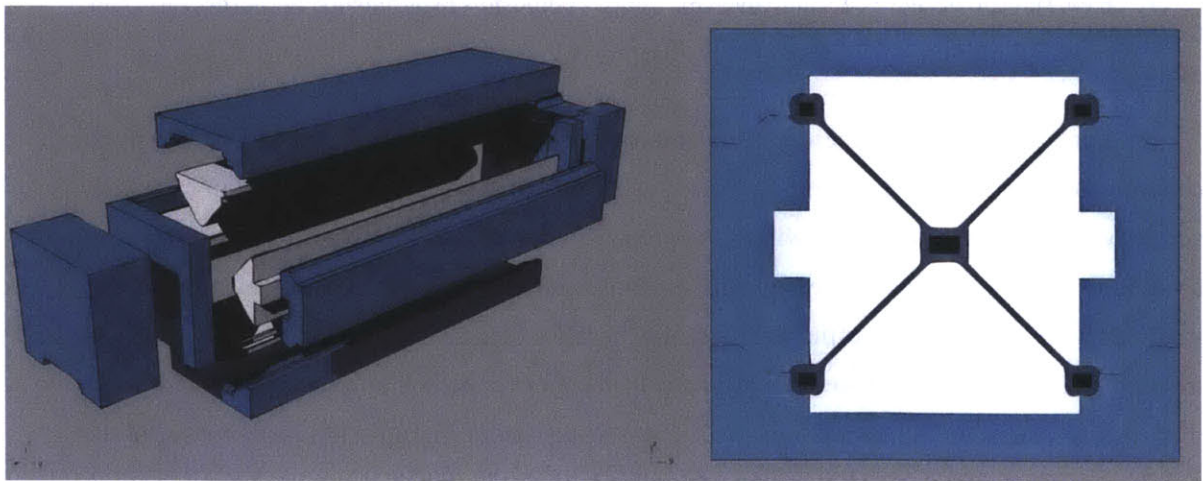


Figure 19 Optimized Part Multiplexed Winding Mold Design

The intended process is as follows:

- 1) Wind each black mandrel to provide an effectively continuous loop of fiber around each hole (which is displaced by the mandrels).
- 2) Wind around the perimeter of the entire part, including the five mandrels. This is ideally done in an automated fashion, as a collapsed winding (around the four extremal windings while held at the proper distance apart, then simultaneously moved together while pressing in with the four tooling parts).
- 3) Place in tooling, clamp in press, draw vacuum pressure, infuse, cycle to temperature, demold.
- 4) Slice into individual parts.

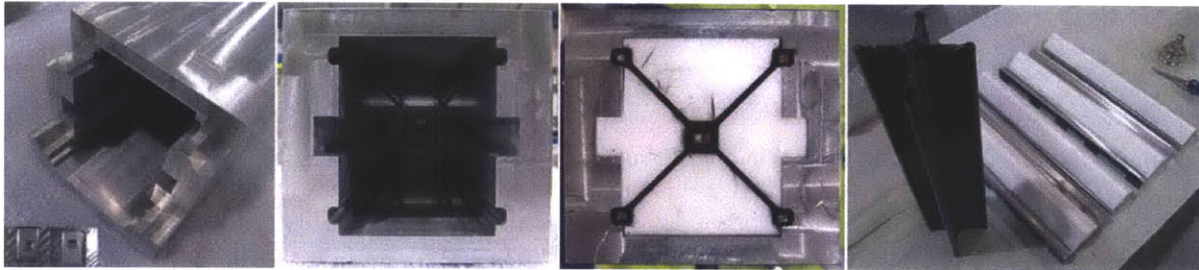


Figure 20 Optimized Part Multiplexed Winding Mold Assembly

In practice, step two was done in four pieces, with continuous strips running from the center of the part to the end of each strut member, around the end (with its sub-winding), and back to the center, with substantial overlap across the neighboring perimeter sections. The reason for the PTFE inserts is two-fold.

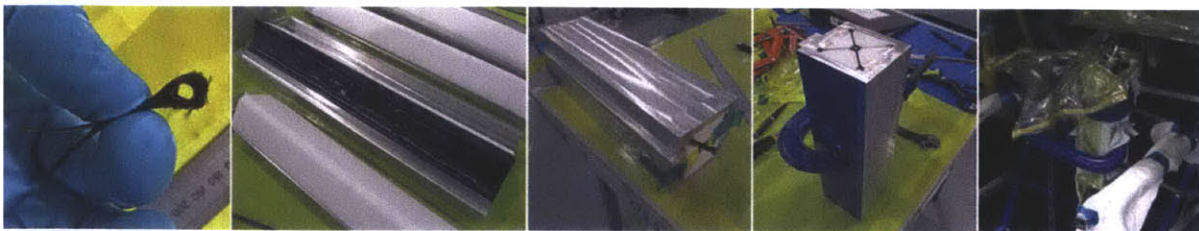


Figure 21 Optimized Part Multiplexed Winding Process

PTFE has a substantially greater coefficient of thermal expansion, when compared to either the aluminum tool or the carbon fibers. Since the system is temperature cycled from room temperature to 180C during the initial phase of the cure cycle, the expansion of the PTFE provides for even fiber consolidation, by exerting pressure on areas of the part for which the dimensional tolerances are less important than the structural quality. The only areas where dimensional tolerances are important are the interiors of the bearing holes, and the extremal half of the end of each strut member, around the bearing hole at the end. The other function for the PTFE inserts was for mold release.



Figure 22 Optimized Part Multiplexed Winding Slicing

Following de-molding, the winding was sliced into individual parts using a wafer saw (Isomet 1000 with 7" 20HC blade at 175 rpm, with water coolant). Qualitatively, it was immediately apparent that these parts were stiffer per weight than the comparison parts made from quasi-isotropic stock.

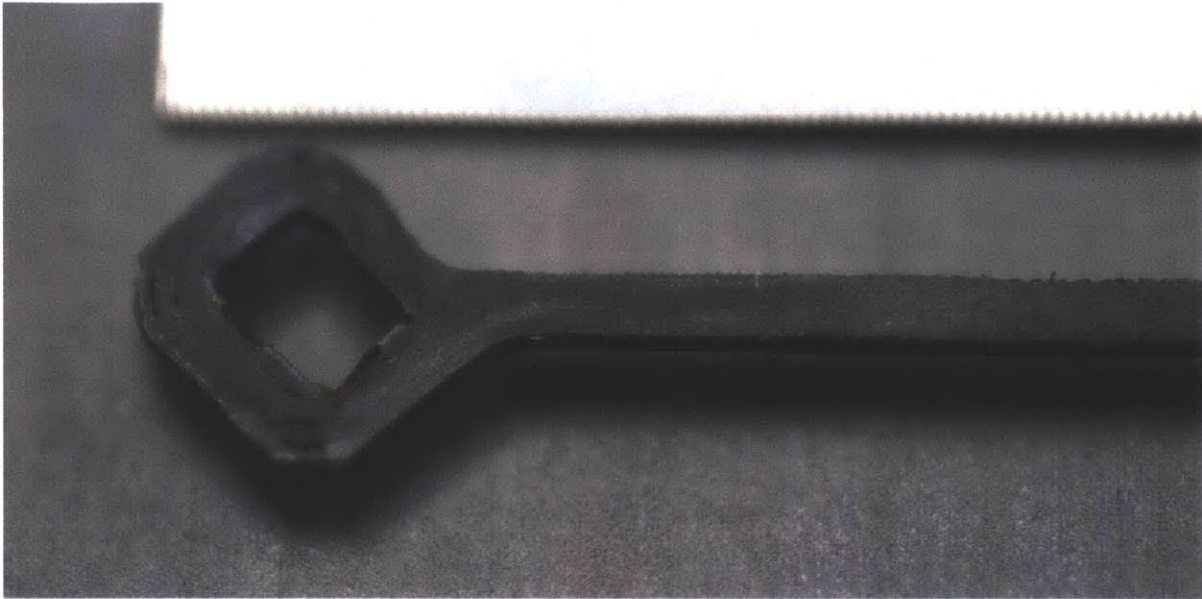


Figure 23 Close-up view of part produced by multiplexed winding. Gradations on scale are 100ths of an inch.

The industry standard method of designing a part with load bearing holes is to assemble a quasi isotropic laminate from which load bearing holes are drilled or milled. For these parts, I designed a thin (1mm) laminate using the 0.125mm per ply unidirectional pre-preg that I used for the multiplexed winding. The layup schedule of 0,45,90,-45,-45,90,45,0 was pre-cut with a cnc profiler, and laid up by hand onto 0.25" thick aluminum tool plates with frekote pre-applied. This was followed by traditional vacuum bagging, using fiberglass strips as air flow media at the edges, peel ply, a caul plate for top side surface finish, breather felt, and vacuum film sealed with silicone tape. Like the multiplexed winding tool, these were placed in an oven with continuous vacuum supply to the bag, for the duration of the cure cycle. Each laminate was then divided into eight 11"x11" sheets for processing on the Center for Bits and Atoms Hurco VM10U machining center.

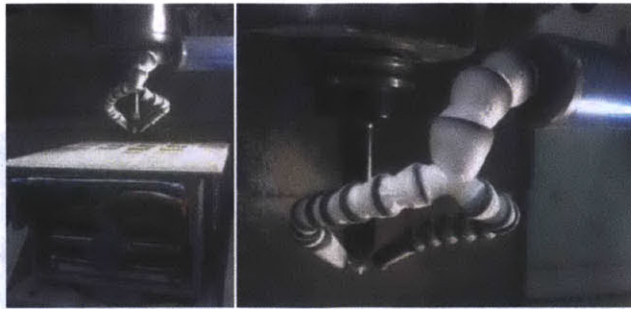


Figure 24 Comparison CNC Milling of Quasi-isotropic Laminate Process – Vortex Tube Cooling, Diamond Coated Tooling

Tooling was diamond coated 3/32" diameter four flute square end mills with 30 degree helix angle, run at standard feeds and speeds, but with air cooling provided by a vortex tube. Tool life was comparable to carbide tooling, but with much cleaner cuts throughout the life of the tool. It is thought that the reason for the matched tool life is that the diamond coating insulates the tool and does not allow it to cool as effectively, under the vortex tube stream. The vortex tube was chosen for its efficacy over liquid coolant in allowing the fixturing to remain stable.

The laminate sheets were fixtured with thin 3M double sided tape with clear VHB adhesive and polyethylene film carrier, to an aluminum sacrificial planar layer. The carrier is important for de-fixturing, as it allows remaining adhesive to be removed efficiently. Wax (over a heated platen) and other tapes were found to be inadequate, noting that the relevant specification seems to be peel strength. With the 30 degree helix angle that was available, particularly high peel strength was necessary to maintain fixturing. For each cycle, after thorough cleaning of surfaces with alcohol, the tape was first applied to the sacrificial plate with a hard plastic laminating roller, then the laminate was placed on top and the laminating roller was used to apply pressure across the top of the laminate. This process would leave some adhesive residue on the cut sides of the parts, which was easily removed by hand.

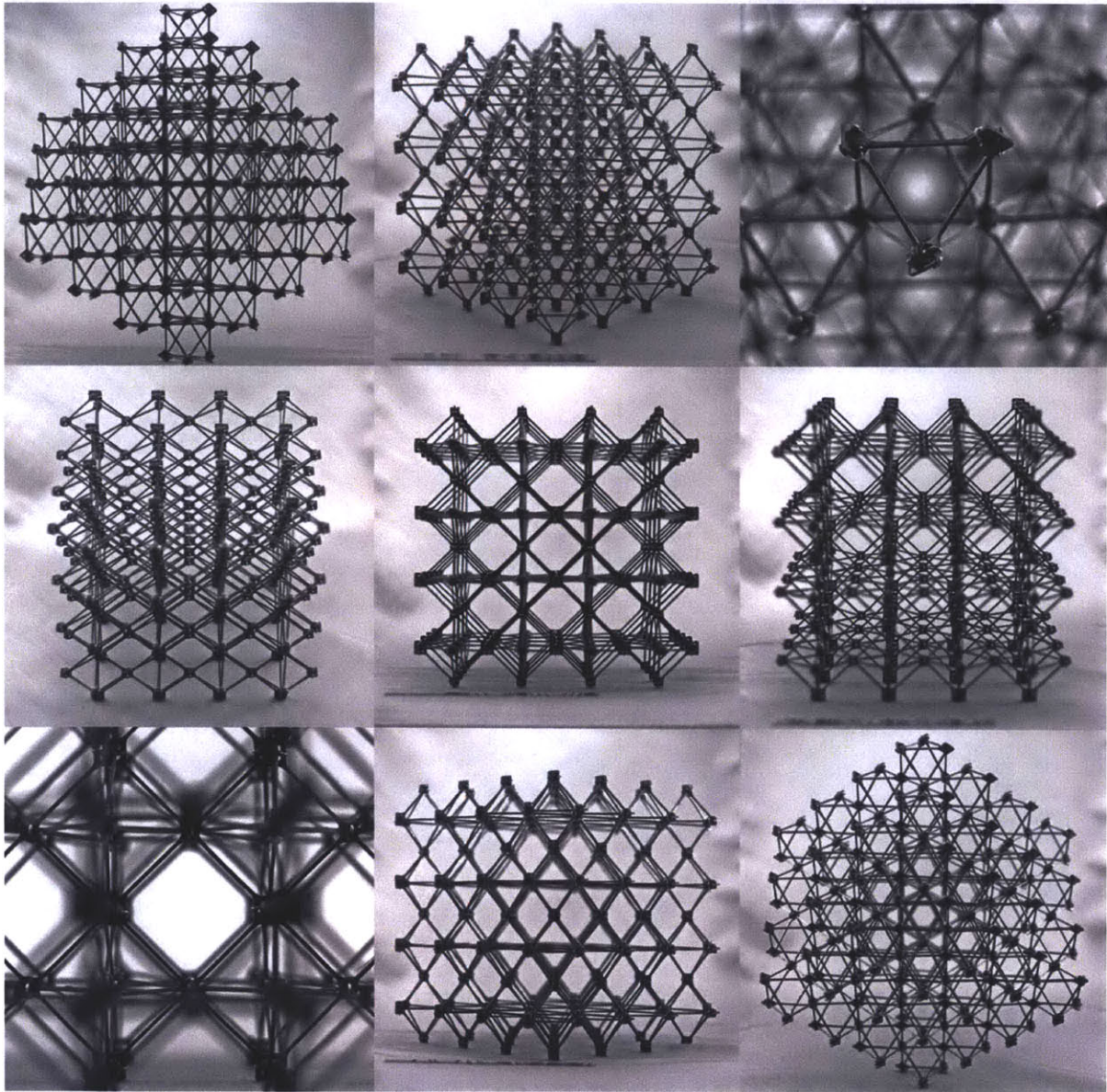


Figure 25 Photographs of Digital Composite test specimen



Figure 26 preliminary connection testing (instron 4411)

### Physical Testing Method

Physical testing of the bulk properties of digital materials is fairly straightforward, as they are treated as classical bulk materials. Of primary interest are elastic modulus, strength, and isotropy. Testing was performed with traditional apparatuses: an Instron 5985 (250kN) for final cfrp assemblies and constituent solid testing, and an Instron 4411 (5kN) for component and small sub-assembly testing.

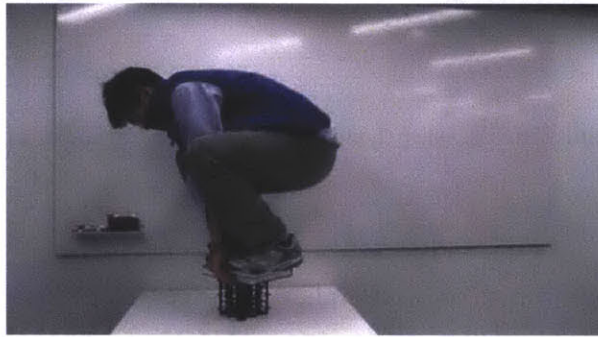


Figure 27 physical testing of an early Digital Composite sample

To prove both the assemble-ability of early digital material system designs, as well as key load transfer principles, initial ad-hoc testing of the tensile strength of digital composite chains were performed. This preliminary testing is described in more detail in the Appendices. The results of this test showed that building strong chains from snap-fit fiber composite parts was plausible. A brief detour focusing on a comparison to shear honeycomb materials convinced us that beginning by concentrating instead on a general isotropic system would be more fruitful. An explanation and discussion of this matter is provided in the Appendices. For the remainder of this section, I focus on the process of testing the cuboct truss design.

The testing methods employed followed a component-to-assembly strategy. This allows for proper estimation of fixturing and load requirements, as well as providing qualitative and quantitative information towards explaining the behavior of complete assemblies. I began by testing the axial and bending modulus and strength of the strut members of the actual components. Strut members were tested in tandem, held near their convergence point to aluminum tabs with

high shear strength epoxy (Loctite Hysol 60HP, cured at 50C for 24 hours), which was then held in the grips of the load testing machine (Instron 4411).



Figure 28 Initial Part Constraint Testing; Setup, Load Testing with Sliding Constraint, Load Testing with Fixed Constraint

The lower constraint was either a glass plate with steel guides (to allow sliding motion, but constrain it to the part plane), or a plate with machined holes into which the ends of the strut members were also adhered (to provide full constraint). I considered the data from the latter experiments as providing an estimation of the upper bound on per-strut-member stiffness and strength, based on balanced axial loading of the parts. The former experiments provided us with a lower bound that is based on transverse beam bending behavior.

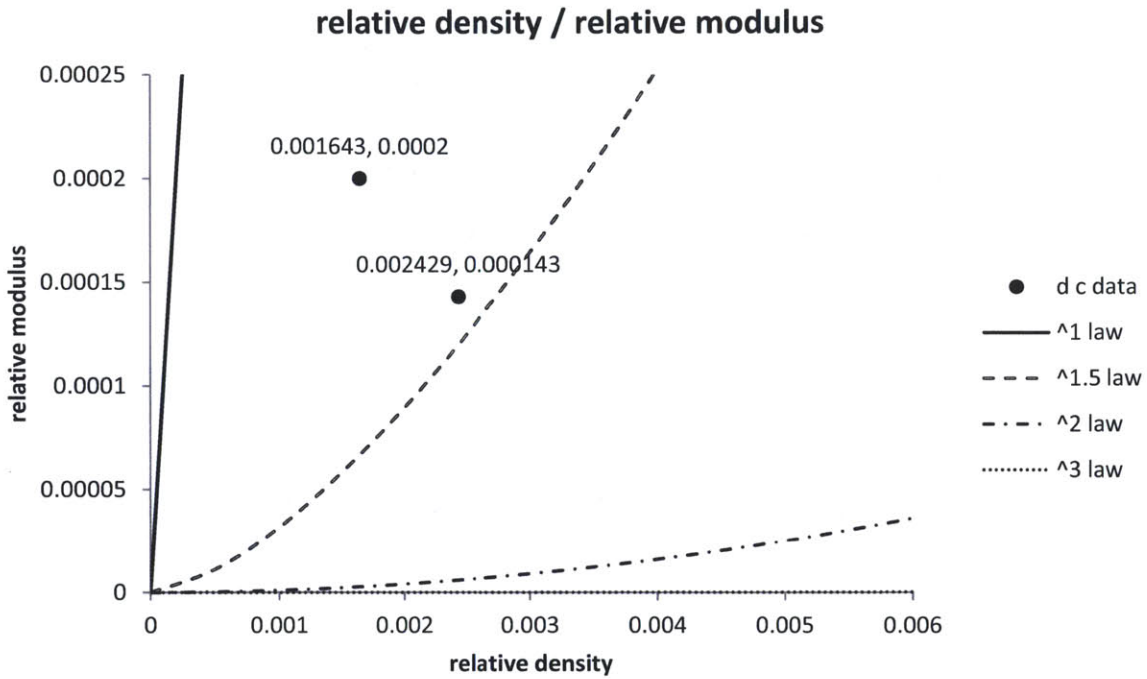


Figure 29 Initial Results Constraint Testing, providing Upper Bound

Continuing this element-wise methodology, the connections were tested with very short attached strut members, in order to confirm connection design. This was performed across various axes, as well, to establish the isotropy of the connection.

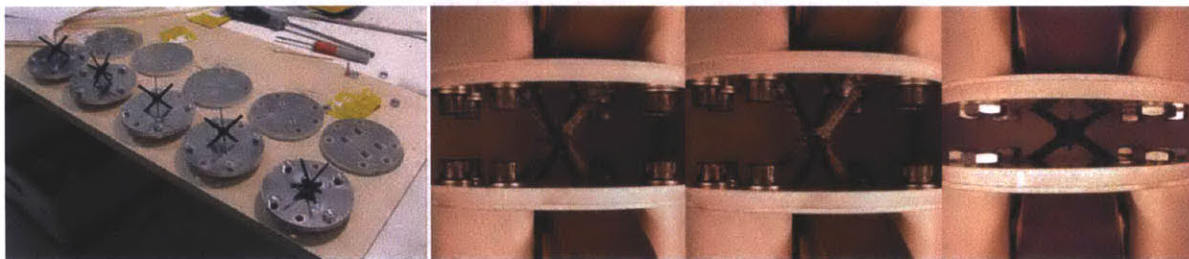


Figure 30 Connection Testing

To test isotropy of the lattice geometry as a whole, I used 3d printing (a dimension elite fdm with abs plastic material, and an inversion si with uv curing acrylic) to generate samples that were computer sliced at arbitrary spatial angles, for load testing. To measure the uniformity of the assembled samples, I used radiography to visually check for alignment of the denser nodes (full ct scans were not particularly informative, since little more than one cell size worth of the structure fit into the operational scanning volume of the machine at any one time).

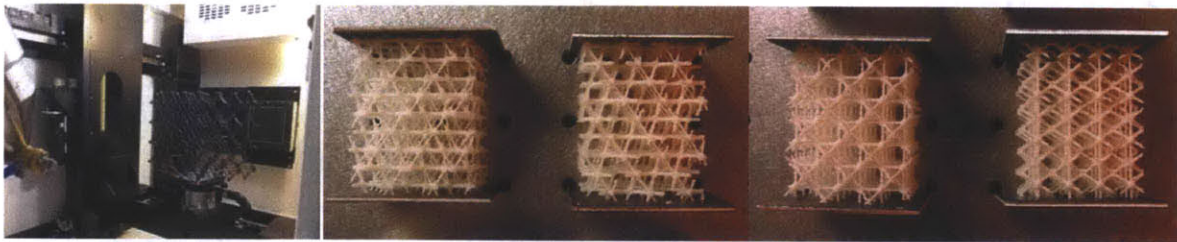


Figure 31 Dimensional Tolerance Evaluation, Isotropy Measurement Samples

The final test samples were fixtured with a single bonded plate for each perimeter node, which was subsequently bolted to a larger coupling plate which was in turn bolted to a large platen fixture that was fixed to the load testing machine (Instron 5985).

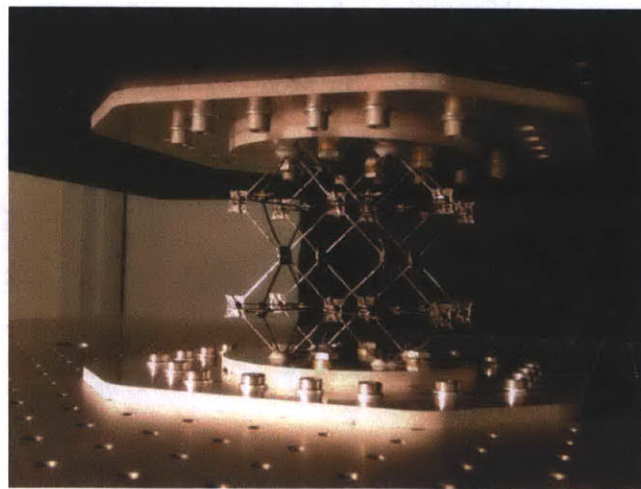


Figure 32 2x2x2, optimized parts

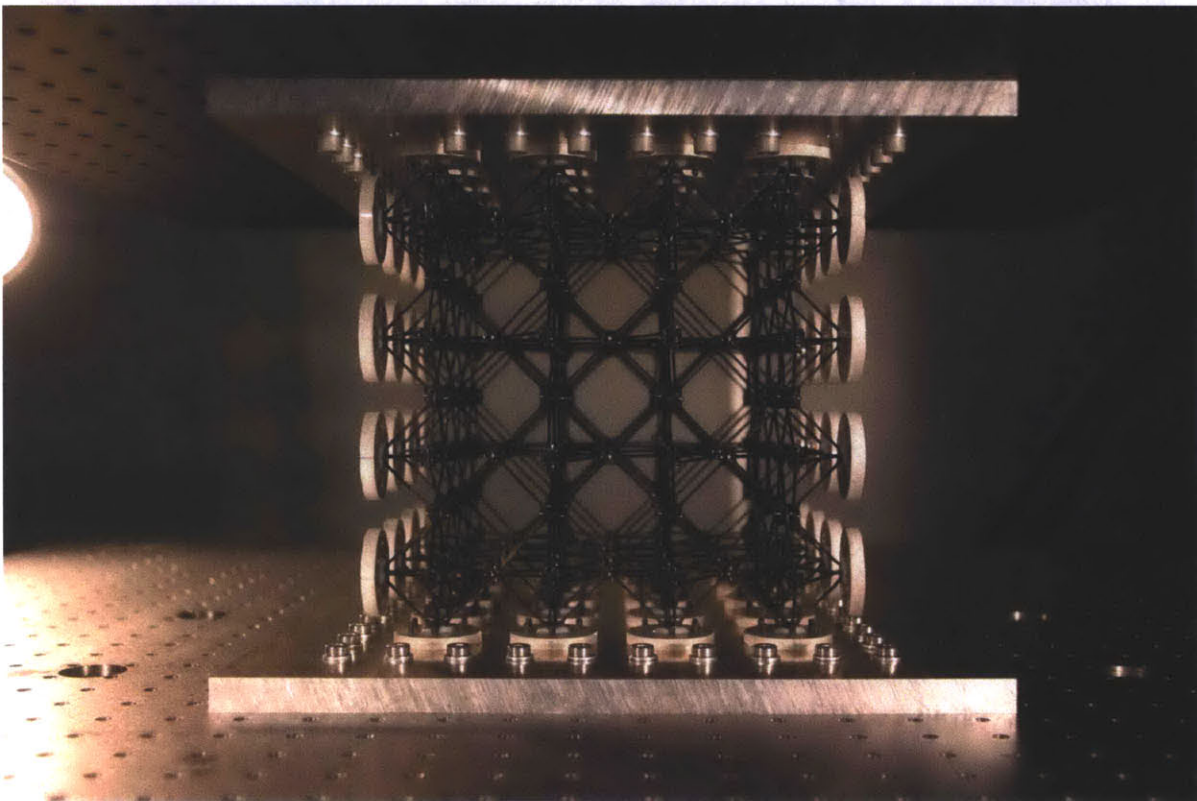
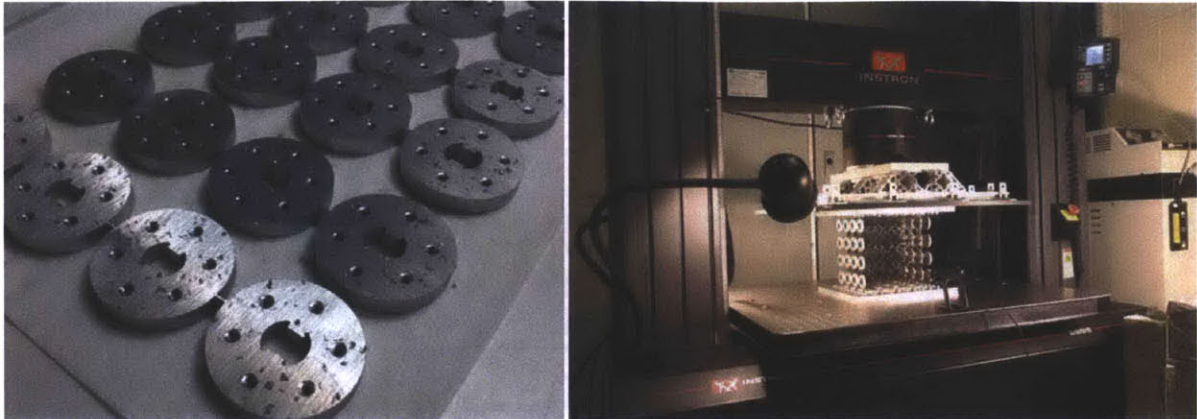


Figure 33 Fixturing and Final Testing

A large solid aluminum block was also machined and tapped so that it could be fitted as a sample, so that the compliance of the fixturing setup could be measured. The compliance of the machine and fixture was repeatably measured to equate to a virtual modulus of  $\sim 325$  MPa at the cross section of the sample, with linear behavior across tension and compression. As this is over an

order of magnitude greater than the observed experimental sample compliance, we may not expect that machine and setup compliance significantly affected the experimental results. Backing out the fixture compliance, with a linear adjustment based on force, from the results confirms this, as seen in the graphs below.

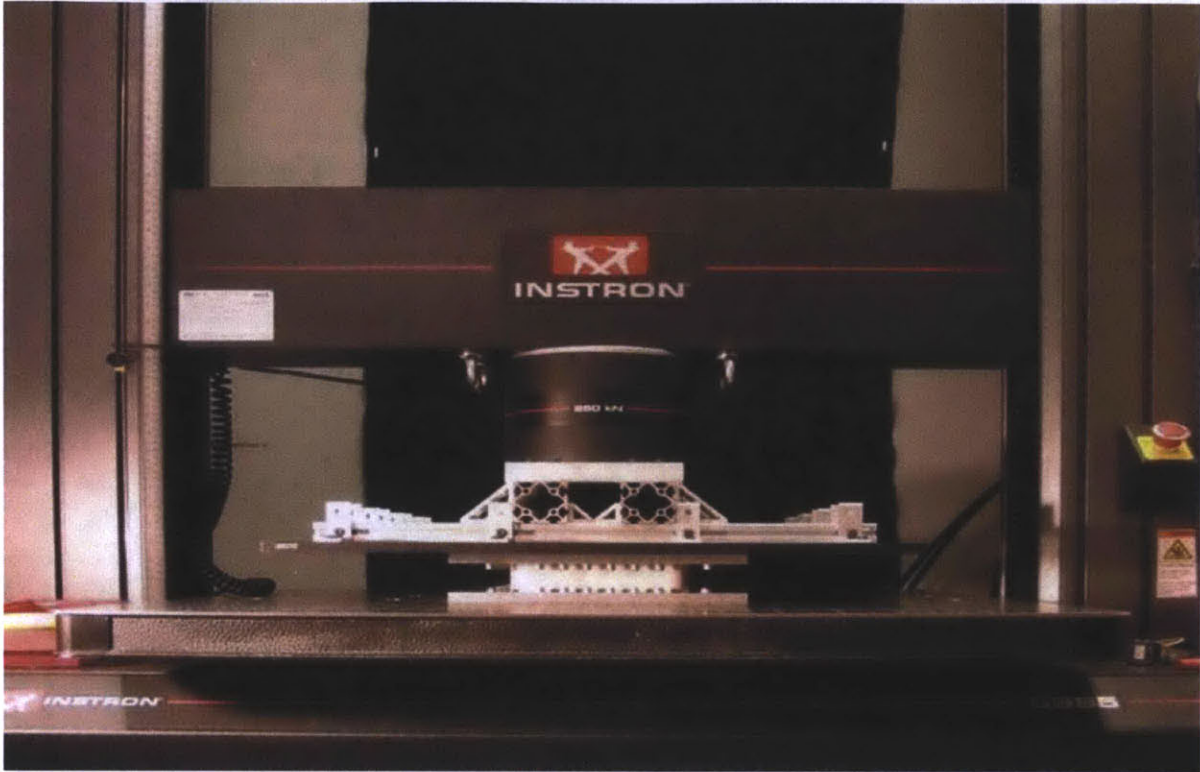


Figure 34 Fixture Compliance Testing with solid aluminum block

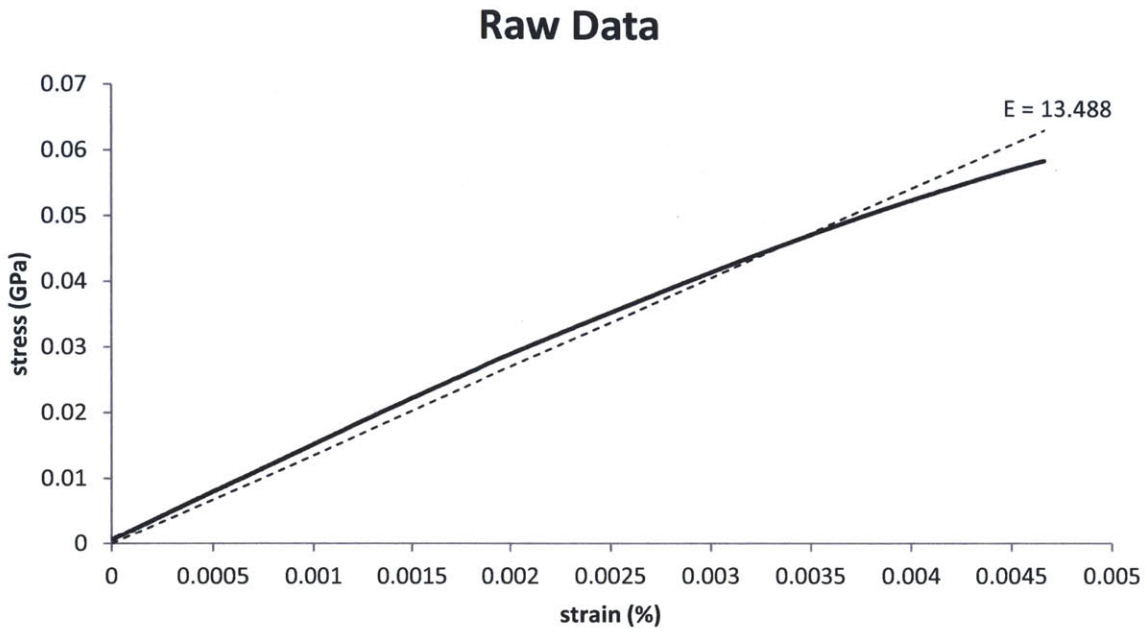


Figure 35 Raw Data, without compliance correction

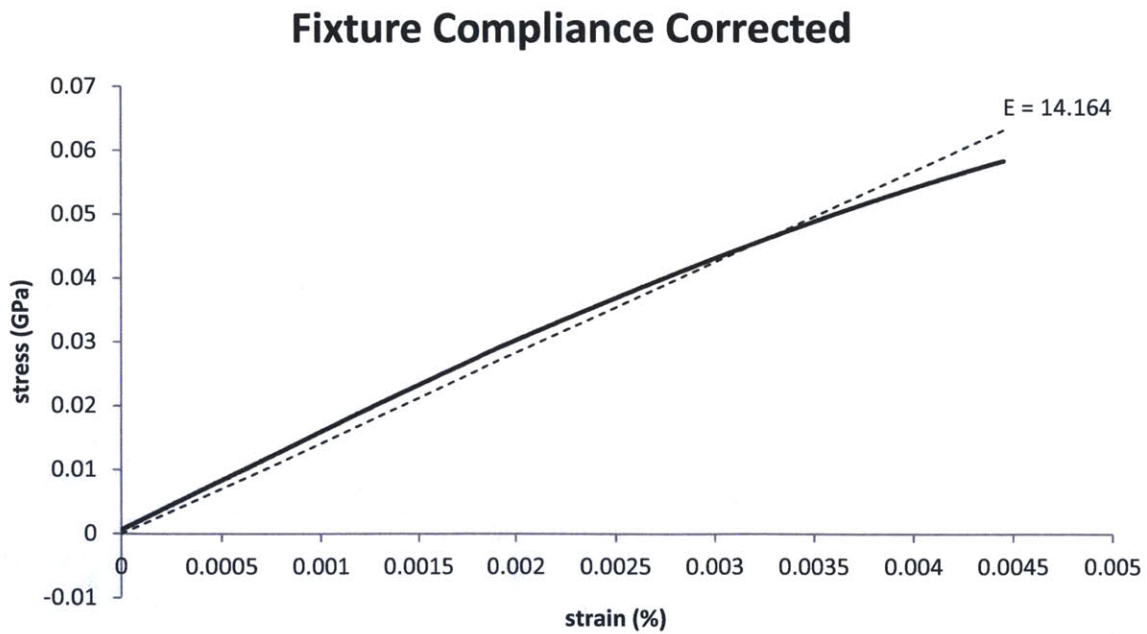
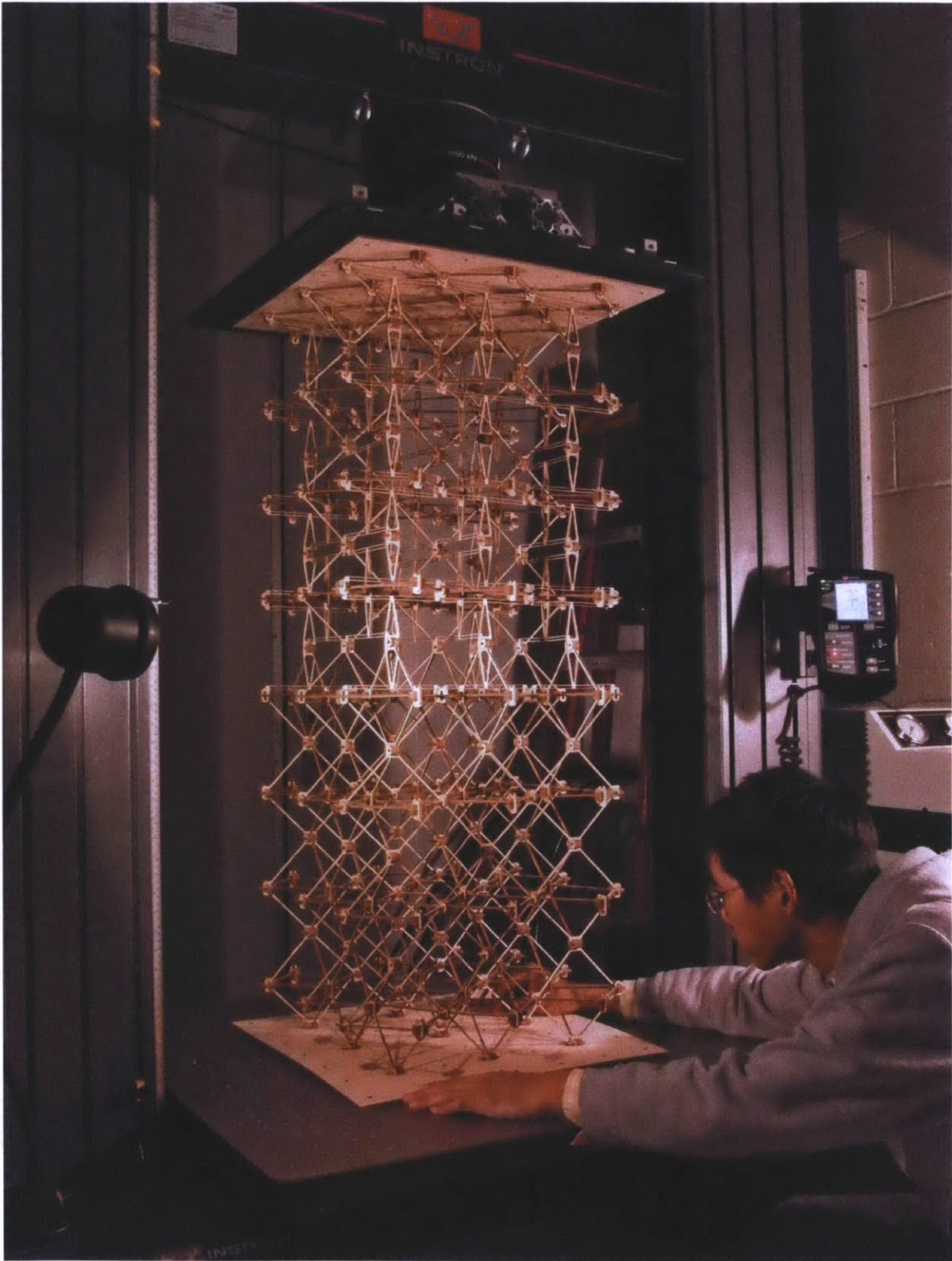


Figure 36 Compliance Corrected Data



## Results

### Density

Both methods of fabrication yielded parts that were assembled into ultra-light digital composite materials. The parts produced with multiplexed winding yielded a material with a density of 0.0048 grams per cubic centimeter – on par with aerogels. The parts produced by milling quasi-isotropic stock yielded a material with a density of 0.0096 grams per cubic centimeter, in the same regime.



Figure 37 Optimized Parts and Conventional Parts,

### Mechanical Performance

Mechanical performance of the parts met expectations – improving upon the conventional quadratic rule of thumb scaling law for lightweight cellular materials, and far improving upon the cubic rule of thumb scaling law for ultra-light materials. One of the most interesting results, however, can be seen in the graph below, which shows cyclic compressive and tensile loading of specimens, which display a linear elastic regime followed by a non-linear elastic regime with

gradual reduction in stiffness. This effect is nearly symmetric in both tension and compression. I explain this effect as a transition to coordinated elastic buckling of the strut members.

## 2x2x2 digital composite (oriented) load cycling

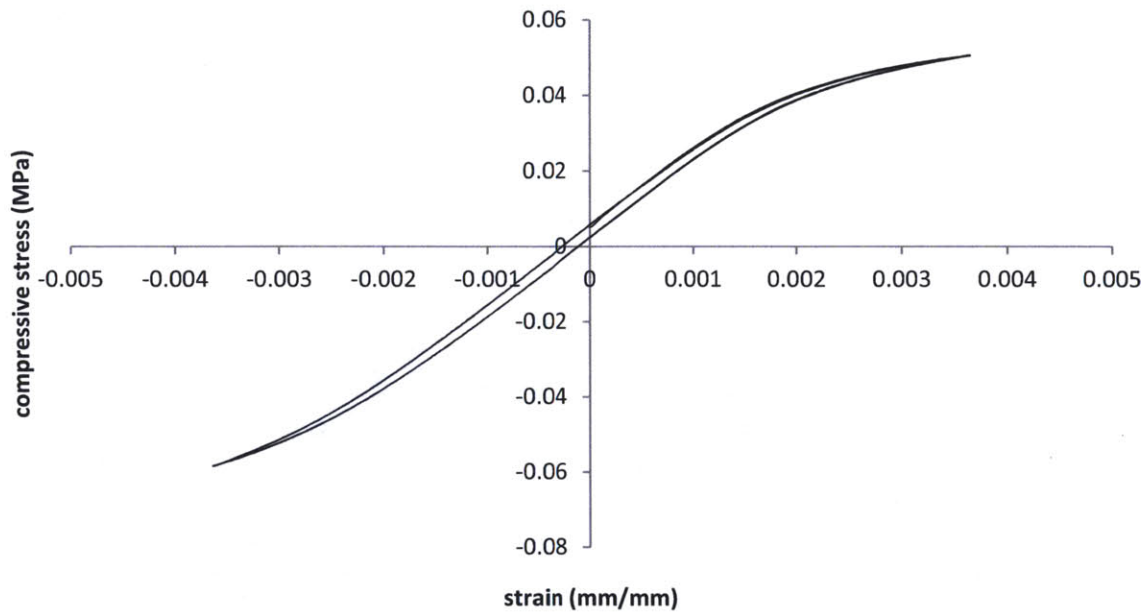


Figure 38 Tension and Compression Cycling showing transition from linear to non-linear elasticity with low hysteresis

Such an elastic instability, or pleating across a structure, had been described in two dimensional sheets before (Bertoldi et al 2010), but to our knowledge this is the first example to be described in three dimensions. The following photos of load response of single cells may provide an indication of what is occurring, here. The left photo shows the strut members in the basal plane buckling in a coordinated fashion, resulting in rotation of the lateral end nodes. The right photo shows twisting of the entire structure about the loading axis, which can be seen as twisting of the top and bottom end nodes.

## digital composite elastic collapse

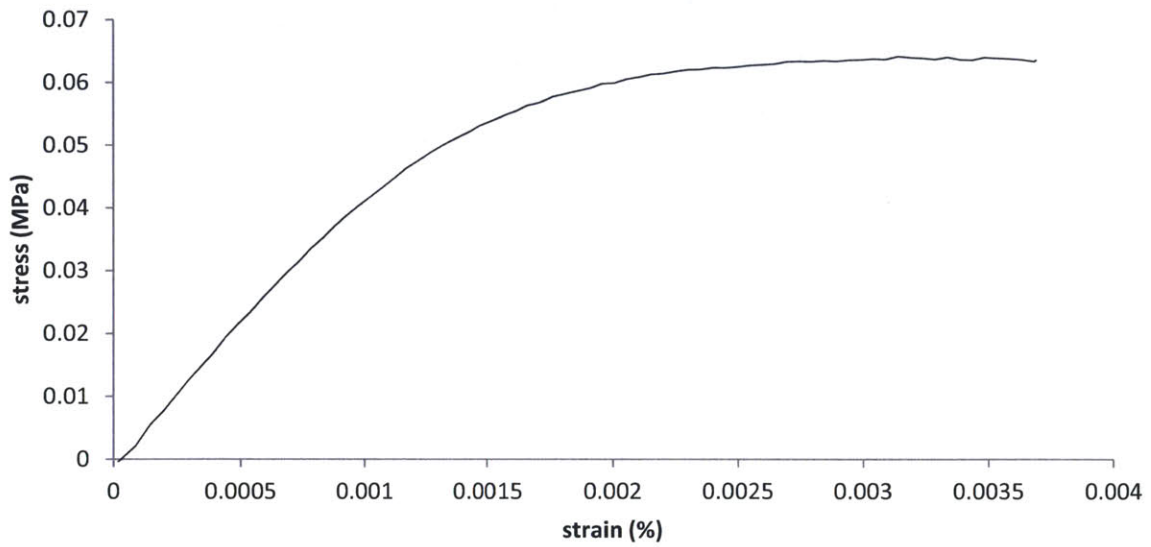


Figure 39 stress strain chart for the samples shown in the photographs below.

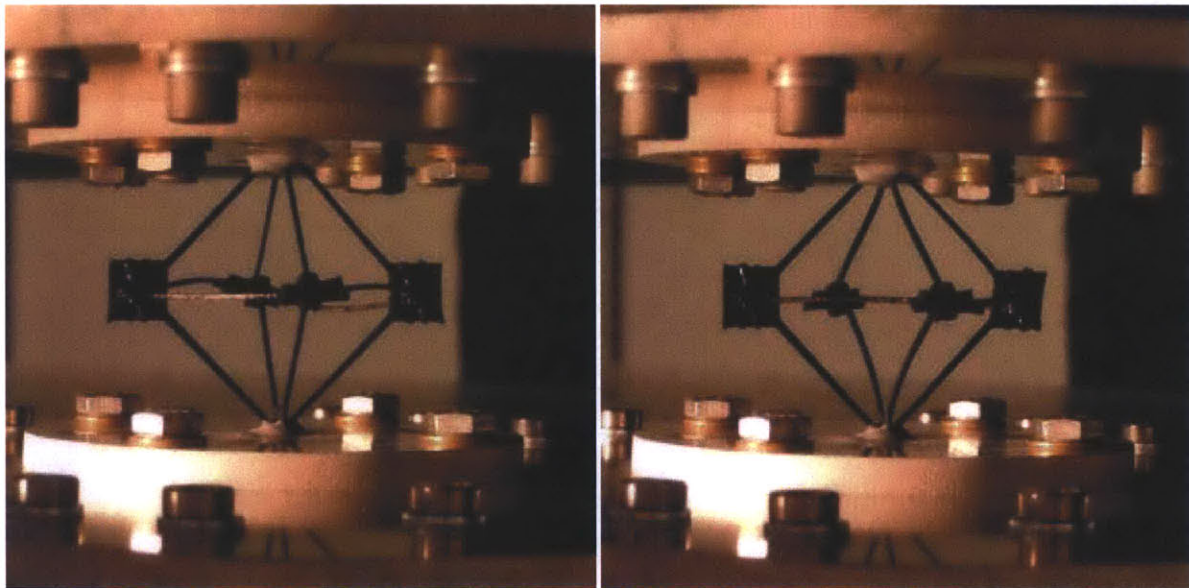


Figure 40 single unit (unconstrained on edges) response to tension (left) and compression (right) showing coordinated buckling.

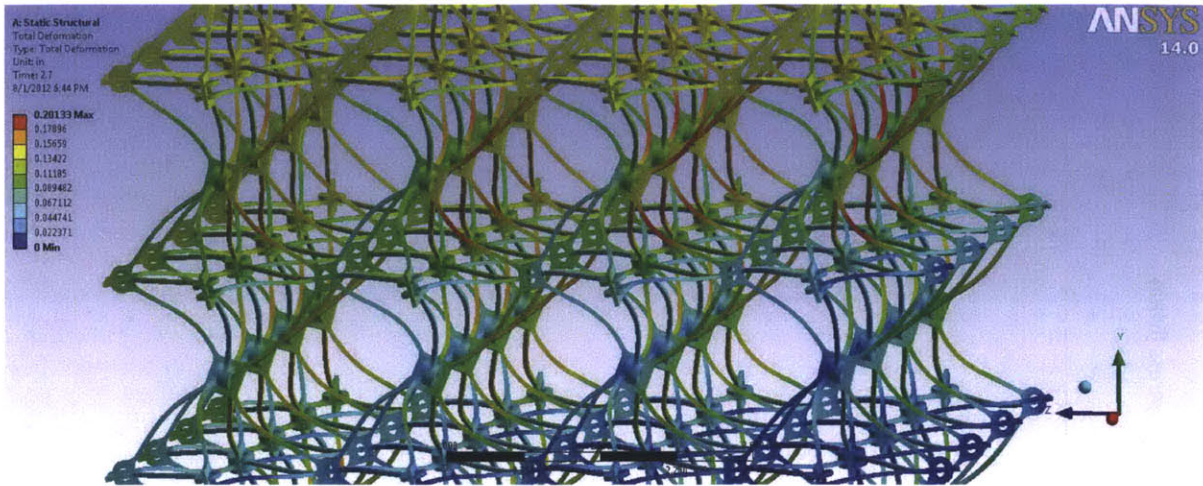


Figure 41 ANSYS simulation with deflection multiplier showing coordinated buckling mode

Finite element simulations of assemblies corroborate this idea, as shown in the above simulation. Note the coordinated rotations of the nodes about the global principal axes. These simulations also examined edge effect. As can be seen in the chart below, edge effect generally conforms to prior studies (Andrews et al 2001), with minimal influence on overall results beyond characteristic dimensions exceeding several units.

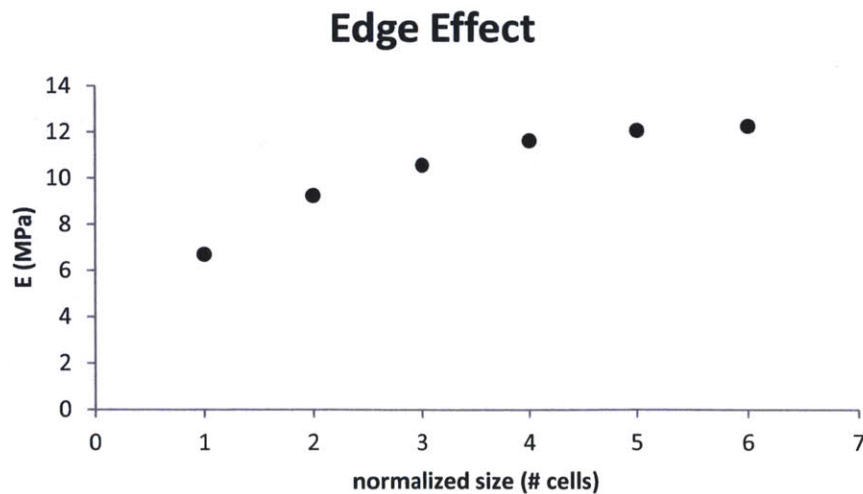


Figure 42 Modulus plotted against normalized size (# cells), ANSYS simulation

The graph of the relative material properties of our samples, below, shows improved scaling for relative material properties, relative to other materials in this weight regime. Included in this graph are printed acrylic samples, which were taken from a computer model at arbitrary angles, and which show the isotropic behavior of the geometry.

As expected, the properties fall shy of the ideal proportional scaling limit, and predictions from full constraint preliminary strut member tests, The strength and modulus are, however, well above the lower bound predictions from pure bending strut member tests. This indicates successful implementation of additional constraint not typically seen in cellular solids.

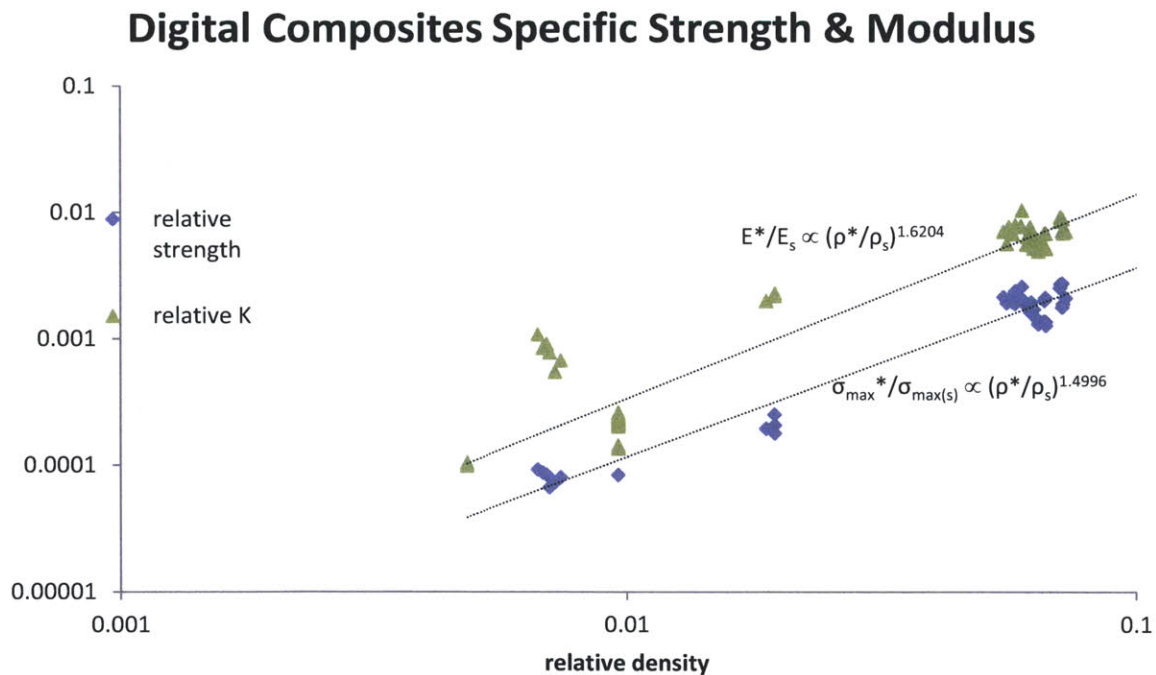


Figure 43 Relative strength and modulus of digital composites

Since this case study was designed without connection release mechanisms, these digital composites behave in tension and compression as an elastic-superelastic-brittle cellular solid, with a pronounced non-linear elastic regime at higher strains. This is in comparison to a classical elastic brittle cellular solid, which displays linear elasticity followed by a brittle crushing plateau and

densification (Gibson & Ashby 1988). Densification of our structures is irrelevant, given their sparseness. While there is a small periodic densification effect during the brittle crushing phase, a true analogy to densification does not occur until extremely high strains (>95%) are reached. Instead of having a linear elastic regime determined by cell edge bending and a collapse plateau associated with cell edge buckling failure, this material displays linear elasticity in compression that has a significant stretching component (in addition to cell edge bending), and an elastic plateau that is associated with elastic strut member buckling. This is similar to observations for periodic metallic cellular truss structures (Wadley et al 2003), but with the non-linear plastic regime of the metallic structures being supplanted by this elastic buckling.

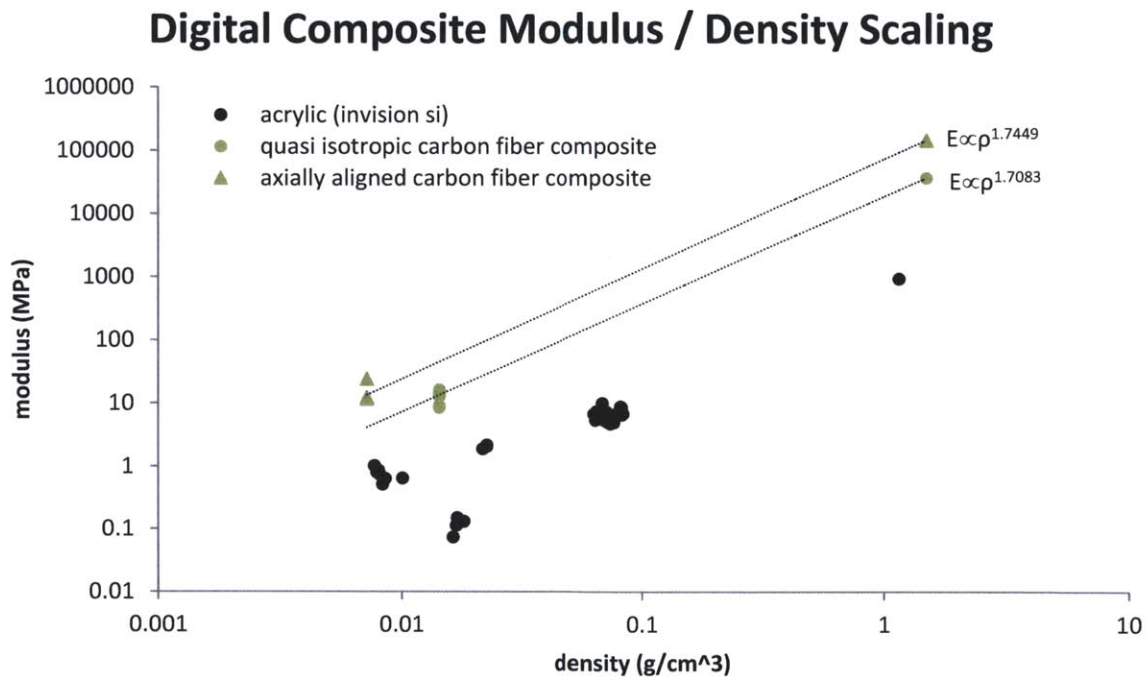


Figure 44 digital composite modulus scaling with density

In tension, linear elasticity again has a significant axial contribution. On the whole, this design behaves in tension in ways that are symmetrical to the way it behaves in compression, as an elastic-superelastic-brittle cellular solid. The tensile superelastic phase is marked by elastic buckling of interstitial strut members, which are placed in compression under tensile loading of

most orientations of the lattice. The initial modulus and strengths are within measurement error across orientations, irrespective of these orientations.

For these digital composite part types, the geometry initially results in simultaneous axial and transverse loading of elements that may be modeled as beams that are fixed on one end and guided on the other end, and therefore I consider the joints to be capable of transmitting a significant bending moment.

This is where I depart from the bulk of the cellular solids literature, which successfully models a wide range of observed cellular solids as pin jointed systems. It has been observed that biological fiber based mesh structures do not seem to obey even modern forms of the Maxwell rigidity criterion. This is recently explained by a mechanical model that assumes that the fibers behave in a manner that transmits significant bending moments across nodes in the structure (Broedersz et al 2011). While the total explanation for this apparent violation of convention is still debated, considerable support is given by the relative magnitude of inter-molecular forces that are present in these biomaterials (Jacobs et al 2001). The result is an addition to the typical two dominant phases of frameworks or trusses in mechanics – a stretch bend coupled phase, that is situated between the stretch dominated and bend dominated structures. If this is indeed the true explanation for the strength and stiffness of biomaterials, which exceed the expectation given by their topology, then we should be able to produce this stretch bend coupled phase in macro-materials. Remember that intrinsic to our design is the fact that for the eight strut members that meet at each node, four of them are actually part of a monolithic unit. With that, I proceed with a mechanical model that considers this adjustment to the typical cellular solids analysis, noting that the axial and transverse loads on the strut member both contribute to the maximum bending moment [Timoshenko & Gere 1961].

$$\delta = \delta_{\text{axial}} + \delta_{\text{bending}} \propto Fl/E_s t^2 + Fl^2/E_s I \propto Fl^2/E_s I \text{ (for low } \rho/\rho_s\text{)} \quad \text{Equation 31}$$

Where

$\delta$  = change in length

$E$  = modulus of elasticity of structure

$E_s$  = modulus of elasticity of constituent solid

$$\sigma = F/A_c$$

$$\varepsilon = \delta/L_c$$

for a cuboct structure,  $A_c = 8l^2$ , and  $L_c = l\sqrt{2}/2$  for single beam ( $A_c = 32l^2$ , and  $L_c = 4l\sqrt{2}$  for entire cell)

Equations 32

from which  $E = \sigma/\varepsilon$  gives an expected relative modulus of:

$$E/E_s = (FL_c/A_c\delta)/E_s$$

for a cuboct structure,  $E/E_s = (1/(8\sqrt{2}))((F/l\delta)/E_s)$

Equations 33

thus, we may assume  $E/E_s = C_g((F/l\delta)/E_s)$  and

$$E/E_s = C_g((F/l\delta)/E_s) \propto C_g \frac{F}{l(Fl/E_s t^2 + Fl^2/E_s l)E_s} \propto C_g \left( \frac{t^2}{l^2} + \frac{l}{l^3} \right) \quad \text{Equation 34}$$

assuming, from above, that  $\rho/\rho_s \propto t^2/l^2$  and  $l \propto t^4$ ,

$$E/E_s \propto t^2/l^2 + t^4/l^3 \propto (\rho/\rho_s) + (t^2/l)(\rho/\rho_s) \propto (\rho/\rho_s) + (\rho/\rho_s)^n \propto (\rho/\rho_s)^n \quad \text{Equation 35}$$

where, given the assumptions of low relative density and high strut member aspect ratios,

$$(\rho/\rho_s)^1 < (\rho/\rho_s)^n < (\rho/\rho_s)^{3/2} \quad \text{Equation 36}$$

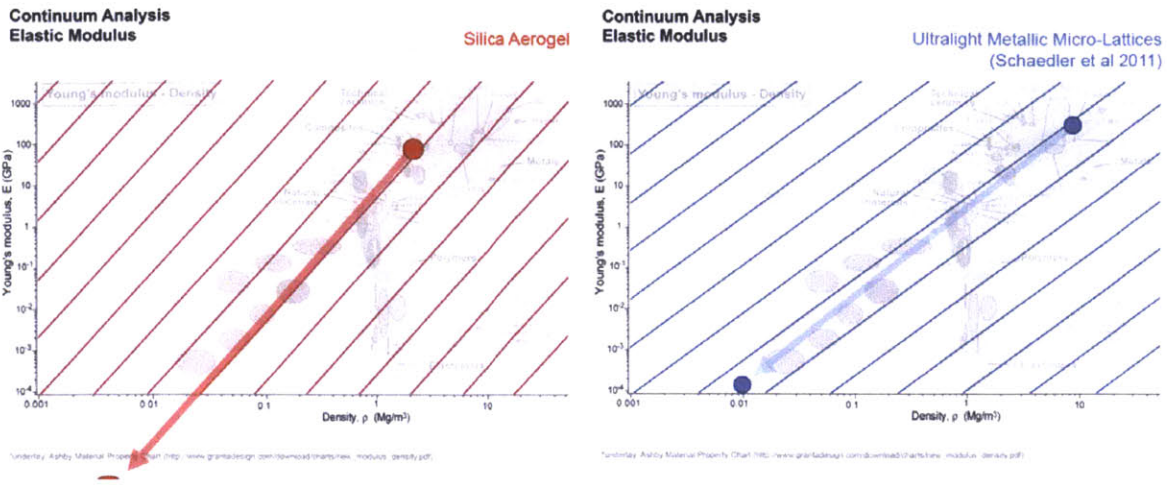


Figure 45 previously known ultra-light materials

How does this fit in with other materials? Considering the ultra-light materials that are adjacent in density, we see considerable improvement. For some time considered the lightest material, aerogels have a relatively poor stochastic structure that results in inverse cubic scaling of modulus with decreasing relative density. Simply achieving three orders of magnitude of reduction in density was an achievement at the time. More recently, materials have been reported (metallic microlattices, aerographite) that display inverse quadratic scaling of modulus with decreasing relative density. While this is standard for stochastic foams of all kinds (metal foams, polymer foams, etc.), the achievement, again, is related to the ability to achieve three orders of magnitude reduction in density.

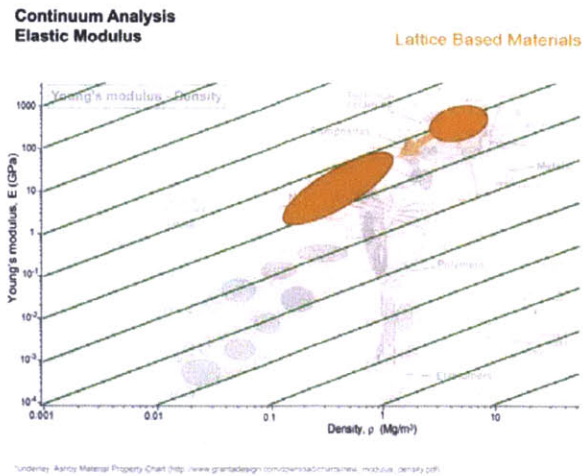


Figure 46 previously known cellular materials with better than quadratic density modulus scaling properties

Near linear scaling of modulus with density has been reported in non stochastic cellular solids for many years, but only with structures that span about one order of magnitude reduction in density, or less. These materials range from those that are effectively modeled as a solid with some holes in it (Gibson & Ashby 1988) to ordered periodic truss materials with strut member thickness to diameter ratios around or greater than 0.1 (Wallach & Gibson 2001). Our digital composites, in contrast, show a three order of magnitude reduction in density, while maintaining better-than-inverse-quadratic scaling of modulus with relative density, and therefore access a new area of the materials property chart. One explanation for the prior lack of success, in producing similarly strong and light structures from other materials that are near to the material properties of solid composites, is the prevalence of “morphological quality” issues that are intrinsic to other production methods, such as casting (Evans et al 1998, Wadley 2002), which results in an inability to produce ordered structures of very slender columns.

## Ultra-Light Materials

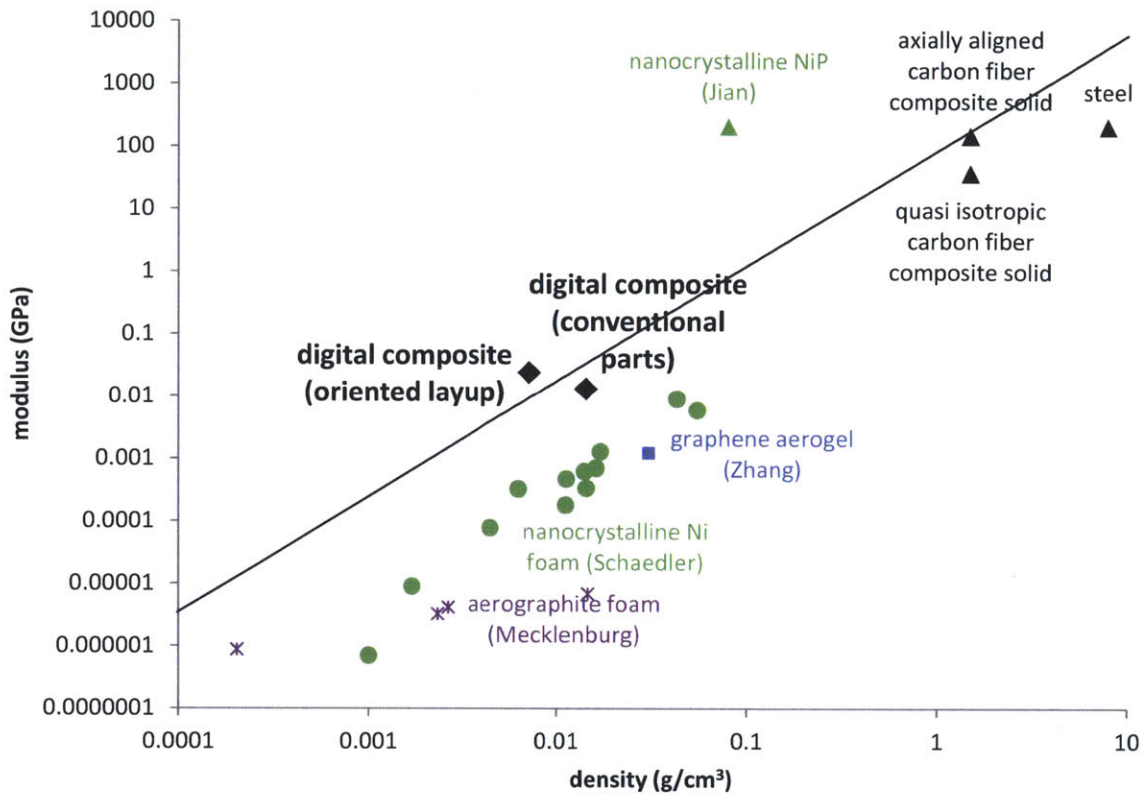


Figure 47 Digital Cellular Composite Material performance – the line represents quadratic scaling from the ideal axially aligned carbon fiber composite solid.

### Failure Modes

A perceived disadvantage to using carbon fiber composites is its failure mode. Where many structural materials display a plastic yielding plateau that absorbs energy, carbon fiber composites are known to remain nearly linear elastic up to the point that they break. A consequence of this is that the breakage event involves the rapid elastic unloading of the broken parts, which can cause further damage to a superstructure, as well as present a significant additional safety hazard. Digital composites, in contrast, display relatively graceful degradation when overloaded, whereby incremental defects are accompanied by a gradually decrease in the modulus of the overall

structure. The graph below shows cycling loading of the same specimen, through overloading induced damage events.

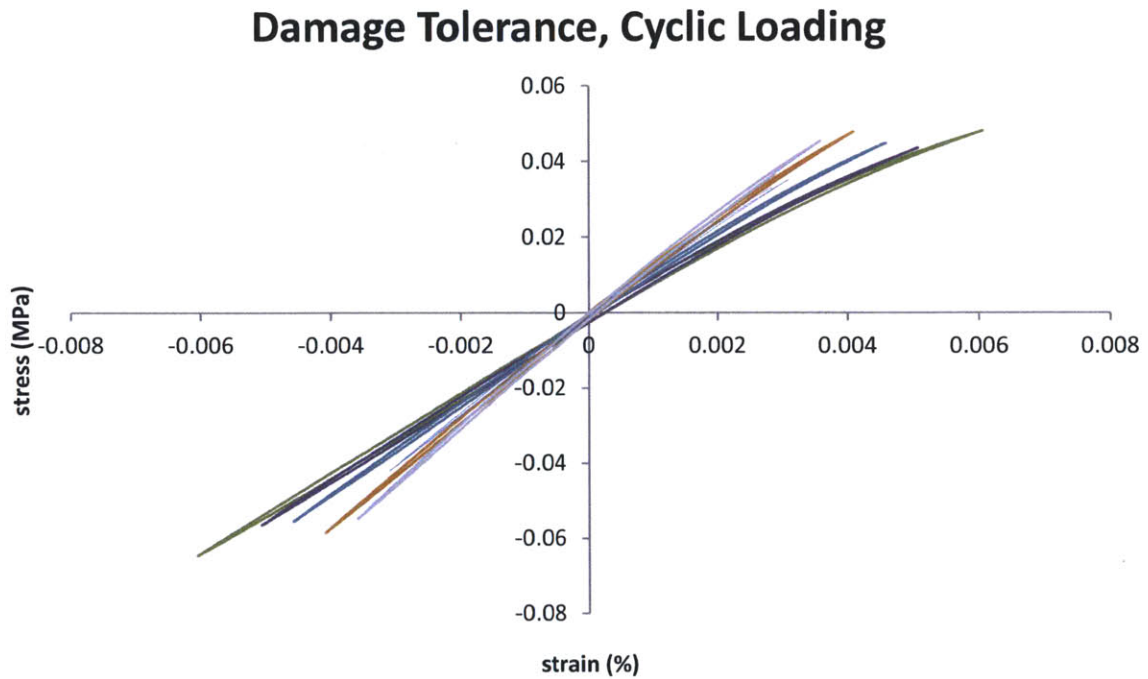


Figure 48 sequential cyclic loading after failure events, showing gradual reduction in effective modulus

It is expected that natural lattice features such as dislocations can be easily designed into digital material structures with results that are analogous to work hardening – modulus may be increased at a strength cost, by effectively producing internal preloading. With a scheme for self detachment and reattachment of connections, this type of process can occur dynamically, but for now, it suffices to address static reconfiguration to achieve such states.

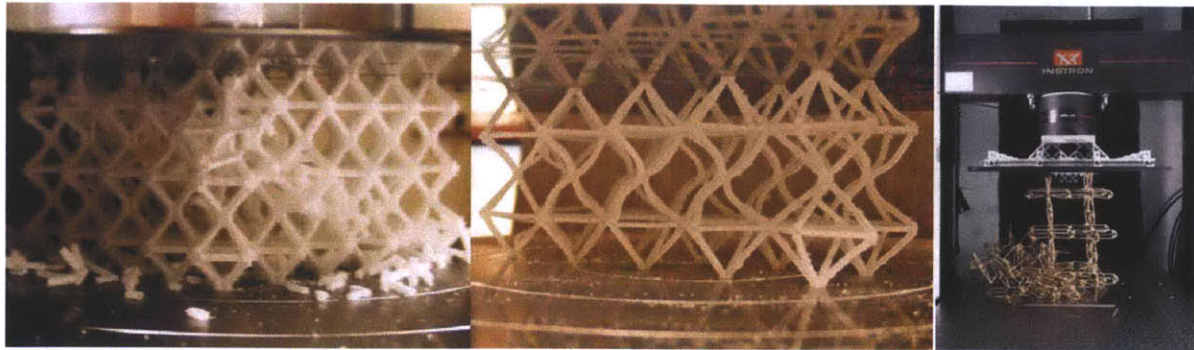
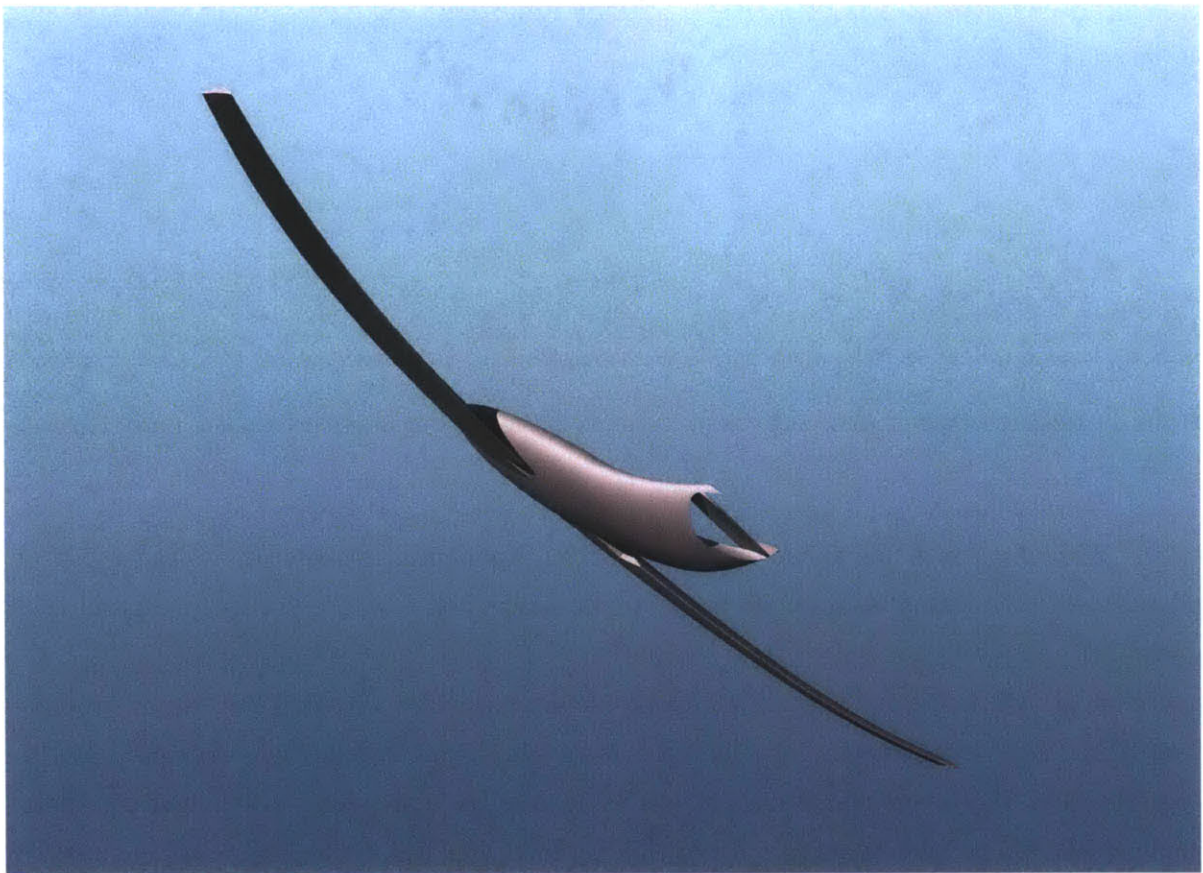


Figure 49 designer failure modes: crack propagation, non-linear elasticity by elastic buckling, brittle crushing

With progress in unmanned vehicle technology, experience has shown that rogue or poorly piloted vehicles represent a significant danger to people and property. This is particularly true of unmanned aerial vehicles, which pose a ballistic hazard to manned aircraft during normal operation. If civilian unmanned aerial vehicles are to become widely accepted, then they need to be constructed in a manner that can be qualified as presenting minimal danger when complete loss of control occurs. This is common practice at a different scale, for tempered glass in human transport applications, and possible through analogous mechanics in digital materials, whereby pre-stress introduced during assembly results in predisposition of the material to fracture in ways that span the entire structure.

Digital composites enable the design of aero-structures with precise failure modes, because of the tunability of the constituent elements. On the other extreme from the previously mentioned damage tolerance, a structure that is strong and light enough for flight can rapidly self-disassemble upon impact with another object. This may ideally manifest as bulk structure disintegration without exceeding the linear elastic limits of the individual parts (or certain parts in the assembly), and I refer to this as digital elastic frangibility.



## Applications

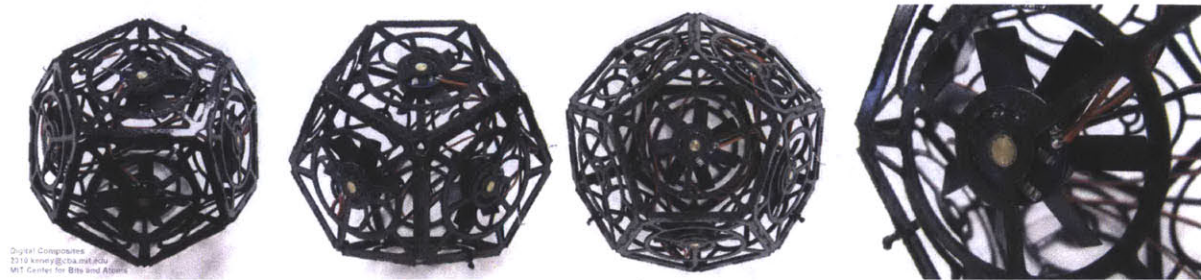


Figure 50 Imperial Probe Droid

Many fields have applications that call for strong, lightweight, and precisely shaped surfaces. Many of these applications have turned to fiber reinforced polymer composite technology for the ability to tune the mechanical properties of the parts. This work proposes that the ability of fiber reinforced polymer composite digital materials to reconfigurably form tuned structures makes it a particularly efficient and functional prototyping and manufacturing tool for these applications. The nature of Digital Composites – as having designed anisotropic strength characteristics of individual part types – allows assemblies to be highly tunable in terms of their shape, density, and corresponding mechanical properties.

### Reconfigurability

Cellular solids engineering has already enabled the use of materials with greater elasticity than previously commonly employed, most significantly with polymer foams. A result has been recent progress with both regular (Wang et al 2011) and irregular (Hiller & Lipson 2012) arrangements of discrete quantities of material throughout space, to simplify complex material design problems. While these examples both use dense analog 3d printing technologies (and are digitally designed), digitally assembled cellular solids can allow a greater range of properties for engineered structures, with cell sizes and strut member aspect ratios that are outside of what is practical with foams. A potentially interesting application for this is large scale lightweight high performing shape morphing structures.

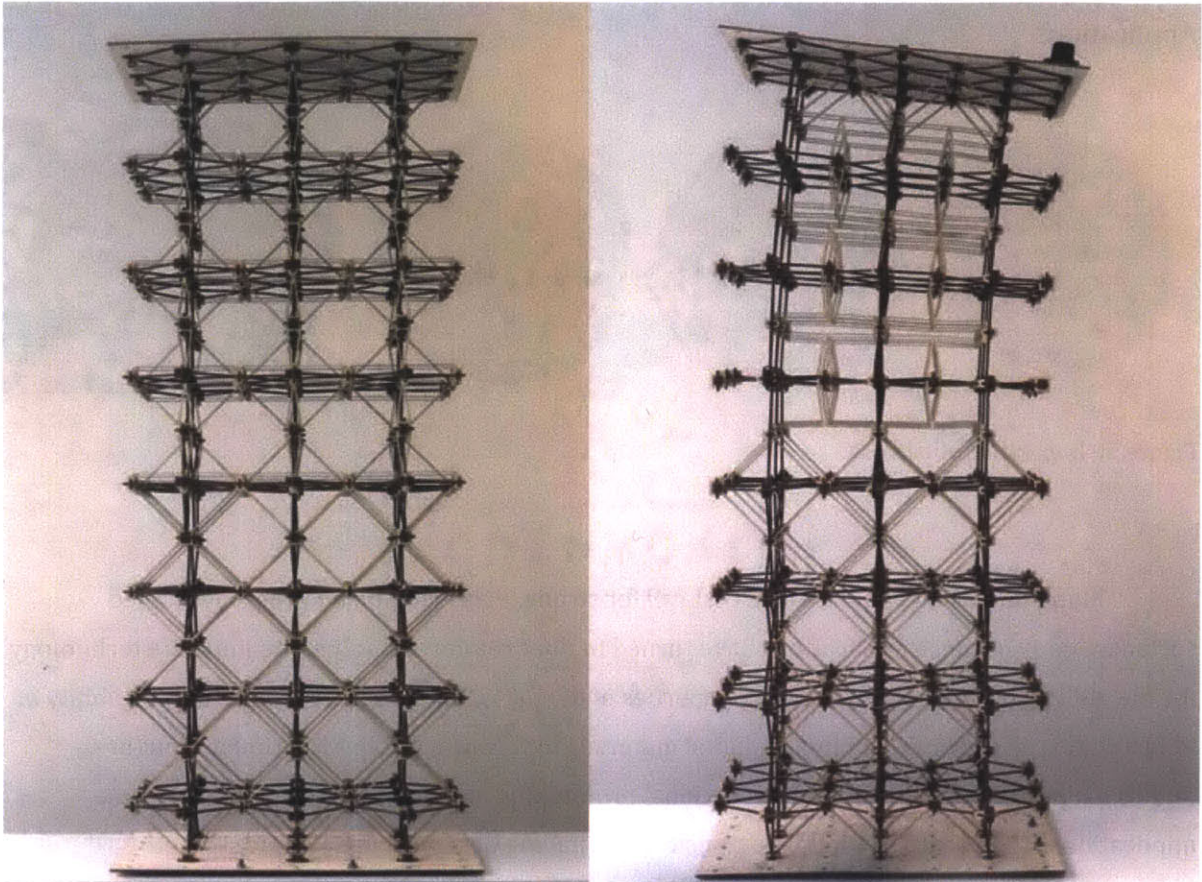


Figure 51 Tunable Elasticity

Continuously shape morphing structures have mostly focused on traditional kinematics with flexural components accounting for continuous deformation and/or high density and high cost materials such as piezoelectric ceramics, shape memory alloys, and electro-active polymers. This has limited the size, degrees of freedom, and manufacturability of shape morphing structures to date. Digital materials allow for the design of materials with many small and inexpensive actuators that combine to deliver large displacements with large forces, and/or tunable elastic phases in a lattice geometry that allows for deformation with simple large scale actuation and low actuator degrees of freedom.

The following example illustrates this programmability of deformation modes in a Digital Cellular Solid. Using identical quantities of two part types, these structures differ only by the spatial arrangement of these parts. Under identical constraints and loading condition (provided by a cable

running through the center of the structure, we see pure axial compression in one example, simple Euler buckling (biased to occur on a single axis) in another example, and complex buckling in the third example.



Figure 52 Test Flexure Tower Setup

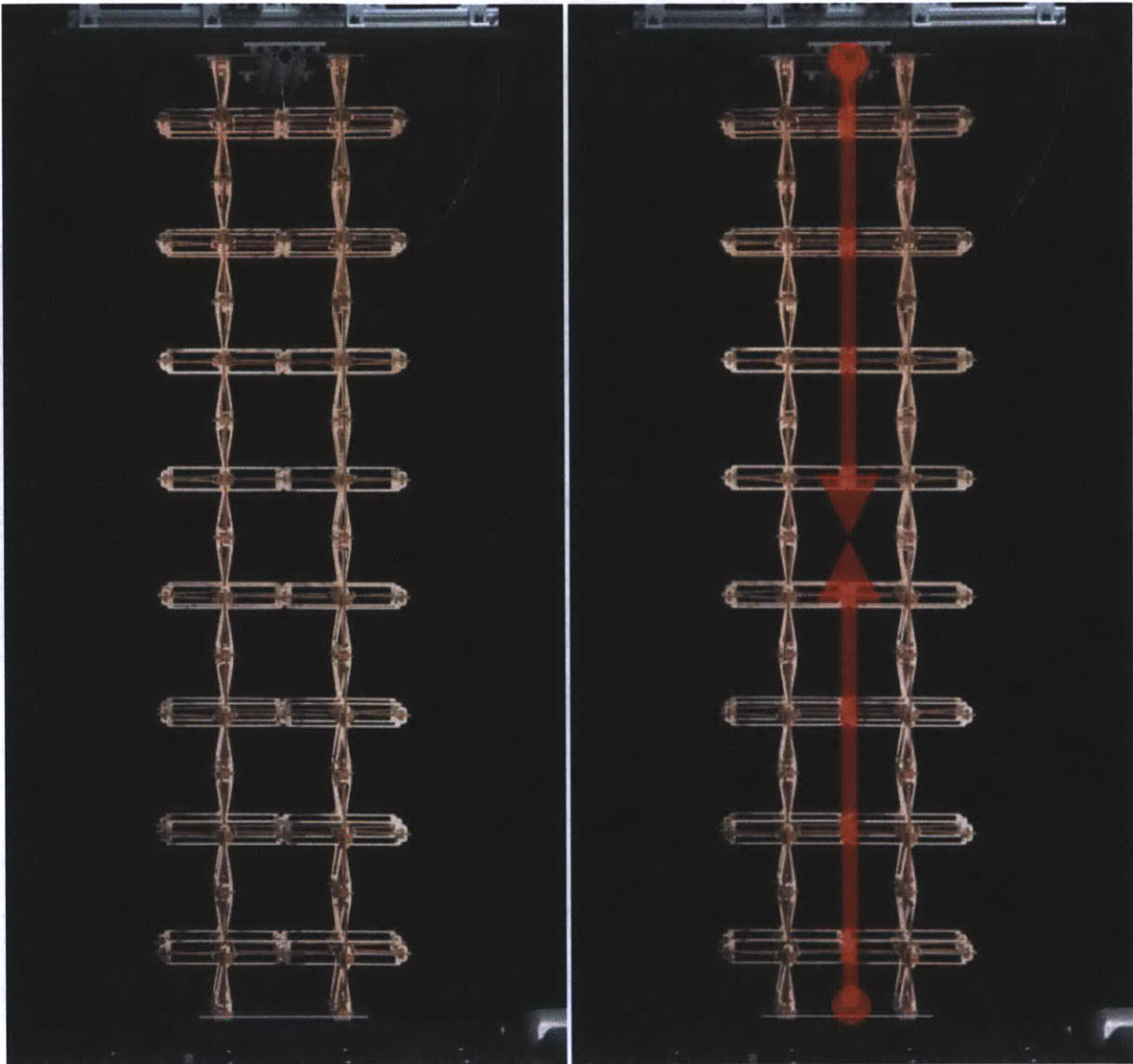


Figure 53 digital composite column profile, loading scheme, (photographs)

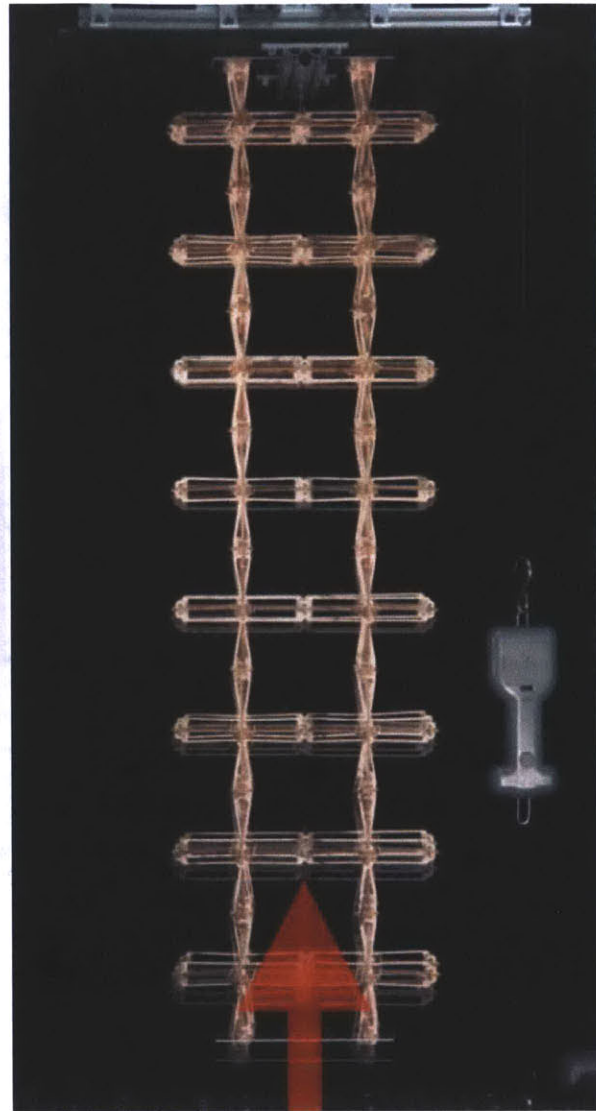
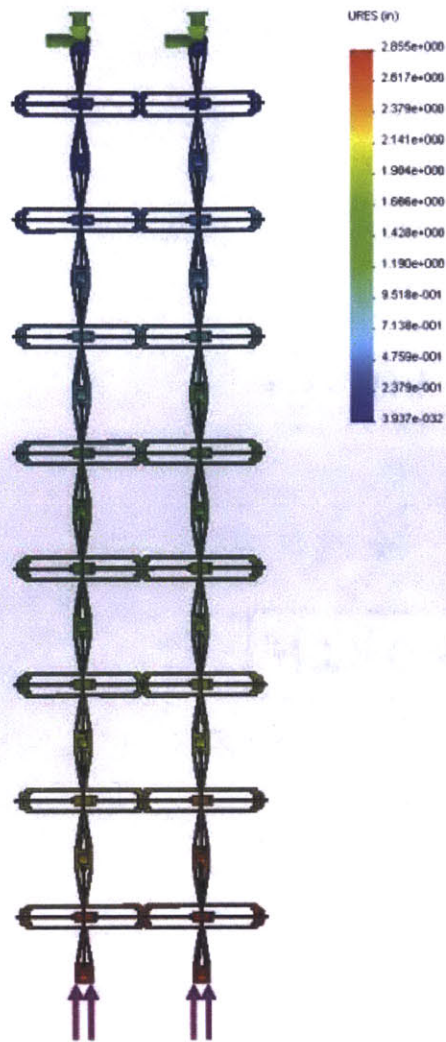


Figure 54 digital composite column profile, simulation and actual experiment (photograph) for first assembly, showing pure axial compression

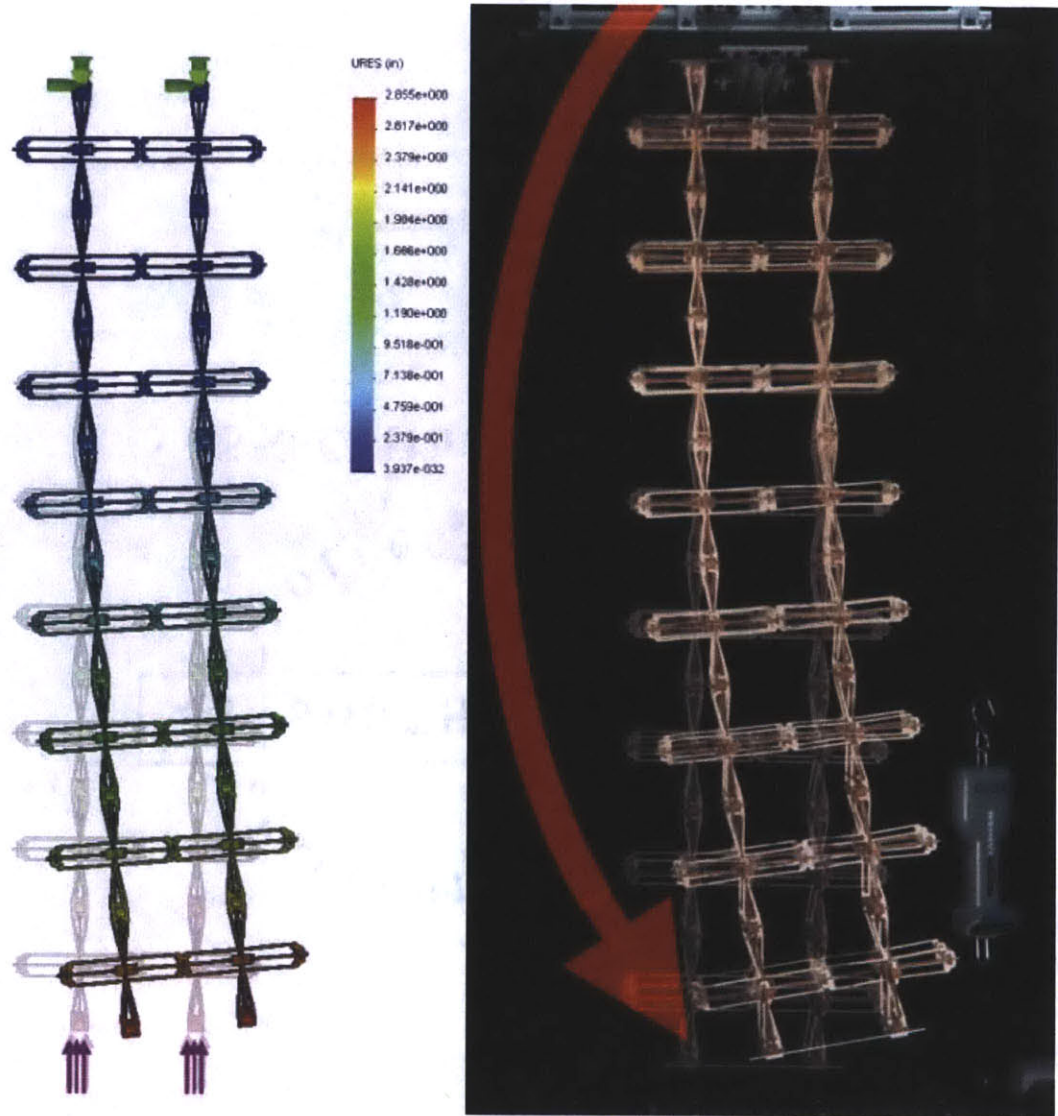


Figure 55 simulation and actual experiment (photographs) for simple single axis buckling assembly

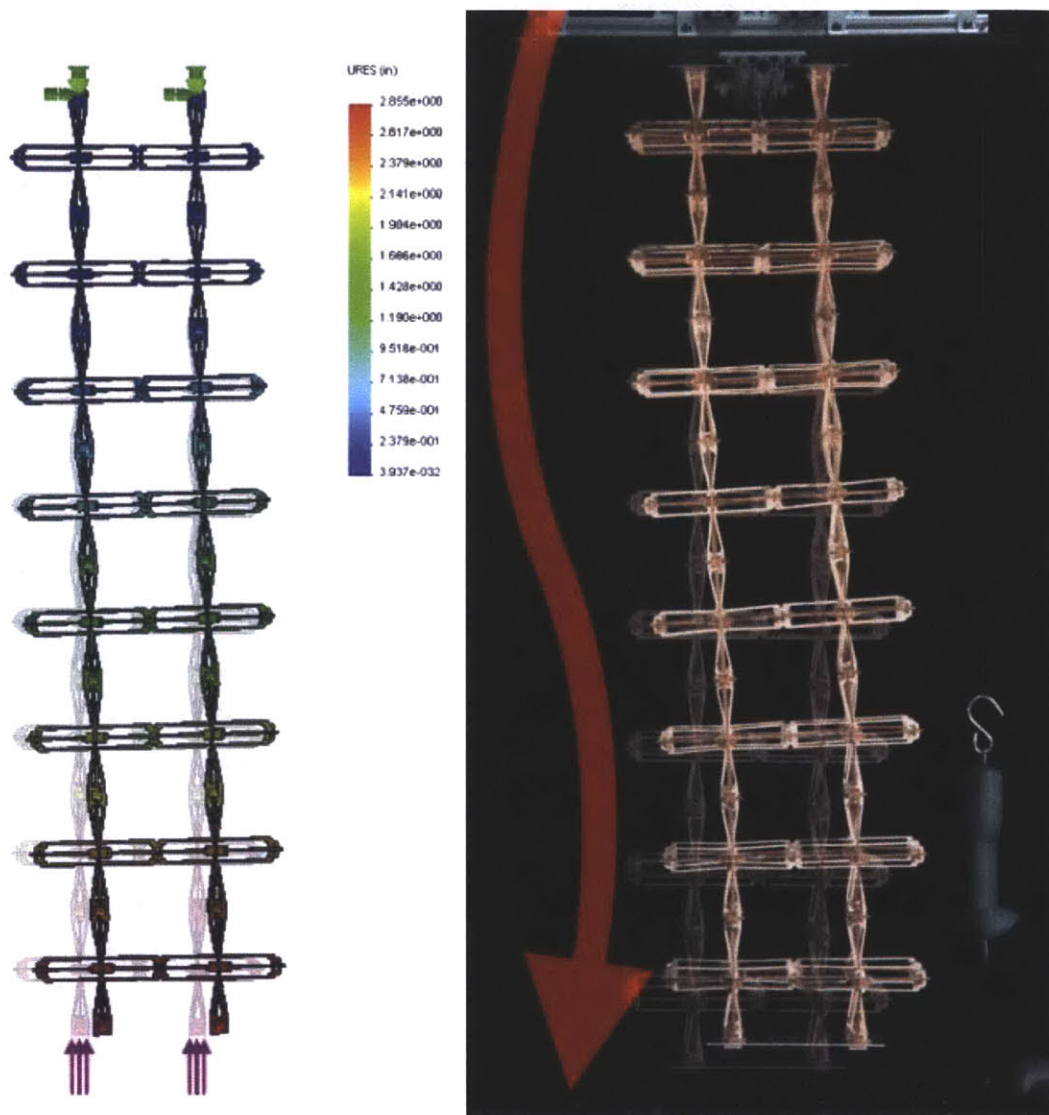


Figure 56 simulation and actual experiment (photographs) for complex buckling assembly

A potential application of this is shape morphing structures. Variable geometry mechanisms have been employed in many fields including structural and vehicle (sea, air, or land) design. The purpose is often to adapt to varying environmental physical conditions (such as which result from differences in sunlight and temperature or differences in airspeed), and the devices themselves are typically active and have been implemented with extrinsic control and actuation. Digital materials

allow for structures with similar changes in geometry by design, but which occur as passive responses to changes in environmental condition.

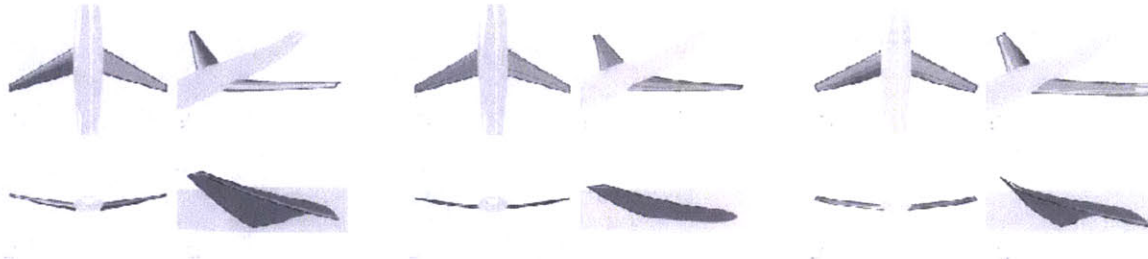


Figure 57 wing shape morphing schemes (high lift, cruise, control/flap); airfoil shapes for different aerodynamic regimes

Utilization of this principle dates as far back as the beginning of engineered flight (Wolko 1987). There are many current engineering examples of aircraft that employ actuated structures that change many aspects of wing shape (effective airfoil camber, chord, thickness, angle of incidence, sweep, etc.) specifically because idealized wings for low speed (where the need to achieve high lift provides significant constraint) applications are very different in shape to idealized wings for high speed (where drag, controls, and structural stress provide significant constraint) applications. Since aircraft need to pass through low speed and high lift regimes on their way to and from high speed cruise conditions, it is natural for an engineering design goal to include good performance under both conditions. Current solutions rely on control and actuation systems that are extrinsic to the primary aircraft structure. Digital Composites can present a solution that accomplishes a tuned global deformation with a single degree of freedom tendon actuator that spans the chord-wise direction of the airfoil.

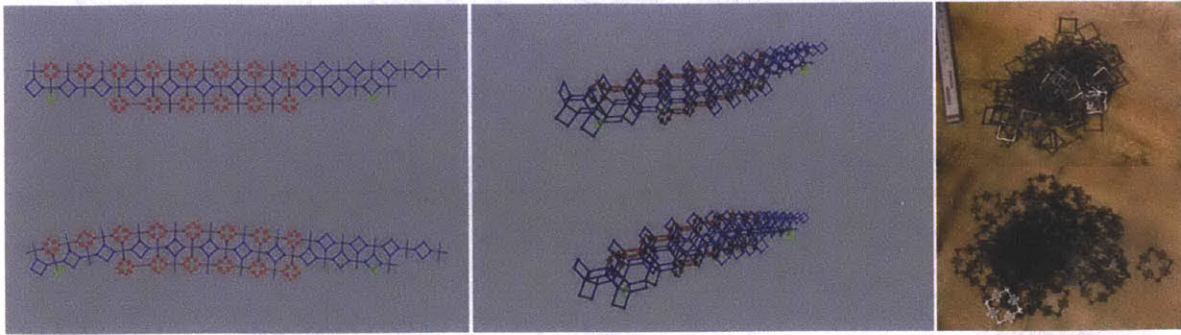


Figure 58 Digital Airfoil Shape Morphing scheme, parts

This structure is designed to bend elastically as a variable camber airfoil, and is composed of two part types, similarly to the previous column buckling example. The leading edge area of the structure retains the highest compliance for the bending axis, which results in the most curvature; the mid-section retains intermediate compliance (again, for the bending axis), and the trailing edge maintains a relatively flat surface, as it includes none of the high compliance part type. Wind tunnel testing provided performance figures for lift per airspeed, and qualitative assessment of the stiffness of the system, discussed further in the next section.

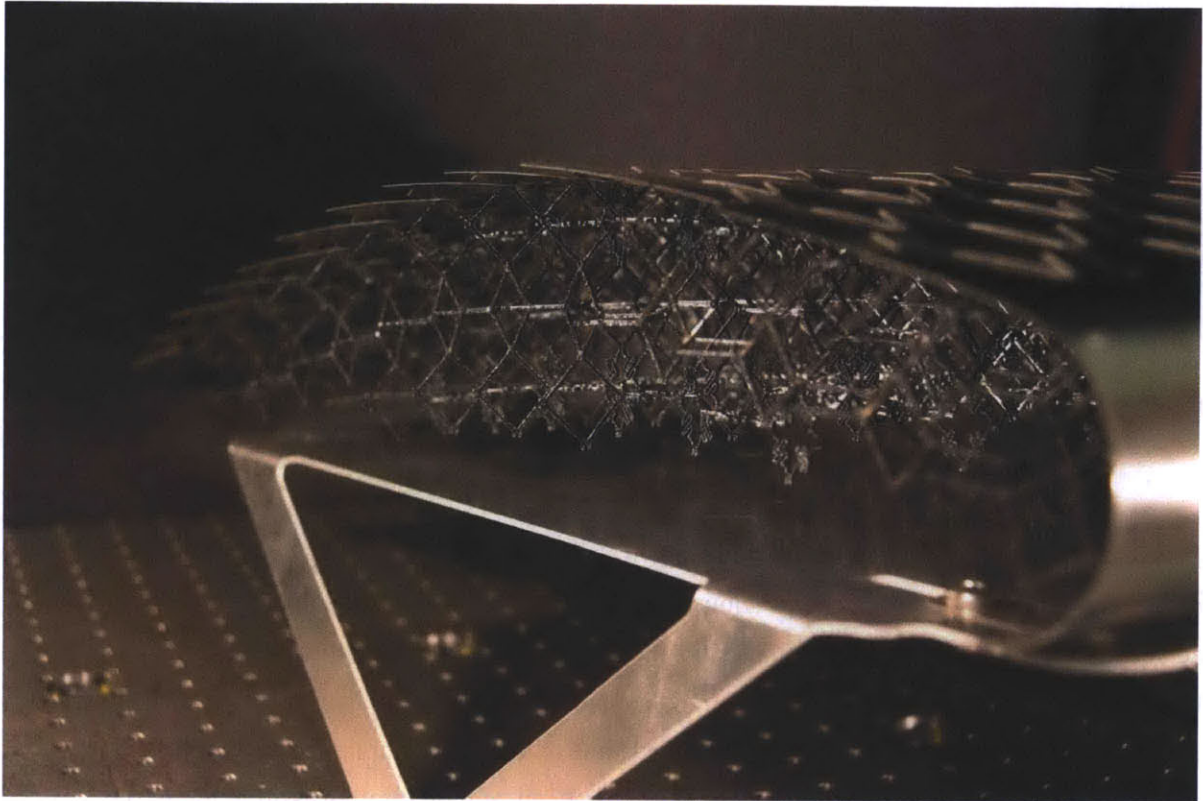


Figure 59 Digital Cellular Airfoil

### Interfaces

The goal of these materials is to efficiently distribute loads across structures. For applications such as transport, this requires the ability to transmit loads to the external environment, in order to achieve a net force vector in the desired direction of travel. A method of interfacing between the periodic digital structure and the outside environment provides two important capabilities. If the characteristic length scale of variation in the application load map is less than the digital material cell size, then this allows for local distribution of loads onto the structure, via a cellular skin. If there are peaks in the application load map that exceed the design limits of small areas of the structure, then effective smoothing of this load map can be accomplished with a skin design whereby cells also distribute loads onto neighboring cells. An extreme limit of such a digital cellular skin is essentially a digital composite in surface form, with tunable response to hoop stress, but for now I will focus on the more basic architecture where each interface or skin cell is responsible for transferring load only to the underlying lattice unit that it is attached to.

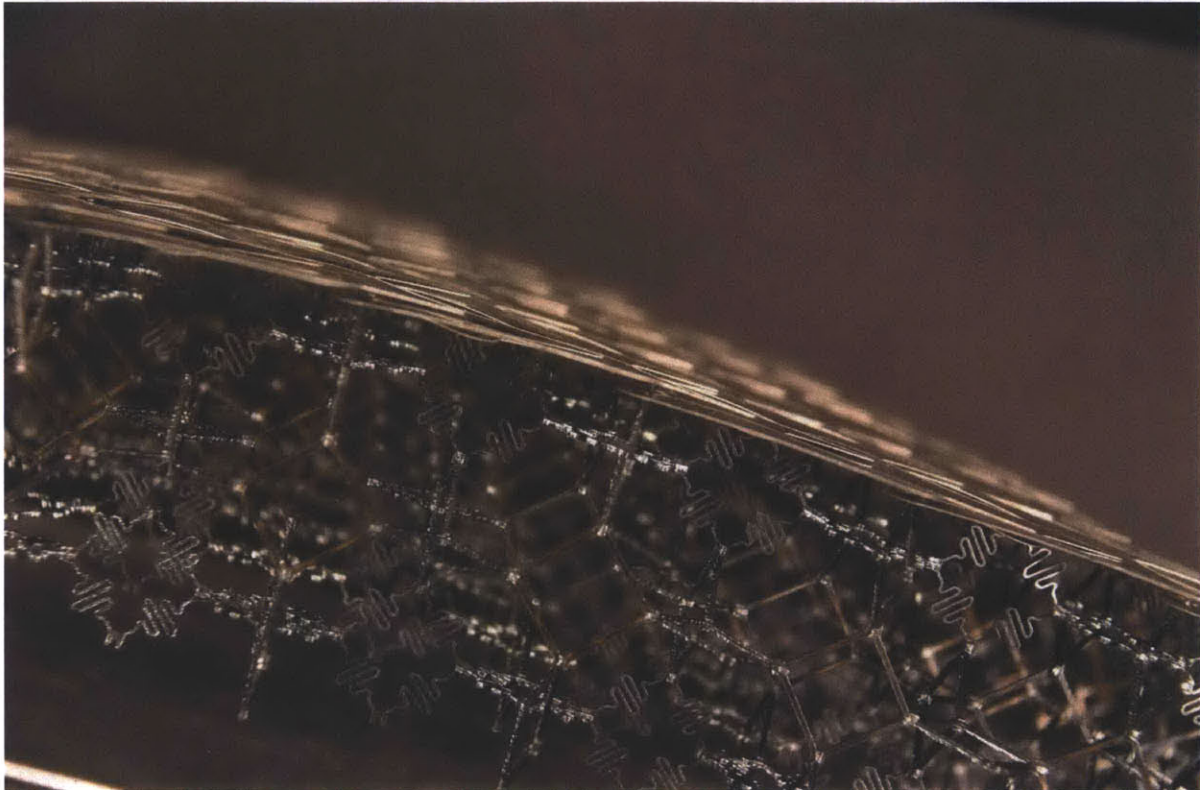


Figure 60 Digital Cellular Airfoil: interface between structure and airstream provided by cellular skin

### **Skins (two-dimensional digital cellular materials)**

The skin is discretized just like the structure, as scales or feathers, and is free to conform to the changeable shape of the structure. Each skin cell is only required to carry the aerodynamic loads of a parcel of the surface, according to the pitch of the supporting digital composite. In this example, there is some minor structural coupling between skin cells, which allows for smoothing of the surface.

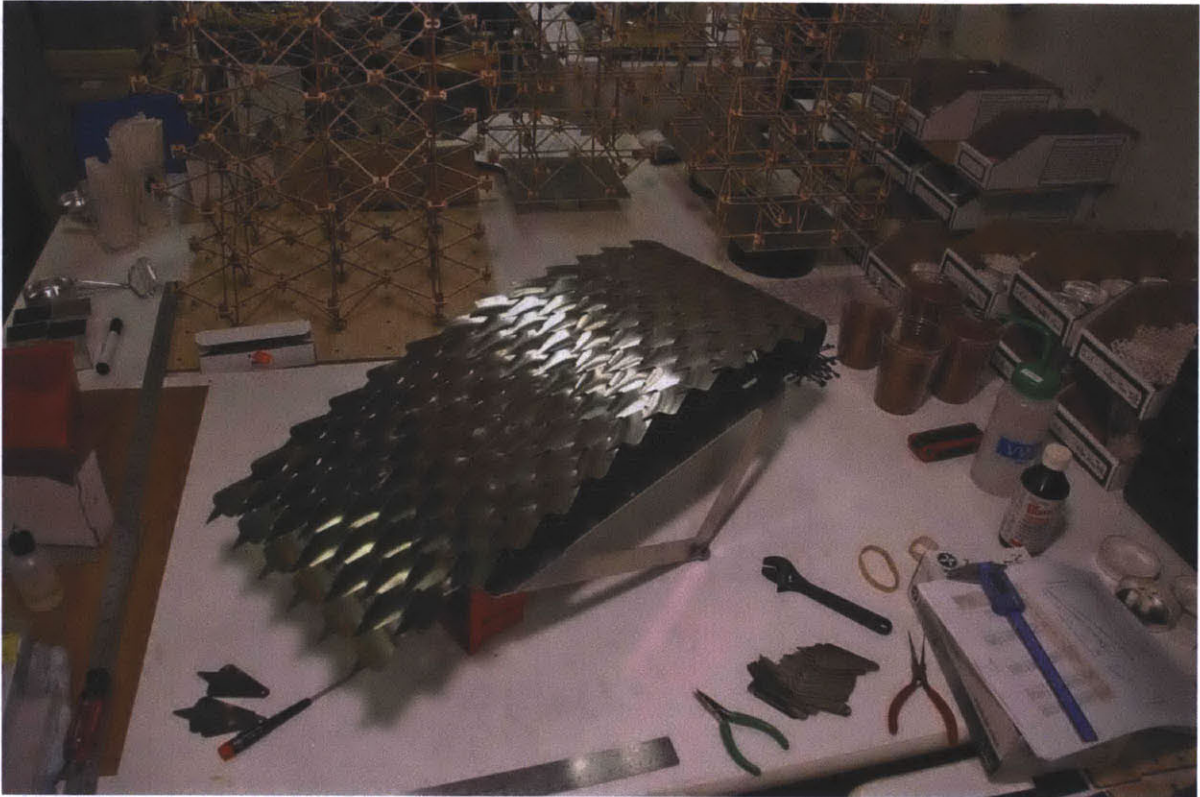


Figure 61 Digital Cellular Airfoil

The skin cells are tessellated overlapping units, each with a single attachment to the digital composite structure underneath. Since overall shape is controlled by the structure underneath, this skin handles negligible hoop stress, and primarily serves to transmit normal stress - so, it allows for free deformation of the surface within the plane of the surface. There are some details that need to be worked out, in order to make it able to maintain a proper pressure gradient for a given aerodynamic regime, and reduce tile-tile friction, but it performed well in the wind tunnel (lift characteristics showed that it worked as an airfoil; could maintain boundary layer attachment at high speed and angles of attack).

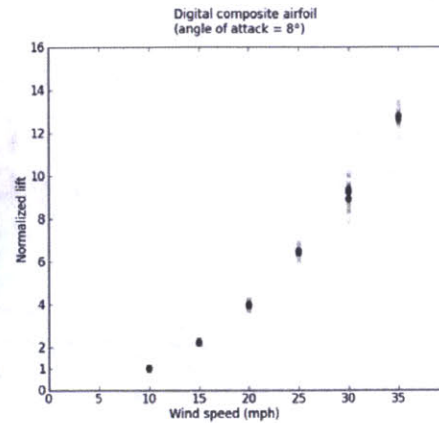
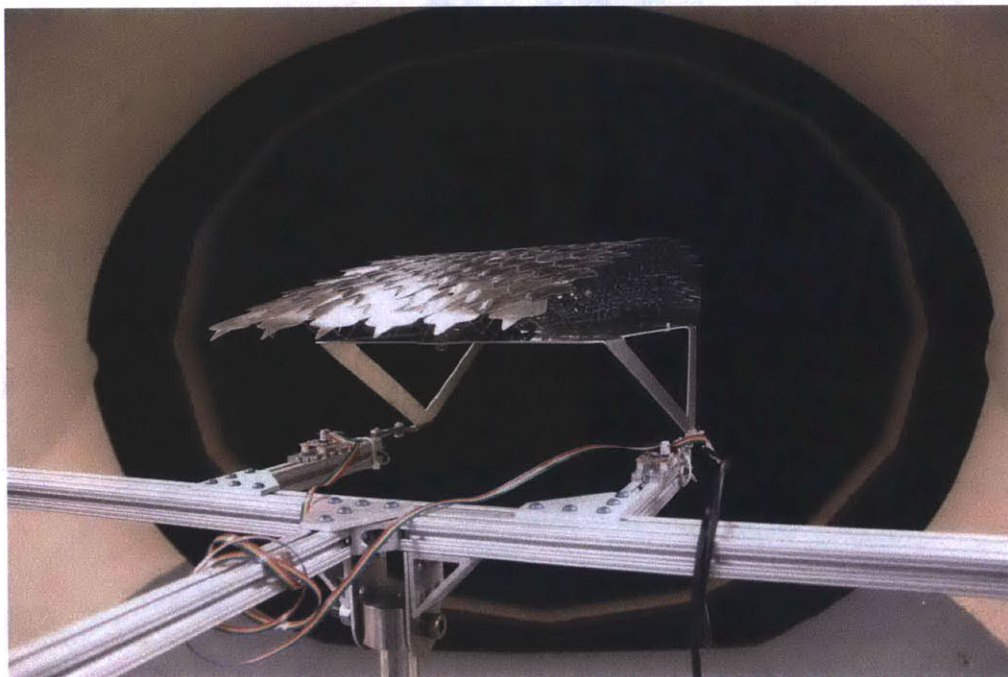
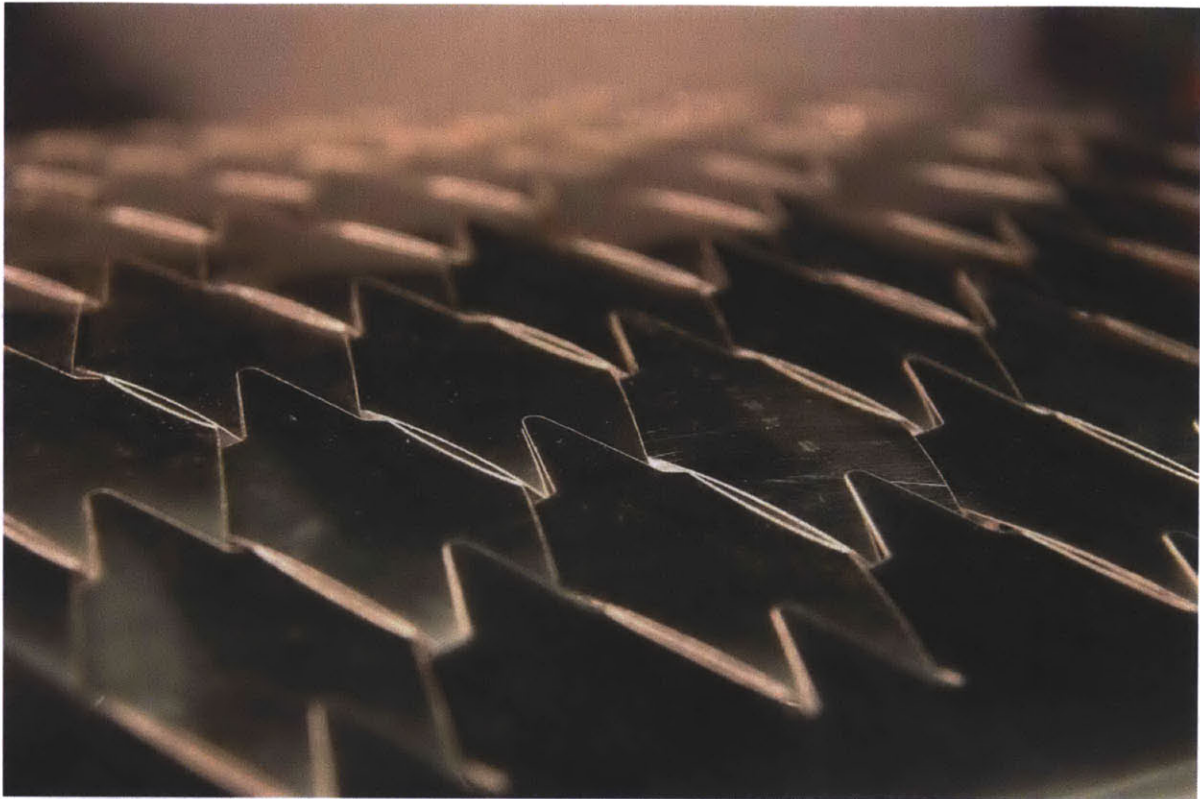


Figure 62 Digital Cellular Airfoil in the MIT Wright Brothers Wind Tunnel

The underlying structure has a two inch cell pitch, and the skin cells are produced from material that is 0.01" thick, constrained to a shape that is curved about the stream-wise axis with a 0.04" variation from the highest to lowest point, relative to the smooth convex hull of the underlying structure. Boundary layer attachment was sustained to twelve degrees angle of attack at thirty five miles per hour. This was the highest angle of attack and highest speed that we tested to. The next step for us is to produce a proper wing with this method.





## Self Assembly

For assembly process, Digital Materials may be classified by spatial dimension of the assembly process. One dimensional systems, or “Digital Strings,” have been demonstrated for the purpose of programming actuated shape, and presents a simple coded strategy for the design of digital assembly processes (“Programmable Matter”) for two and three dimensional structures (Cheung et al 2011). This led to the question of the mechanical properties of completed assemblies.

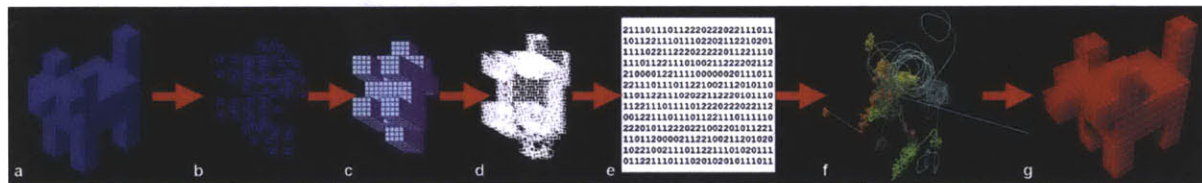


Figure 63 1d → 3d workflow with potential applications to Digital Composite Assembly (Cheung, et al 2011)

The one dimensional mechanical properties of this kind of digital material system in string form is trivial to consider. While some work has been done to analyze and predict the stiffness of folded string structures without strong cross-linking (White et al 2011), generalized usefulness of these systems is generally founded upon the assumption of the string taking on a three dimensional strongly interconnected state.

The ability of the string or surface to reach smooth topologies in three dimensional space may be enabled by explicit degrees of freedom, and may permit the formation of non Euclidean, non-developable surface forms, such as spherical or hyperbolic shells with programmable porosity. Generally, the topology of a digital material assembly may therefore be any surface or volume meshing, with arbitrary node connectivity, as necessary to achieve a specified range of configurations. Regardless of the geometric system, it is useful to automate the description and assembly process. For instance, for digital surfaces, decomposition of any surface as an assemblage of planes, geodesic, and hyperbolic surfaces that can be approximated by the system can be calculated based on the curvature map of the form, and the degrees of freedom inherent in the component design.

It is apparent that both one and two dimensional systems can be developed to form three dimensional interconnected assemblies. For this reason, the analytical section of this work will primarily address regular three dimensional lattice structures. It remains to be seen if the best processes of assembling such structures includes one and two dimensional assembly states, but this question will be left for future work.

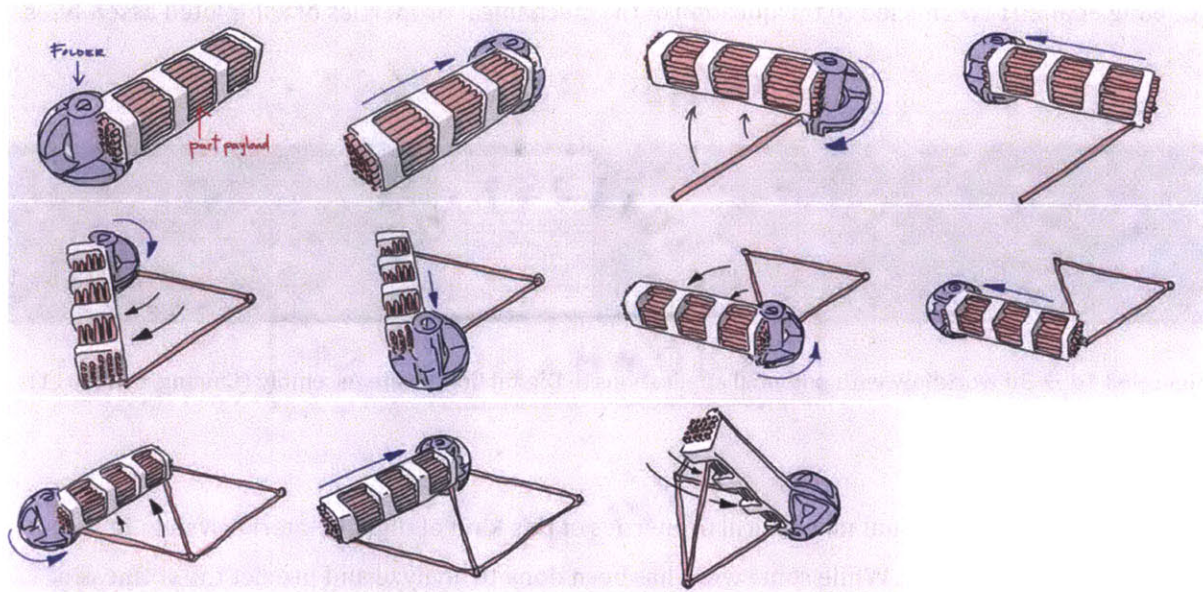


Figure 64 one dimensional workflow for framework construction

## Conclusions

Digital Cellular Solids are cellular solids that exhibit improvements in relative stiffness and strength compared to relative density, over current practices for producing lightweight materials. This is accomplished by assembling lattice geometries that perform better than any that we know how to make with traditional methods. When implemented with fiber composites, the result is not only stiffer and stronger than any previously known ultra-light material, but it presents a new scalable and flexible workflow for applying fiber composites to engineering problems – in particular, those that might benefit from tuned elastic deformation.

The science of cellular solids has enabled the widespread use of lightweight materials to meet important engineering needs, such as passive energy absorption, but they are not in widespread use for structural applications, perhaps due to a large gap between the strength and stiffness to weight ratios of popular classical solids, and the performance of known lightweight cellular materials that are produced from the same constituent material. Stochastic cellular architecture results in distribution towards properties such as low stiffness, low strength, but good energy absorption and low thermal conductivity (Gibson & Ashby 1988). Young's modulus of ultra-light stochastic materials generally follows  $E \propto \rho^3$ , as opposed to the  $E \propto \rho^2$  relationship for random open cell foams with higher relative densities (Ma et al 2001). I show considerable improvements on this, with close to linear scaling over three orders of magnitude in density. Conventional analysis of stochastic cellular solids (i.e. foams) relies on simple mechanical cell models and dimensional arguments, verified with experimentation. Analysis of digital composites with the same methods (except that the mechanical models are not nearly as approximate as with analysis of foams) is shown to yield good predictions of experimental behavior, as well. However, unlike with stochastic foams, direct modeling and measurement of elements (with specific load tests) is possible at these scales.

The engineering of fiber reinforced composite materials has enabled structures with large reductions in weight for given strength and stiffness targets, but at very high design and processing costs, and many challenges producing mechanical interfaces (joints). For the field of fiber composite engineering, digital composites systems circumvent the conventional assumption that efficient composite design is one where micro-scale material features must constantly be adapted towards macro-scale design features, in an analog fashion. This analog simultaneous design and production of materials and components is currently performed at great expense. Performing this

optimization in a digital fashion not only decouples the part design from the low level material design, but it allows for greatly increased design and prototyping freedom within the traditionally difficult realm of lightweight, strong, and stiff materials.

Digital materials promise scalable methods of producing functional things with reconfigurable sets of discrete and compatible parts, but the presence of many reversible connections has raised questions about the performance of the end result. I have shown, here, that for a Digital Cellular Solid lattice structure composed of strut members and joints at intersection nodes, the joint strength can be tuned to have higher load capacity than the buckling load for the strut member in the structure, while still maintaining favorable relative density as well as corresponding relative strength and pre-buckling modulus performance. This is because geometric factors dictate that relative density scaling with connection volume is less dominant than relative density scaling with strut member aspect ratio, and simple column buckling analysis reveals that for slender strut members, there is generous allowable connection volume while still maintaining desirable relative density. The result allows for structures with very low hysteretic losses. With fiber composite parts, this can be accomplished as an ultra-light material and with post-buckling elastic collapse behavior that stays completely elastic over large additional strain, displaying much of the strength/stiffness to weight benefits of solid fiber composites together with a superelastic phase that could be used to circumvent the typical energy release that characterizes conventional carbon fiber composite failure modes.

Strong, lightweight, reconfigurable and precisely shaped structures are desired in many fields (e.g., architecture, aerospace, transport, science). These can range from many kilometers scale elevated light railway infrastructure to meter scale vehicle structures, to low inertia measurement devices with micron scale features. This work proposes that the ability of Digital Materials to reconfigurably form tuned structures makes it a particularly valuable functional prototyping and manufacturing tool for these applications. These systems may be understood as a digital material for rapid prototyping and fabrication of any two-dimensional or three-dimensional shape with discretized resolution, from fiber reinforced composite material. This may be thought of as a kit of parts whose individual fiber layouts and interconnectivity allows for tuned macro-assemblies. Therefore, a primary feature of fiber reinforced composite materials – the ability to engineer very specific mechanical material properties – is enhanced with this kit-of-parts method, whereby functional material properties as well as overall shape are tuned via the strategy for assembly of the parts.

When made from anisotropic fiber reinforced composites, Digital Composites function as a chain of discrete fiber composite parts that can be close to the strength of a monolithic part, as a low density, sparse structural system. Particular advantages over conventional fiber composites include manufacturing processes, serviceability, and reusability, in addition to the tunability and extensibility that are general goals of digital materials. This is accomplished by linking tiles that are individually tuned through their fiber layup, so that forces are transferred between the tiles, rather than having continuous fibers span entire macro-structures.

Collaboration with and review of the commercial aero-structures industry reveals potential benefits in prototyping, manufacturing, and maintenance costs for aero-structures in particular – based on fabrication by discrete addition, subtraction, and sorting. From a total systems perspective, consider that a Boeing 747 consists of approximately six million discrete parts, half of which are fasteners. Estimates for part count of similar planes are within an order of magnitude of this figure, and seem to scale roughly proportionally to volume. For the Boeing 747, commercial price is on the order of one hundred million US dollars.

The current 737 fuselage is comprised of a couple of hundred thousand parts (depending on the sub-model), not including fasteners. Given the parts ratios for the 747, we may assume that an additional couple of hundred thousand fasteners are used to attach these parts to each other. With a factory system of about seven hundred people, about one fuselage per day is completed. Therefore we can estimate that on average, seven thousand parts are added to the assembly, per hour (or ten per person per hour), or about two per second. Not even counting the high level of automation that is integrated into this production process, just the people involved spend more than 1.7 megawatt hours assembling this part, based on well accepted estimated of human metabolic rate (100W per person). Each part costs about ten watt hours of just manual labor to install. Estimating the total structural volume of this fuselage as a cylinder – which is four meters in diameter, forty meters long, and twenty five centimeters thick – gives us about one hundred and twenty cubic meters. This would require about nine hundred thousand parts, if we simply used the cuboct truss presented here. Trained students can place one of the cuboct truss parts every five minutes, so with the same workforce, the job would get done in five days.

Final comparison to conventional aero-structures must be from a functional constraint perspective. Is this a better way to build an airplane – does it more efficiently handle aerodynamic

loads? From a simplified structural performance point of view, it may be useful to see where things are on a chart of strength or stiffness to density. Note on the solid material density to modulus charts,  $E/\rho$  isocurves indicate modulus of elasticity remaining proportional to density. This means that for a given material (such as one that digital material components are made from), if you change the volumetric fill fraction of a continuum of that material and empty space (which gets counted towards the volume, but not the mass), the  $E/\rho$  curve indicates the theoretical upper bound on the modulus of that altered material. The economics of flight dictate that for any given flight mechanism, lighter is better. A given flight mechanism will also depend to a fair degree on material stiffness, in order to push or react against the air.

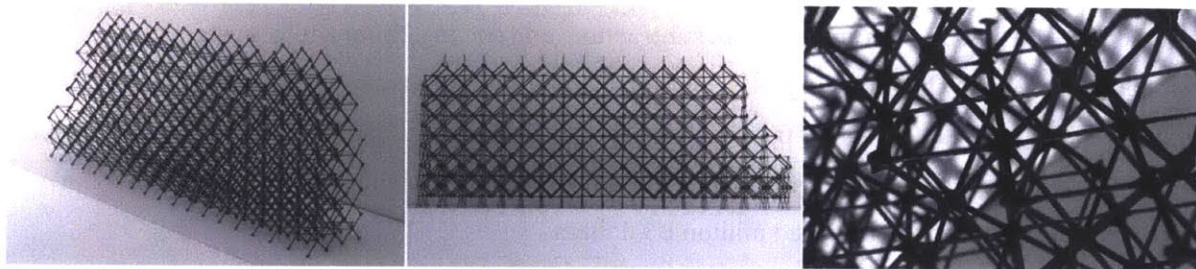


Figure 65 Digital Composite Wing Wedge, Sized to replace existing component on commercial jet produced by spiritaero

Comparison of performance, between conventional aero-structures and Digital Composite replacements, was initially considered to be a simple task – all that is required is to place a digital material replacement part into the same testing apparatus that is used to qualify conventional parts. This, however, presents an interesting problem and point of discussion, since the qualification methods are tailored towards the structural design of the conventional part (they are not qualified to fly, for instance, by seeing if they can fly).

Referring to the loading test specifications for an actual aero-structure assembly, we see that the complete structural system does not have extreme loading requirements. Aerodynamic loads are intrinsically quite distributed. In fact, it is clear that if the part were fabricated entirely as skinned commercially available structural honeycomb, it would far exceed the part specification (by three orders of magnitude, depending on the product). This latter method of construction is assumed to be prohibitively difficult, since there are various non-structural systems that need to

reside in the interior of the part. Furthermore, it would suffer from the same production issues that partially compel this application for digital composites in the first place (for instance, larger monolithic structures provide fewer opportunities for qualification before the cost of a failed qualification test becomes too high).

An overall aero-structure deflection test may include a wing tip load that is applied via a winch cable attached to a bolt on the wing tip, for which a spar leading to the wing root is probably fairly close to an idealized structure. However, as a test of (especially extreme) operating conditions for a plane, this relies on an important assumption – that the surface material's (i.e. skin panels) contribution to the structural performance when the assembly is point loaded on a spar - gives you enough useful information about the spar's contribution to the structural performance when the assembly is surface loaded, such as in flight. This is justified if actual flight data (for wing deflection) matches the test deflections.

While the testing method may be well reasoned for the conventional structure, it is simply apples to airplanes to compare with digital material volumes in the same test. An entire digital composite wing, in the testing fixture for the conventional structure, would need special interfacing elements (which could be floating within the structure, in this case), in order to distribute the point loads of the conventional test. Yet, this kind of point loading remains just an approximation for the forces that these structures are subjected to in flight. It is possible that an airworthy digital material wing under conventional structure testing operations would simply have a handful of digital composite units rip loose at the loading points. The wing would otherwise stay intact (and undoubtedly still airworthy).

Perhaps it only will be a fair comparison when considered in terms of first principles of flight and definitions of safety factor. Additionally, conventional control surface structure attachment points represent perhaps unnecessary localized loading as a result of conventional design, and we may just look ahead to morphing structures, whereby the safety factor would need to be redesigned.

A metric such as weight per span can be seen as a size independent indicator of flight efficiency, for given materials and construction methods. For instance, all birds are basically made out of the same materials with the same method of construction, and their wing performance per weight is known to follow a basic similarity law, regardless of their size (Helmholtz 1873). The critical aspect of materials and construction that affect flight is mechanical performance in beam

bending (Cleveland 1970). Beam performance can be optimized for stiffness to weight via a beam performance index that is defined as the square root of the modulus of a material divided by the material density, for a given cross sectional shape (Ashby and Cebon 1993). A chart of the beam performance indices of digital composites in comparison to traditional aero-structure materials is shown below.

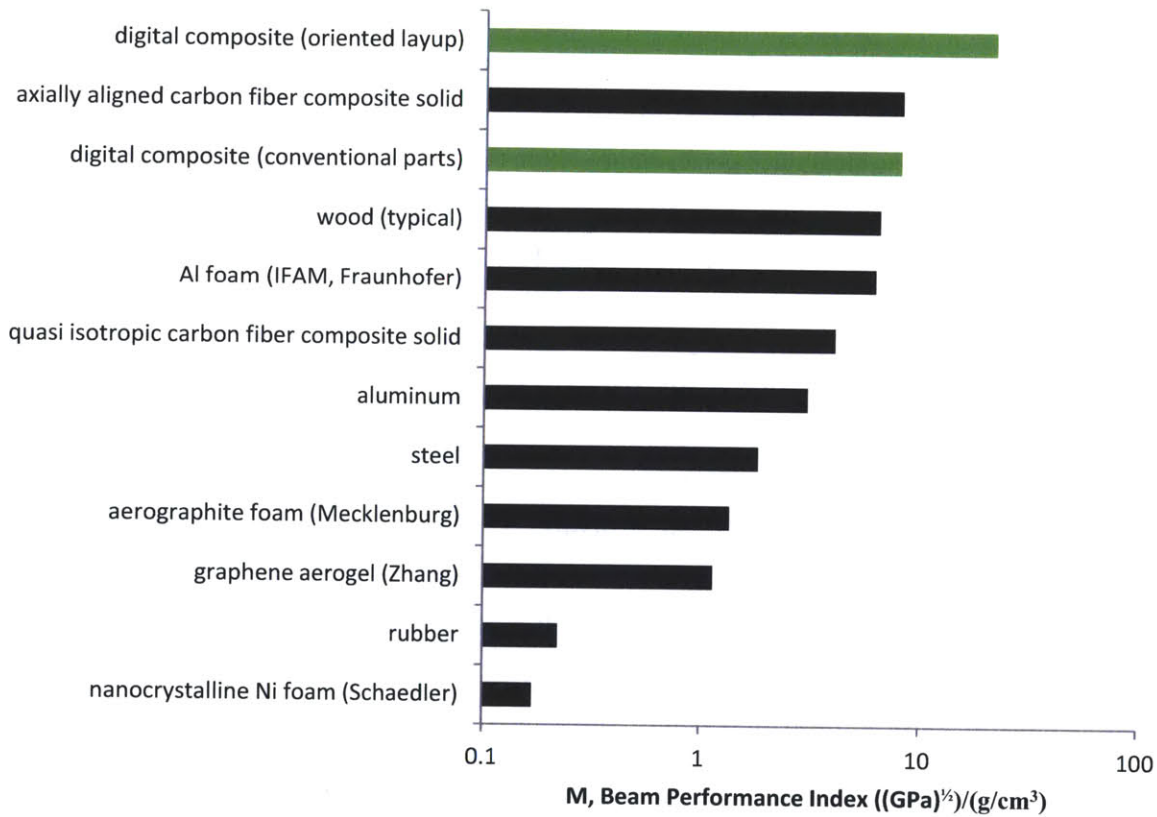


Figure 66 beam performance index for various materials

The continually evolving quest for more efficient aircraft has always included a focus on strength to weight ratios (Kelly et al 2002). If an aero-structure can be made a modest amount lighter for the same stiffness (and therefore aerodynamic performance, by current convention), then a considerable weight of fuel is saved. This is because an initial fuel savings itself incurs a reduction in weight, which incurs additional reductions in aero-structural requirements, and additional reductions in weight (Cleveland 1970). Digital composites may therefore present an

opportunity for a significant increase in engineered efficiency for high performance structures, including large scale static aero-structures. With the apparent opportunities to design structures with complex elastic modes, we may be also able to access uncharted design space for structural kinematics, including with engineered flight, with digital composites.

Recent work in engineered flight is exploring the possibility that flapping wing flight can save aerodynamic power compared to fixed wing flight, by mechanisms such as interaction with self induced wakes (e.g. Pesavento & Wang 2009). To do this, relative to engineered flapping wing craft (ornithopters), it has been shown that biological flight employs a greater range of coordinated wing motions, including wing twist, span-wise bending, vertical flap, and horizontal flap (Lehmann & Pick 2007; Heathcote et al 2008; Jongerius & Lentik 2010). The mechanical systems that achieve this in biology is observed to rely on sparse, lattice like arrangements of material, ranging from avian bones to insect wing cuticle (Wang et al 2008). Both examples employ considerably dense and stiff bio-materials, as constituent solids, for aero-structures with very low weight per span (Vincent & Wegst 2004), and which digital composites bear a passing resemblance to.



Figure 67 Andean Condor

(This page intentionally left blank)

## Grand Challenges

### #1 – Engineered Molecular Digital Composites

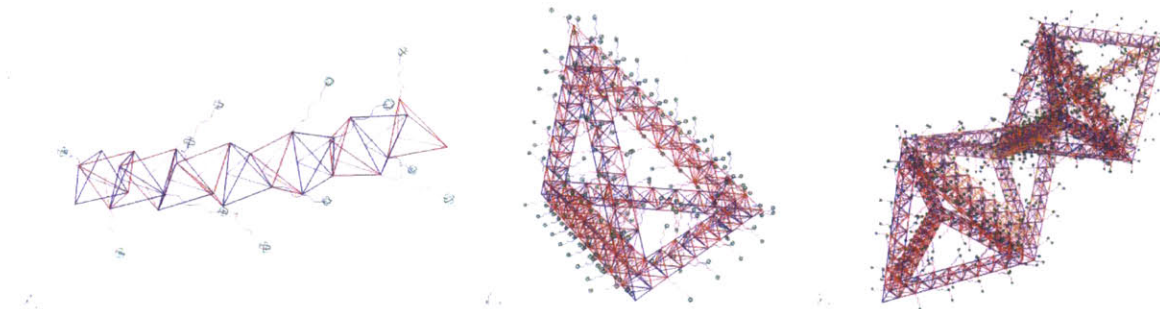


Figure 68 Engineered Molecular Digital Composites

The ability to making our own materials with part size and placement at the molecular level would revolutionize the way that we make things. This will require hierarchical methods, and utilize much of the machinery of biological molecular assembly, with small modifications. A version would be a soup that needs to be fed energy and an inorganic substrate in solution, which the biomachinery in the soup is designed to organize into Digital Cellular Solids. This could be used to create bulk material, or guided by formwork, energy, or food, to create specific shapes and variations (e.g. certain environmental pressures result in changes in ratios between parts, and corresponding changes in mechanical properties).

## #2 Digital Composite Electronics Reconfigurator

Even in its densest form, Digital Material structures can maintain an integral and redundant set of communication channels (three dimensional mesh network) that allow for the diffusion of information, such as signaling of the need to adapt the structure. This means that the material can also be employed as part of sensing and monitoring equipment. For example, structural carbon fiber may be employed as strain gauges, heating elements, temperature detectors,<sup>5</sup> capacitive energy storage devices, and more. Possible uses include structural health monitoring and even computational logic.<sup>6</sup> Digital Material construction presents the ability to deploy this type of equipment in a scalable manner. Furthermore, active or passive electronic circuits can be embedded in Digital Material structures, allowing for the storage of information that may be used for purposes ranging from passive monitoring to altering overall shape.

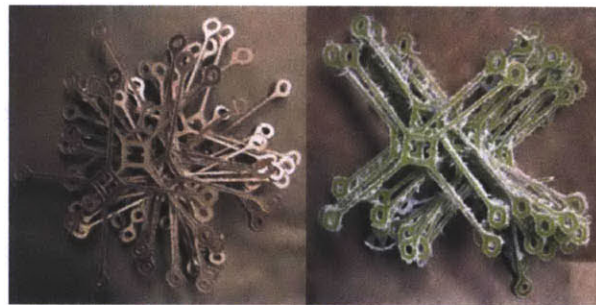


Figure 69 Conductive and Insulating Digital Composite Parts

Imagine having a container that any electronic “trash” can be tossed into for rapid disassembly by mechanical enzymes. This process would take vastly less energy than mining individual elements from the assemblies. The constituent parts are fundamental – power electronics, simple microprocessors,, input devices, and output devices – get automatically evaluated for reuse, and organized into groups, floating around in the container. The same mechanisms in the container are capable of assembling the units to make new devices, according to codes passed in to the container. It is like a printer that takes old printed material as its feedstock.

---

<sup>2</sup> Carbon fiber heating elements are commercially available, and the use of graphite resistors as Resistance Temperature Detectors is common practice. With Digital Composites, the interfaces between parts would be set up to couple to each other (e.g. through carbon fiber), either conductively or electromagnetically.

<sup>6</sup> Commercially available in situ fiber reinforced polymer sensing and monitoring systems are very expensive, and many rely on custom designed schemes for embedding non structural components within parts.

### #3 – Digital Flexural Mechanisms

Many engineered mechanisms could be replaced by digital flexural materials, as the latter provides for exponential tunability.

A good example is medical orthoses and prostheses, which require tunability, extensibility, and very high strength and stiffness to weight ratios. These constraints have resulted in leading devices that cost around the same as conventional personal vehicles, which renders them inaccessible to many patients. Current prosthetics methods rely on expensive stocks of materials and parts with very limited reusability or recyclability. A digital composite kit could provide the tunability required of these devices, at a much lower cost and weight, with reusable parts.

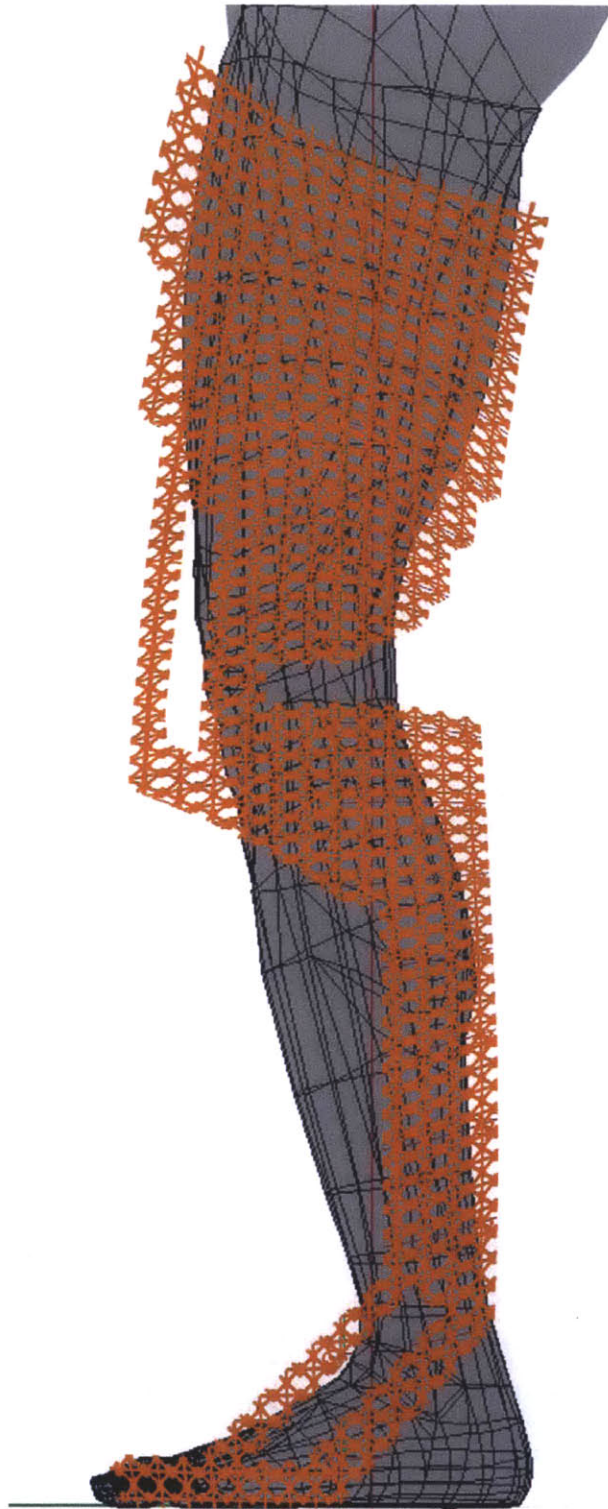


Figure 70 Digital Composite Orthoses and Prostheses

#### #4 Passive Shape Optimization and Resonant Aerodynamic Propulsion

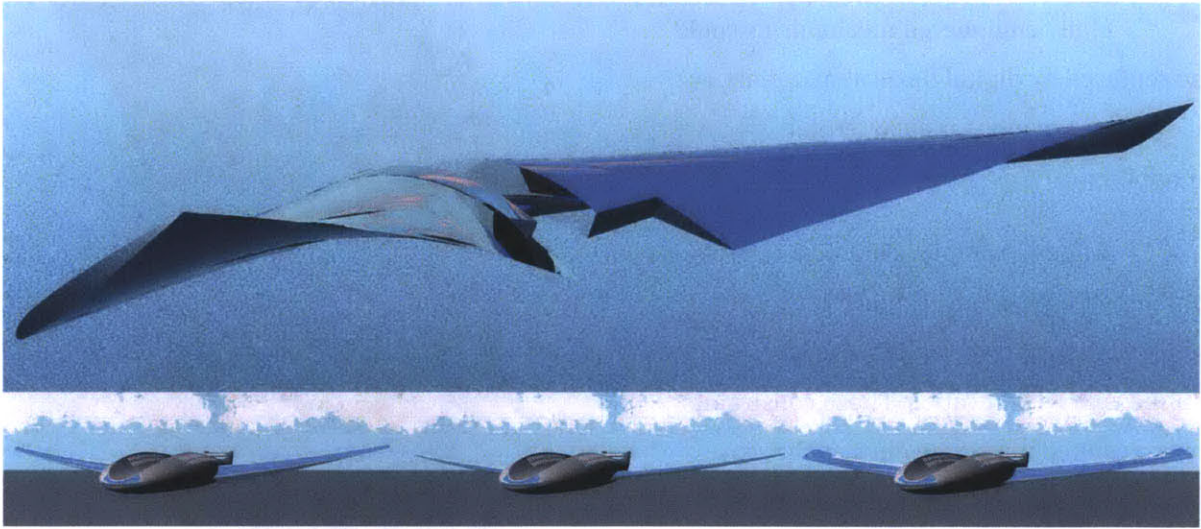


Figure 71 Digital Composite Shape Morphing Wings

A wing with digital material structure could be tuned to passively elastically deform to optimal shapes as a response to changes in load, load distribution, or pressure that results from changes in airspeed. Further, the notion of flapping – momentum transfer through non stream-wise motion – need not be restricted to the mass distribution that we commonly observe in nature. Resonant modes across a large structure could be tuned such that only small driving and control inputs are necessary to maintain speed.

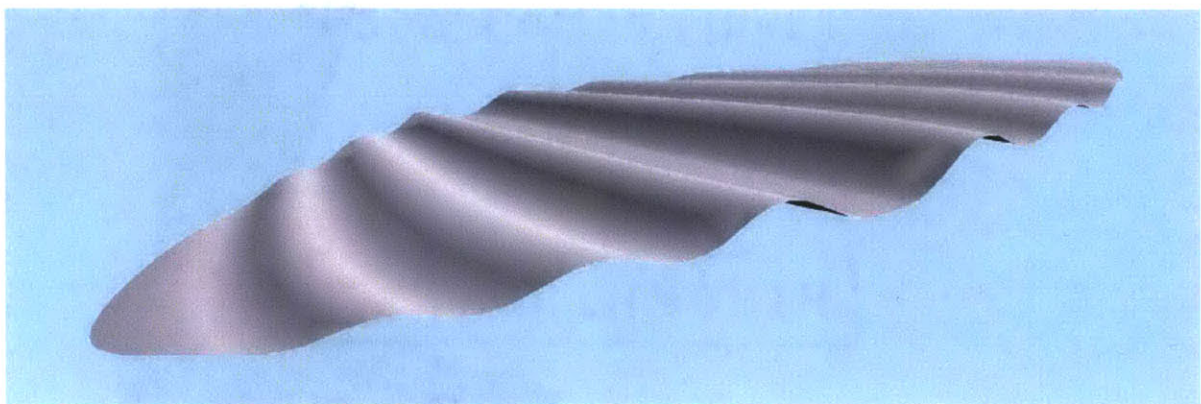


Figure 72 Resonant Aerodynamic Propulsion

### #5 Rapidly Deployable Infrastructure

In the long term, with completion of assemblers, these systems have the ability to gradually adapt to new load patterns, with mobile units that travel over the structure and delete portions of its own structure, as well as other units that are capable of adding new material. This is essentially a large scale version of the reconfigurator mentioned in #2.

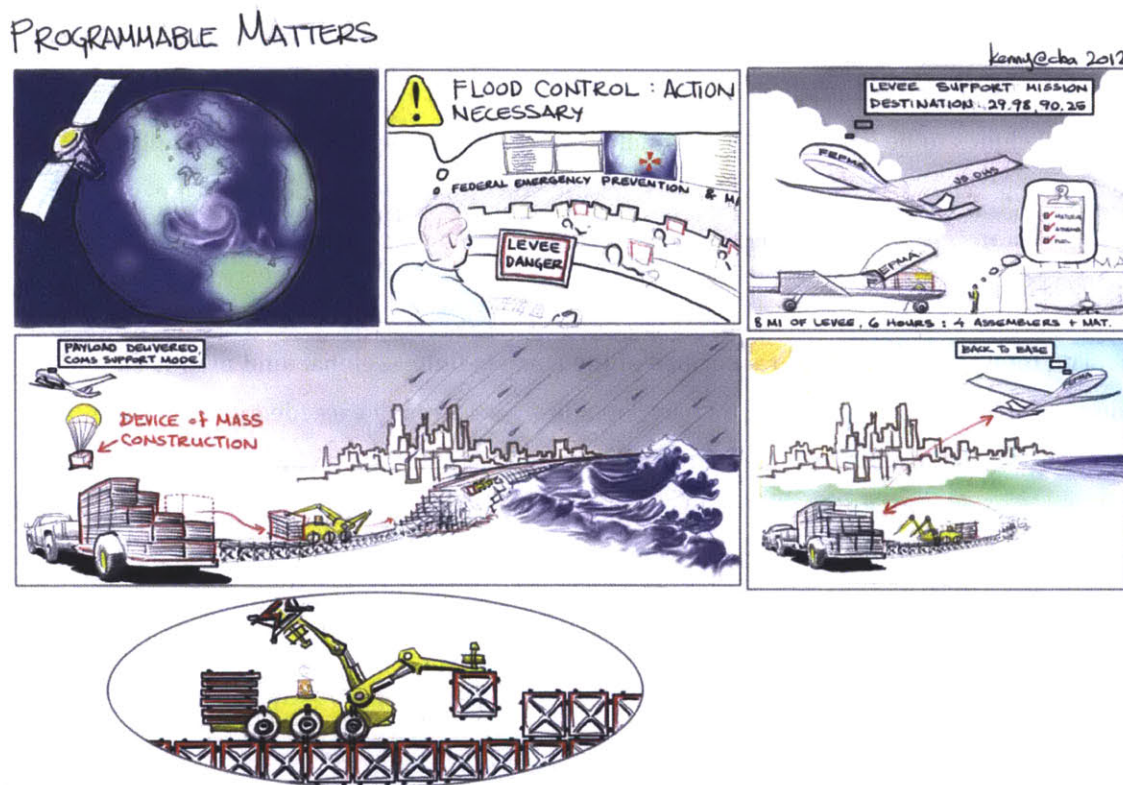


Figure 73 Disaster Relief with Rapidly Deployable Digital Composite Infrastructure

## #6 Three Dimensional Villages

In the field of architectural construction, it is clear that conventional on-site assembly and materials processing methods are vastly less energy and time efficient than that which can be achieved in a factory. Proof of this problem is in the quantity of waste that is commonly produced during on-site building construction, which easily exceeds twenty percent of all solid waste in nations that collect such data (Horvath, 2004; Bossink and Brouwers 1996). With conventional assembly methods, the assembly tools and machines must be larger than the product that is operated upon, to maintain metrology (Gershenfeld 2005). It is not difficult to imagine the realms in which there are distinct efficiency advantages for production methods that allow the assembly tools and machines to be smaller than the final products. While there exist factory built assemblies at the building scale (i.e. airplanes, boats), architecture may always demand site specific and structural customization that precludes prefabrication (and the economics of optimization for transport as large units).

The total inhabitable natural surface of the earth is finite – global land area is estimated to be around  $58 \times 10^6$  square miles. The human population has already exceeded seven billion. It is no surprise that the surface of the earth that has been developed for human inhabitation is increasing, accordingly. Assuming that the inhabitable surface of the earth stays constant, we could use up the earth's entire surface within a few generations. If we are to accommodate a continuously growing population, then we have to find ways to make our cities more population dense.



Figure 74 Aerial Concept View

Truly volumetric villages will have to be evolvable structures – the ability to perform in situ repairs and modifications is critical. In effect, the lifespan of the structure should be infinite. A part of the challenge, here, is to make the dense urban situation not only functional, but more desirable than the suburban condition. If a structure were sufficiently light for its strength and stiffness, it will be possible to sparsely distribute building throughout space, and maintain a very high population surface density. This can serve to consolidate land usage into hyper efficient meta-buildings, leaving the majority of the land available for agriculture and wilderness (Cheung 2005).

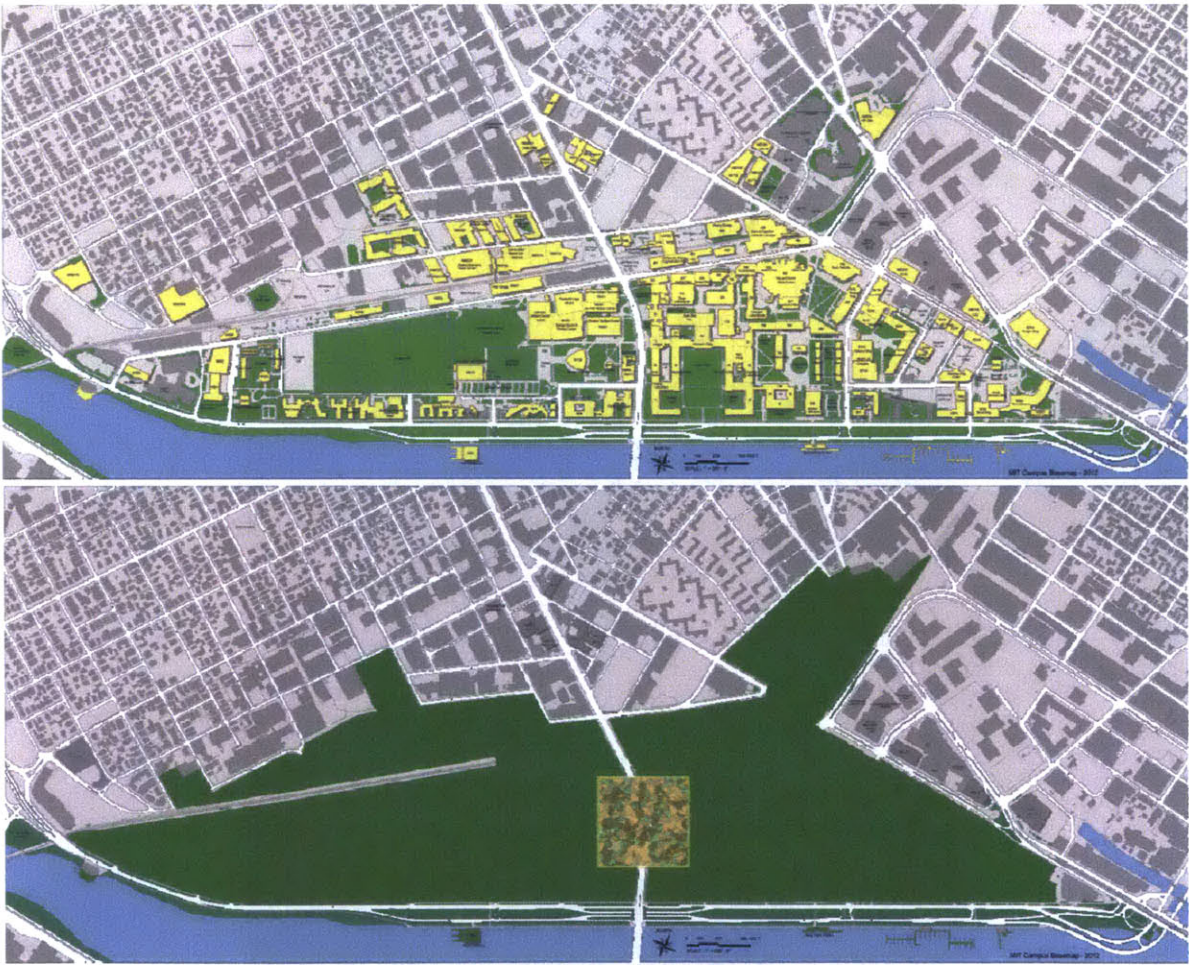


Figure 75 MIT Campus, Consolidated.

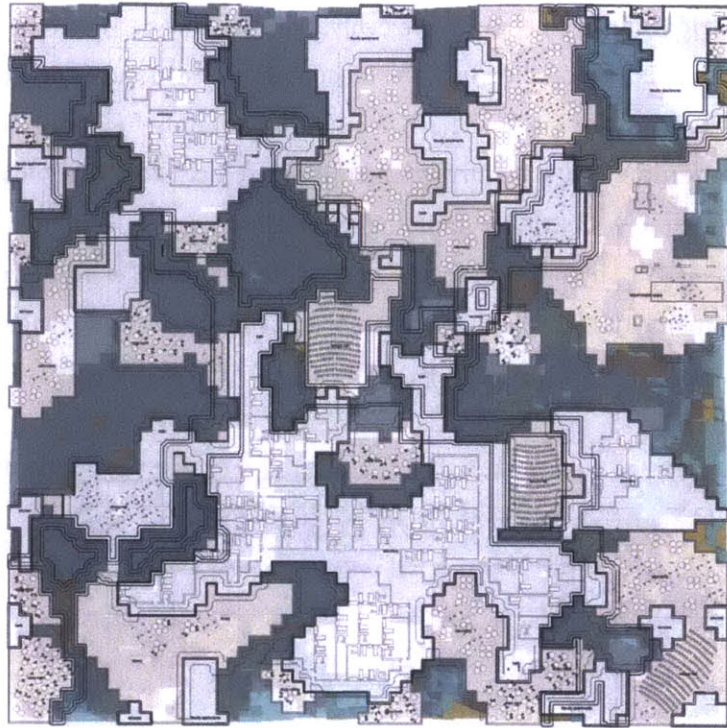
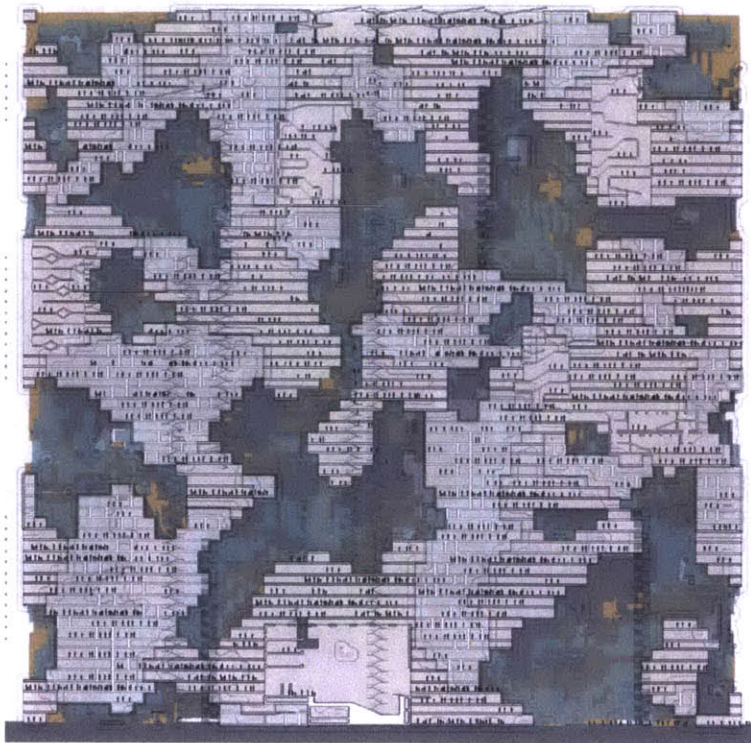


Figure 76 Three Dimensional Village Floor Plan (above), Section (below)



## References

- Aizenberg, A., Weaver, J., Thanawala, M. S., Sundar, V. C., Morse, D. E., & Fratzl, P. (2005). Skeleton of *Euplectella* sp.: Structural Hierarchy from the Nanoscale to the Macroscale. *Science*. V.309. pp275-278.
- Ashby, M. F. (2005). Hybrids to fill holes in material property space. *Philosophical Magazine*. V.85, n.26-27, pp3235-3257.
- Ashby, M. F., & Cebon, D. (1993). Materials Selection in mechanical design. *Journal de Physique IV, Colloque C7, supplement au Journal de Physique III*. V.3.
- Baker, D., Church G., Collins, J., Endy, D., Jacobson, J., Keasling, J. J., Modrich, P., Smolke, C., and Weiss, R. (2006). The BIO FAB Group. Building a Fab for Biology . *Scientific American*. June, 2006.
- Barish, R. D., Schulman, R., Rothmund, P. W. K., and Winfree, E. (2009). An Information-Bearing Seed for Nucleating Algorithmic Self-Assembly. *Proceeding of the National Academy of Sciences*. V.106, pp6054-6059.
- Barish, R. D., Rothmund, P. W. K., and Winfree, E. (2005). Two Computational Primitives for Algorithmic Self-Assembly: Copying and Counting. *Nano Letters*. V.5, n.12, pp2586-2592.
- Bennett, C.H. (1988). Notes on the history of reversible computation. *IBM Journal of Research and Development*. V.32, pp16-23.
- Bertoldi, K., Reis, P. M., Willshaw, S., & Mullin, T. (2010). Negative Poisson's Ratio Behavior Induced by an Elastic Instability. *Advanced Materials*. V.22, pp361-366.
- Boncheva, M., D. H. Gracias, et al. (2002). Biomimetic self-assembly of a functional asymmetrical electronic device. *Proceedings of the National Academy of Sciences*. V.99, n.8, pp4937-4940.
- Bossink, B.A.G. and Brouwers, H.J.H. (1996). Construction waste: quantification and source evaluation. *Journal of Construction Engineering and Management*, V.122, n.1, pp55-60.
- Broedersz, C. P., Mao, X., Lubensky, T. C. & MacKintosh, F. C. (2011). Criticality and isostaticity in fibre networks. *Nature Physics*. V.7, pp983-988.
- Chen, J. H. & Seeman, N. C. (1991). Synthesis from DNA of a molecule with the connectivity of a cube. *Nature*. V.350, pp631-633.
- Cheung, K. C. (2005) educational union. B.Arch. Thesis. Cornell University
- Cheung, K. C., Demaine, E. D., Bachrach, J. R., and Griffith, S. (2011). Programmable Assembly With Universally Foldable Strings (Moteins). *IEEE Transactions on Robotics*. V.27, n.4, pp718-729.
- Cleveland, F. A. (1970). Size Effects in Conventional Aircraft Design. *Journal of Aircraft*. V.7, n.6, pp483-512.
- Connelly, R., Fowler, P. W., Guest, S. D., Schulce, B., & Whiteley, W. J. (2008). When is a symmetric pin-jointed framework isostatic? arXiv:0803.2325v2 [math.MG] 27 Sep 2008.

- Deshpande, V. S., Ashby, M. F., & Fleck, N. A. (2001). Foam Topology Bending Versus Stretching Dominated Architectures. *Acta Materialia*. V.49, pp1035-1040.
- Deshpande, V. S., Fleck, N. A., & Ashby, M. F. (2001). Effective properties of the octet-truss lattice material. *Journal of the Mechanics and Physics of Solids*. V.49, pp1747-1769.
- Evans, A. G., Hutchinson, J. W., & Ashby, M. (1998). Cellular Metals. *Solid State & Materials Science*. V.3, pp288-303.
- Evans, A. G., Hutchinson, J. W., & Ashby, M. (1999). Multifunctionality of cellular metal systems. *Progress in Materials Science*. V.43, pp171-221.
- Franco, M. I., Turin, L., Mershin, A. & Skoulakis, E. M. C. (2011). *Proc. Natl Acad. Sci. USA* doi:10.1073/pnas.1012293108
- Fujibayashi, K., Zhang, D. Y., Winfree, E., Murata, S. (2008). Error suppression mechanisms for DNA tile self-assembly and their simulation. *Natural Computing*, (on line, July 2008).
- Fuller, R. B. (1961) Octet Truss. US Patent Number 2986241.
- Gershenfeld, Neil A. (2005). *Fab : the coming revolution on your desktop--from personal computers to personal fabrication*. Basic Books. New York.
- Gibson, L., & Ashby, M. (1988). *Cellular Solids, Structure and Properties*., Cambridge University Press., Cambridge, UK.
- Gibson, L. J. (2005). Biomechanics of cellular solids., *Journal of Biomechanics*. V.38, pp377-399.
- Griffith, S., Goldwater, S., and Jacobson, J.M. (2005). Self-replication from random parts. *Nature*. V.437, pp636-636.
- Guest, S. D., & Hutchinson, J. W. (2003). On the determinacy of repetitive structures. *Journal of the Mechanics and Physics of Solids*. V.51, pp383-391.
- Heathcote, S., Wang, Z., & Gursul, I. (2008). Effect of spanwise flexibility on flapping wing propulsion. *Journal of Fluids and Structures*. V.24, pp183-199.
- Hiller, J., & Lipson, H. (2012). Automatic Design and Manufacture of Soft Robots. *IEEE Transactions on Robotics*. V.28, n.2, pp457-466.
- Horvath, A. (2004). Construction Materials and the Environment. *Annual Review of Environment and Resources*. V.29, pp181-204.
- Hull, T. (2006). *Project Origami: activities for exploring mathematics*. AK Peters. Wellesley.
- Huybrechts, S., & Tsai, S. W. (1996). Analysis and Behavior of Grid Structures. *Composites Science and Technology*. V.56, pp1001-1015.
- Jacobs, D. J., Rader, A. J., Kuhn, L. A., & Thorpe, M. F. (2001). Protein Flexibility Predictions Using Graph Theory. *PROTEINS: Structure, Function, and Genetics*. V.44, pp150-165.
- Jongnerius S. R., & Lentik, D. (2010). Structural Analysis of a Dragonfly Wing. *Experimental Mechanics*. V.50, pp1323-1334.

Kelvin, Lord (Sir William Thomson) (1887). On the Division of Space with Minimum Partitional Area. *Philosophical Magazine*. V.24, n.151, pp503.

Lakes, R. (1993). Materials with structural hierarchy. *Nature*. V.361, pp511-515.

Lang, R. J. (2003). *Origami Design Secrets: mathematical methods for an ancient art*. AK Peters. Natick.

Lehmann, F. O., & Pick, S. (2007). The aerodynamic benefit of wing-wing interaction depends on stroke trajectory in flapping insect wings. *The Journal of Experimental Biology*. V.210, pp1362-1377.

Leon, E. J., Verma, N., Zhang, S., Lauffenburger, A., & Kamm, R. D. (1998). Mechanical properties of a self-assembling oligopeptide matrix. *J. Biomater. Sci. Polymer Edn*. V.9, n.3, pp297-312.

Lomander, A., Hwang, W., & Zhang, S. (2005). Hierarchical Self-Assembly of a Coiled-Coil Peptide into Fractal Structure. *Nano Letters*. V.5, n.7, pp1255-1260.

Ma, H. S., Prévost, J. H., Jullien, R., & Scherer, G. W. (2001). Computer simulation of mechanical structure-property relationship of aerogels. *J. Non-Cryst. Solids*. V.285, pp216-221.

Maiti, S. K., Gibson, L. J., & Ashby, M. F. (1984). Deformation and Energy Absorption Diagrams for Cellular Solids. *Acta Metall.* V.32, n.11, pp1963-1975.

Martin, G. E. (1998). *Geometric Constructions*, Springer, New York.

Maxwell, J.C. (1864). On the calculation of the equilibrium and stiffness of frames. *Philosophical Magazine*. V.27, pp294-299.

Mayer, G. (2005). Rigid Biological Systems as Models for Synthetic Composites. *Science*. V.310, pp1133-1147.

Mecklenburg, M., Schuchardt, A., Mishra, Y. K., Kaps, S., Adelung, R., Lotnyk, A., Kienle, L., & Schulte, K. (2012). Aerographite: Ultra Lightweight, Flexible Nanowall, Carbon Microtube Material with Outstanding Mechanical Performance. *Advanced Materials*. V.24, pp3486-3490.

Neumann, J. von. (1955). Probabilistic logics and the synthesis of reliable organisms from unreliable components. *Automata Studies* (eds Shannon, C.E., and McCarthy, J.) 43-98 (Princeton University Press, Princeton, 1955).

Niklas, K. J., Molina-Freaner, F., Tinoco-Ojanguren, C., & Paolillo Jr, D. J. (2002). The Biomechanics of *Pachycereus Pringlei* Root Systems. *American Journal of Botany*. V.89, n.1, pp12-21.

O'Rourke, J. (1988). "Uniqueness of orthogonal connect-the-dots." *Computational Morphology*. North-Holland. pp97-104.

Ozin, G.A. & Arsenault, A. (2005). *A Chemical Approach to Nanomaterials. Nanochemistry*. Royal Society of Chemistry. Cambridge. 2005.

Paul, D., Kelly, L., Venkaya, V., & Hess, T. (2002). Evolution of US Military Aircraft Structures Technology. *Journal of Aircraft*. V.39, n.1, pp18-29.

Perry, T.S. (1988). PostScript prints anything: a case history. *Spectrum, IEEE*. V.25, n.5, pp42-46.

- Popescu, G.A., Künzler, P., & Gershenfeld, N. (2006). Digital Printing of Digital Materials. DF 2006: International Conference on Digital Fabrication Technologies (Society for Imaging Science and Technology, Denver, 2006).
- Roberts, A. P., & Garboczi, E. J. (2002). Elastic properties of model random three-dimensional open-cell solids. *Journal of the Mechanics and Physics of Solids*. V.50, pp33-55.
- Rothmund, P. W. K. (2006). Scaffolded DNA Origami: from Generalized Multicrossovers to Polygonal Networks in Nanotechnology: *Science and Computation*. pp3-21.
- Rothmund, P. W. K. (2006). Folding DNA to create nanoscale shapes and patterns. *Nature*. V.440, pp297-302.
- Rothmund, P.W.K., Papadakis, N., Winfree, E. (2004). Algorithmic Self-Assembly of DNA Sierpinski Triangles. *PLoS Biol* 2(12): e424 doi:10.1371/journal.pbio.0020424.
- Schaedler, T. A., Jacobsen, A. J., Torrents, A., Sorensen, A. E., Lian, J., Greer, J. R., Valdevit, L., & Carter, W. B. (2011). Ultralight Metallic Microlattices. *Science*. V.334, pp962-965.
- Shannon, C.E. (1948). A Mathematical Theory of Communication. *Bell System Technical Journal*. V.27, n.379-423, pp623-656.
- Slocum, A. H., & Weber, A. C. (2003). Precision passive mechanical alignment of wafers. *Journal of Microelectromechanical Systems*. V.12, pp826-834.
- Smith, D.R., Pendry, J.B., Wiltshire, M.C.K. (2004). Metamaterials and Negative Refractive Index. *Science*. V.305, pp788-792.
- Soloveichik, D., Cook, M., Winfree, E. (2008). Combining Self-Healing and Proofreading in Self-Assembly. *Natural Computing*. V.7, pp203-218.
- Soloveichik, D. & Winfree, E. (2007). Complexity of Self-Assembled Shapes. *SIAM Journal on Computing*. V.36, n.6, pp1544-1569.
- Sylvain, V. (2002). Molecular self-assembly of surfactant-like peptides to form nanotubes and nanovesicles. *Proc. Natl. Acad. Sci. USA*. V.99, n.8, pp5355-5360.
- Streinu, I., Whiteley, W. (2001). The spherical carpenter's rule problem and conical origami folds, *Proceedings of the 11th Annual Fall Workshop on Computational Geometry*, Brooklyn, New York.
- Stroscio, J.A., & Eigler, D.M. (1991). Atomic and Molecular Manipulation with the Scanning Tunneling Microscope. *Science*. V.254, pp1319-1326.
- Timoshenko, S. P., & Gere, J. M. (1961). *Theory of Elastic Stability*. McGraw Hill. New York.
- Toth, L. F. (1964). What the bees know and what they do not know, *Bulletin AMS* 70. V.29, n.481, pp468-481.
- USDOD (2002). *Composite Materials Handbook. Polymer Matrix Composites Guidelines for Characterization of Structural Materials*. MIL-HDBK-17-1F 1
- Vincent, J. F. V. & Wegst, U. G. K. (2004). Design and mechanical properties of insect cuticle. *Arthropod Structure & Development*. V.33, pp187-199.

- Wadley, H. (2002). Cellular Metals Manufacturing., *Advanced Engineering Materials*. V.4, n.10, pp726-733.
- Wadley, H. N. G., Fleck, N. A., & Evans, A. G. (2003). Fabrication and structural performance of periodic cellular metal sandwich structures. *Composites Science and Technology*. V.63, pp2331-2343.
- Wallach, J. C., & Gibson, L. J. (2001). Mechanical behavior of a three-dimensional truss material. *International Journal of Solids and Structures*. V.38, pp7181-7196.
- Wang, Z.L., Kang, Z.C. (1998). *Structural Evolution and Structure Analysis. Functional and Smart Materials*. Plenum, New York.
- Wang, L., Lau, J., Thomas, E., & Boyce, M. C. C. (2011). Continuous Composite Materials for Stiffness, Strength, and Energy Dissipation. *Advanced Materials*. V.23, pp1524-1529.
- Wang, X. S., Li, Y., & Shi, Y. F. (2008). Effects of sandwich microstructure on mechanical behaviors of dragonfly wing vein. *Composites Science and Technology*. V.68, pp186-192.
- Warren, W. E., & Kraynik, A. M. (1988). The Linear Elastic Properties of Open-Cell Foams. *Journal of Applied Mechanics*. V.55, pp341-346.
- Weaire, D.; Phelan, R. (1994). A counter-example to Kelvin's conjecture on minimal surfaces. *Phil. Mag. Lett.* V.69, pp107-110.
- White, P. J., Revzen, S., Thorne, C. E., & Yim, M. (2011). A general stiffness model for programmable matter and modular robotic structures. *Robotica*. V.29, pp103-121.
- Whitesides, G. M. & Grzybowski, B. (2002). Self-assembly at all scales. *Science*. V.295, n.5564, pp2418-2421.
- Wilson, E. O. (1992). *The Diversity of Life*. Harvard University Press. Cambridge.
- Winfree, E. (2006). Self-Healing Tile Sets. *Nanotechnology: Science and Computation*. pp55-78.
- Winfree, E., Liu, F., Wenzler, L., Seeman, N. C. (1998). Design and self-assembly of two-dimensional DNA crystals. *Nature*. V.394, pp539-544.
- Wolko, H. S. (1986). *The Wright Flyer, An Engineering Perspective*. Smithsonian Books. Washington, D. C.
- Zhang, S. (2005). Designing Novel Materials and Molecular Machines. *Economic Perspectives*. Oct. pp22-26
- Zhang, S. (2004). Beyond the Petri dish. *Nature Biotechnology*. V.22, n.2, pp151-152.
- Zhang, S. (2003). Fabrication of novel biomaterials through molecular self-assembly. *Nature Biotechnology*. V.21, n.10, pp1171-1178.
- Zhang, S. (2003). Building from the bottom up. *Materials Today*. May. pp20-27.
- Zhang, S & Altman, M. (1999). Peptide self-assembly in functional polymer science and engineering. *Reactive & Functional Polymers*. V.41, pp91-102.

## Appendices

121 Appendix A – Process Development

126 Appendix B – Process Development - Connection Tests

128 Appendix C – Bio-mimicry

129 Appendix D - Natural Cellular Solid Analysis Case Study

133 Appendix E – Conventional Wing Structure Comparison

135 Appendix D – Digital Part Fabrication Processes

139 Appendix E: Other Candidate Manufacturing Processes

141 Appendix F – Strut Member Geometry – a study of asymmetric cross section design

143 Appendix G – Atomic Theory of Digital Materials (a conjecture)

144 Appendix H – Catalog of Digital Composites

146 Appendix I – Directional Connection Schemes

## Appendix A – Process Development

Preliminary volumetric digital composite test pieces perform, in almost all mechanical respects, between the regime of alloy honeycomb or foam cores and prototype carbon micro-truss cores, according to manufacturer's data and control tests. Just from looking at our initial tension tests with randomly oriented glass fiber laminate, it is clear that a bulk digital composite structure that meets the whole-part loading specifications is attainable.

To prove both the assemble-ability of early digital material system designs, as well as key load transfer aspects of the designs, initial testing of the tensile strength of Digital Composite type C was performed. An important feature of the design was the cam action under load, which was intended to increase connection strength with load. If the connection surfaces properly increase in normal (therefore frictional) force when the design load is applied, then it is expected that within-part strut members will fail before the connections between parts.

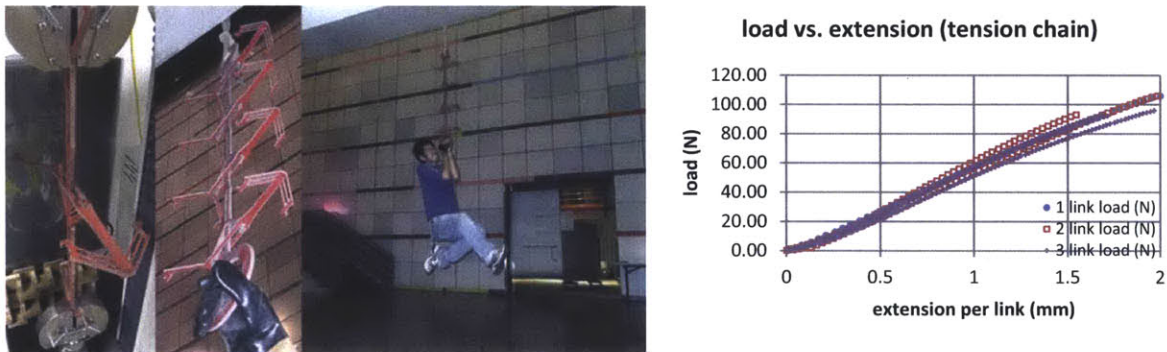


Figure 77 Preliminary Chain Testing

The designs require snap-fit preload for new parts only required at the normal to the already built structure. Therefore, to add to a part, you only need to take new pieces and push them onto the outside of the part, which allows an automated assembly mechanism to have a single degree of freedom for the procedure of installing a new part. This example has a breaking strength of 1kN with low variance, and effectively transfers load to orthogonal elements. At the lattice spacing of this particular part, the equivalent maximum (negative, on a surface) pressure is about

three pounds per square inch. This is easily tunable by increasing the cross section of the parts – the sparseness of the structure allows for this particular design to be trivially adjusted to sustain an equivalent maximum pressure of thirty pounds per square inch (with the trade-off of increased mass density).

Repeated trials were performed with up to three connection long chains (the longest that would fit in our load testing machine), in order to check for consistent behavior with increasing length. The results confirm consistent behavior, so we took some samples over to the atrium of our building to swing around on them, as a sanity check.

At this stage, we found a more specific subject – “thing to build better with digital composites” – for case study. We have received positive feedback from collaborators in the commercial aero-structures industry<sup>7</sup> on the potential for benefits in prototyping, manufacturing, and maintenance costs for aero-structures - based on this idea of doing fabrication by discrete addition, subtraction, and sorting. They have provided an example part together with qualification test specifications. The original part design is shown on the left side of Figure 84 – a static metal spar-and-ribs structure with composite skin panels containing honeycomb filler. The test part will be a bulk volume of digital composites, similar to the examples shown in Figure 96, completed with a skin.

Replacing just the honeycomb was identified as an early and simple opportunity - it is good in compression and shear, but poor in bending, torsion, and maintenance under typical environmental conditions (water infiltration and retention is a major problem). The problems with it are enough for the industry to identify it as a “pain point.” So, our initial task was to compare the bulk mechanical properties of conventional honeycomb with performance of test Digital Composite assemblies. Figure 84 on the right shows automated inclusive filling of the envelope with Digital Composite type A.

To test bulk compression modulus, we prepared example volumes of Digital Composite A, B, & C, as well as aluminum honeycomb, aluminum-fiberglass honeycomb, and rigid polyurethane foam. Images of test pieces and the test setup are shown in the figure below. Approximately 4.5”x4.5”x4.5” cubes of material were constrained (epoxied) to fiberglass test plates and compressed using a 5kN NC load frame. Specimens were crushed well past the yield point to a 1” height in order to observe a complete response curve, including crush strength.

---

<sup>7</sup> Spirit Aerosystems



Figure 78 Process Development Testing

The test results are summarized in the table below, together with published properties of commercially available structural honeycomb products, for comparison.

Table 2	density (kg/m <sup>3</sup> )	compression strength (KPa)	bulk modulus (MPa)
Experimental Data			
digital composite A (cik)	17.8735	150.025	87.27
digital composite B (pushCam)	15.1366	38.631	62.80
digital composite C (pullCam)	16.9449	34.309	11.90
aluminum honeycomb composite	73.5298	259.635	157.50
aluminum honeycomb fiberglass composite	102.4596	262.926	355.20
polyurethane foam A	92.6656	*	123.04
polyurethane foam B	93.7539	1112.634	45.69
aluminum beverage can	33.3611	248.372	97.44
Manufacturer Data			

ultracor PBO HC	40.0462	889.423	75.84
ultracor carbon/cyanate HC	12.8148	255.106	64.12
ultracor corrugated carbon	112.1292	1179.003	89.63
ultracor triax HC	48.0554	2702.745	326.81
ultracor quartz HC	45	1489.268	102.04
hexcel 5052al ld HC	16.0185	137.895	68.959
hexcel 5052al hd HC	198.6289	13100.039	4481.59
hexcel HRP glass/phenolic ld HC	35.2406	861.844	89.63
hexcel HRP glass/phenolic hd HC	192.2216	12410.563	1792.64
hexcel HRH glass/PI ld HC	51.25908	1516.847	186.16
hexcel HRH glass/PI hd HC	128.1477	6894.757	689.48
hexcel HRH aramid/PI ld HC	24.0277	586.054	41.37
hexcel HRH aramid/PI hd HC	128.1477	11031.612	413.69

\*specimen reached load cell maximum

It is not trivial to match the compressive strength and modulus of commercially available core materials, however, these initial tests suggest that it is quite possible to do so with Digital Composites (even just refined manufacturing methods for the parts might make up the difference observed in these tests). Regardless, the most compelling result is in terms of mass density. Our un-optimized test samples show similar compressive strength to the commercial core products that we tested, but at a considerably lower density.

However, referring back to manufacturer's data on the best commercially available core products (i.e. carbon honeycomb core products), we see that our preliminary digital composite test pieces are between this regime of alloy honeycomb or foam cores and carbon honeycomb cores (which are still considerably lighter for their strength than our test results).

This is not bad. To see why, we refer to the loading test specifications for the part. Just from looking at our initial tension tests with randomly oriented glass fiber laminate, it is clear that a bulk digital composite structure that meets the whole-part specifications would not be overly difficult. In fact, it is clear that if the part were fabricated entirely as skinned commercially available structural honeycomb, it would far exceed the part specification (by three orders of magnitude, depending on the product). We guess that this latter method of construction is prohibitively difficult, since there

are various non-structural systems that need to reside in the interior of the part. Furthermore, it would suffer from the same production issues that partially compel this application for digital composites in the first place. Larger monolithic structures provide fewer opportunities for qualification before the cost of a failed qualification test becomes too high.

These initial tests therefore suggest that while it seems possible, Digital Composites may not be a particularly good candidate material for replacement of carbon fiber laminate cores. However, results do suggest that Digital Composites can meet the structural specifications for entire assemblies.

## Appendix B – Process Development - Connection Tests

In order to understand design constraints, I did a quick round of initial tests on connection strength, modulus, and failure modes.

Tests were performed with tooling grade carbon fiber laminate (mcmaster-carr 8181K32, 0 90 (50/50)), which was provided with estimated elastic modulus of 65 GPa at the 0 and 90 axes. The constituent fibers are described by the manufacturer as having an elastic modulus of 234 GPa, and the fiber fill fraction of the laminate is 55% by volume. The mass density of the laminate is specified as 1.4 grams per cubic centimeter.

The part design tested was an early version of the dcx3 part, with principal part dimension  $u$  (center of peripheral bearing hole to center of adjacent peripheral bearing hole) of 3.0000 inches, nominal ligament length of 2.1213 inches, thickness of 0.03125 inches, and width of 0.125 inches. Average principal part volume is 0.0385436 cubic inches, with an average pin part volume of 0.00441604 cubic inches. A resulting octahedral unit cell is composed of three parts and three pins, therefore its constituent solid volume totals 0.12887892 cubic inches for a cellular volume of  $u^3$ , or 27 cubic inches. The mass of the cell is 2.9567 grams, giving a total cellular material density of 0.006683 grams per cubic centimeter, and a relative density of 0.004773.

As reference, note that since the constituent solid modulus is expected to be  $\sim 65$  GPa, the expected ideal modulus for a material composed of this solid and vacuum, at this density, is around  $\sim 310$  MPa (typical for low density plastics). However, because of conformational constraints the expected ideal modulus for a stochastic cellular solid composed of this solid and vacuum, at this density, is instead around  $\sim 1.48$  MPa (typical for elastomeric rubbers).

At  $\sim 0.007$  grams per cubic centimeter, this material is on par with the density of the lightest foams – any lighter, and we would be drawing comparisons with sparsely structured ultralight materials such as aerogels, for which the maximum modulus of a material composed of this solid and vacuum, at this density, is  $\sim 7.07$  KPa (typical for biological tissue).

It is rather expected that the ligament end constraints will behave as guided constraints – rotationally fixed but with affine partial translational freedom (as they are co-constrained by the other seven ligaments meeting at any connection). As such, we predict that simultaneous axial and fixed-guided transverse beam loading will dominate the behavior of the structure. The resulting

estimate for the ligament bending based modulus of an ideal material with this geometry is  $\sim 21.4\text{MPa}$ . Considering that we are using 0 90 biaxial laminate for omni-directional loads, instead of ideally oriented fibers, we may expect  $\sim 50\%$  of this ideal stiffness, giving us an expected stiffness of  $\sim 10.7\text{MPa}$  (typical for elastomeric rubbers).

The tests performed here purely address the strength of a connection assuming half-length ligaments with fixed constraints on the ends, as worst-possible-case behavior. The objective was to look at the connection properties only. Any extension to overall material properties is predicated on the strong assumption that the connection dominates the behavior of the material, which is not actually expected.

$E \sim 12\text{MPa}$  failure at ligaments

$K \sim 19\text{MPa}$  failure at central load bearing feature

Second iteration tests are aimed at layup optimization. The part design tested was initially designed around existing development tooling, with principal part dimension  $u$  (center of peripheral bearing hole to center of adjacent peripheral bearing hole) of 2.0000 inches, nominal ligament length of 1.4141 inches, thickness of 0.03937 inches, and width of 0.04000 inches. Average principal part volume is 0.0158205 cubic inches, with an average pin part volume of 0.003394132 cubic inches. A resulting octahedral unit cell is composed of three parts and three pins, therefore its constituent solid volume totals  $0.0474615$  (part) +  $0.010182396$  (pin) cubic inches for a cellular volume of  $u^3$ , or 8 cubic inches.

Continuing with calculations for the same material as above, the mass of the cell is 1.3224599 grams, giving a total cellular material density of 0.01009 grams per cubic centimeter, and a relative density of 0.007207. The expected ideal modulus for any material composed of this solid and vacuum, at this density, is around  $\sim 468\text{MPa}$  (typical for plastics). Again, because of conformational constraints, the expected ideal modulus for a stochastic cellular solid composed of this solid and vacuum, at this density, is instead around  $\sim 3.38\text{MPa}$  (typical for elastomeric rubbers), and the ligament bending based modulus of an ideal material with the prescribed non-stochastic geometry is  $\sim 39.8\text{MPa}$ .

## Appendix C – Bio-mimicry

Biological materials can be seen as proof of the feasibility of accomplishing designed digital materials in general, and provides potential foundations for the design of simplified de novo fabrication mechanisms. However, in using biological fabrication as a basis for engineered digital fabrication, I strongly resist the application of the term “bio-mimicry.” This position comes partially as a result of popular conception of bio-mimicry as the practice of adopting natural forms for engineered applications with perceptually similar constraints, without the requirement of whole understanding and analysis of how these forms specifically satisfy the constraints of the application. Moreover, some of the engineering achievements that are labeled as bio-mimicry seem to be cases of biologists applying engineering knowledge, rather than vice versa. From cactus that survive desert winds (e.g. Niklas 2002) by implementing some of the same structural principles of radio towers, to flies that may integrate a form of vibrational spectroscopy (Franco et al 2011), there are countless examples where the design of something precedes our understanding of nature. In such cases, there is no question that the natural form or functional requirement preceded the design, but what seems often missed is that our understanding of what we see as our own design problems interplays with what we see as the fit functions in nature. The introduction and success of bioengineering is happily starting to render this distinction – between the biologist and engineer – obsolete.

Few now assert, as scientists or engineers, that we have reason to think that biological form is optimal (e.g. Toth 1964). Even if we assume that biological form is optimal, it is only reasonable to assume that the space of dimensions, which any given biological form is optimized across, is exceedingly large in comparison to practical dimensions of merit for our engineered systems. If life necessitates survival in perpetuity, then we do not endeavor to create engineered life.

## Appendix D - Natural Cellular Solid Analysis Case Study

In order to gain a better understanding of the structure of bone in general, I initially compared the structural morphology of terrestrial mammalian (pig) and avian (duck) bones, using computed tomography (CT) scanning. The images below are of 10x magnified fused deposition modeling (FDM) prints of ankle bone from the respective specimens.

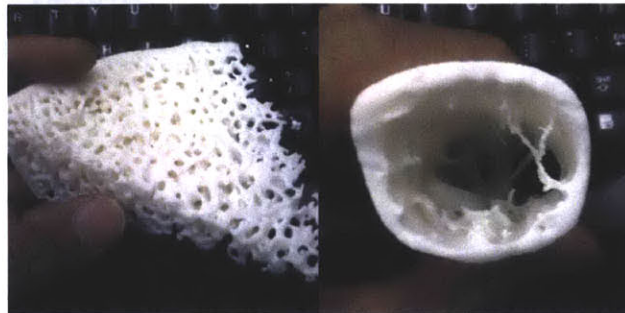


Figure 79 3d printed (x10 scale) CT scan data from bones

The suitability of CT scanning for collecting data on the positioning and arrangement of trabecular bone is clear from this initial experiment, so I proceeded to examine avian bones in finer detail. The particular objective function, of needing to be light-weight, is most important, here. Attention was paid in order to obtain a specimen would have been able to practice flight. Shown below are some of the prepared pheasant bones, from left to right: radii, ulnae, left carpometacarpus, right carpometacarpus, humeri, tibiotarsi, femurs.

A potential goal of this research is to attempt to produce a compelling predictive model for bone loading patterns, given its shape and internal structure. For this, one approach would be to look at cellular automata models, as the data is already in the form of a lattice. Another approach is to clean the CT data into mesh models that FEA packages can handle. For now, we will discuss this latter approach (although not for lack of interest in the former).

As the CT data is in the form of a three dimensional density map, there is a fair amount of data processing required as part of this analysis. A screenshot of a custom application written for this purpose is shown, below. The histogram (red) shows clearly separate modalities for materials present within the scanning volume. The bone presents a similar density to the glass specimen jars, which is not ideal – choosing a more differentiable container material will make things easier, in the future. It is interesting to note that even samples which cropped out the air surrounding the

specimen jars often indicated the presence of air in the histogram, because many of the bones exhibited pneumatization – the presence of air sacs in the interior of the bone. It is not known if these serve any function other than to greatly reduce skeletal mass density, which is certainly a positive attribute for flight.



Figure 80 Custom CT Data Processing Software

A simple thresholding algorithm for producing a mesh representation of the isosurface at a chosen density (or around a chosen density range) creates the surfaces shown, below. The datasets are large enough to require subdivision of the files, in order to ease the pruning of extraneous elements (i.e. the glass jar), before reassembling the figure in software. The lower portion of the figure below shows a pruned and assembled data set, including a cutaway image of a trabecular region.

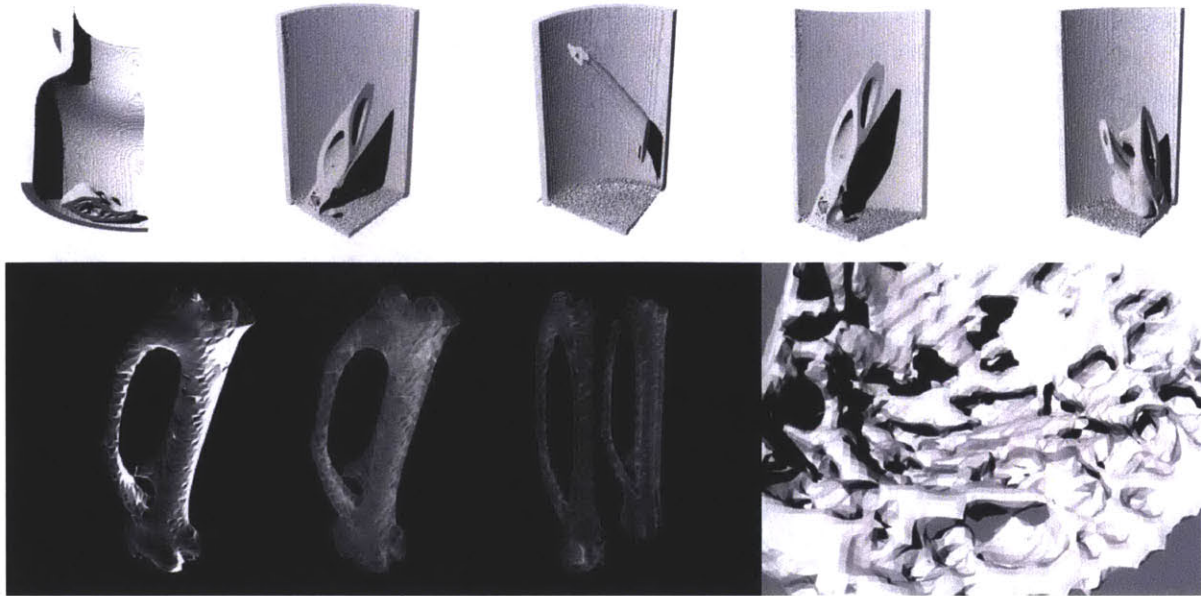


Figure 81 CT Data Renderings

Further simplification is necessary, in order to reduce these to elemental topologies. In order to simplify a mesh without broadly clipping the feature size, it is possible to perform clustering decimation with a threshold on curvature for all vertices. A nice test of this sort of high pass curvature filter may be useful for taking an undevelopable surface in three dimensional space and finding the critical seams that allow approximate fabrication from flat material. The image below shows code progress on this, from left to right: the original stanford bunny mesh, high surface curvature points automatically picked out, the same without the mesh, curves (seams) automatically generated from the point cloud,<sup>8</sup> and a surface automatically generated from one of these curves (essentially rebuilding the model as vector surfaces, instead of facets).



Figure 82 Curvature Based Crease Finding on Stanford Bunny Model

<sup>8</sup> most of them... a few of them were added by hand, across a low curvature area, connecting high curvature seams

After the simplified solid forms have been prepared, it is possible to simulate loading strategies, and to compare the different types of structures. Below is a preliminary simulation of rods under bending load. The first is a solid cylinder, the second is a hollow cylinder, and the third is a hollow cylinder with a rib through the middle, representing simplified internal structure (trabecula). The outer envelopes of all three shapes are the same, with identical loading conditions. The mass of all three are also the same, meaning that the first is made from relatively low density material, and the second is made from high density material (the third is somewhere in between). As expected, the simulation shows the second shape to be the strongest for a simple bending condition with idealized constraints, with the first one performing most poorly. However, one can imagine that the third shape is ideal for some specific set of constraints. Experience might lead one to easily mention three point loading as a loading condition under which this third shape will perform particularly well, but what if we could produce such a loading condition quantitatively?

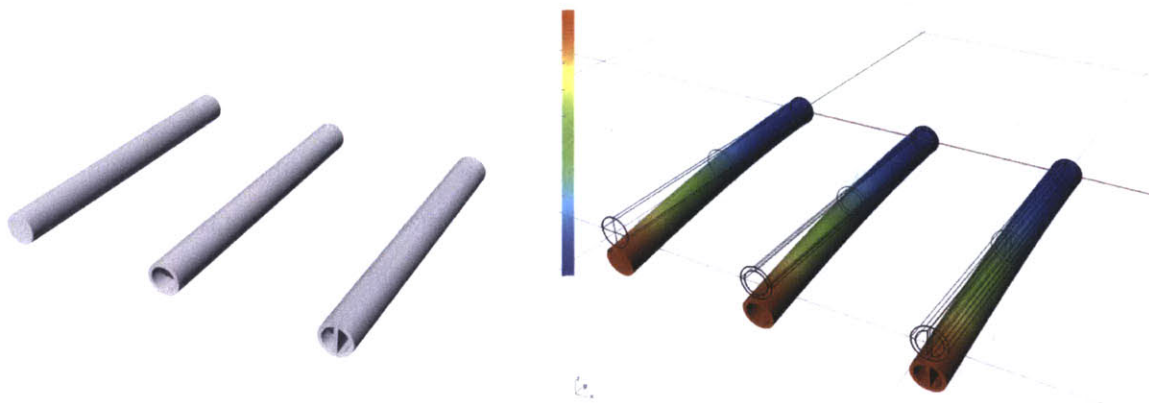


Figure 83 Preliminary Material Distribution Characterization Method

## Appendix E – Conventional Wing Structure Comparison

Conventional aircraft wing structural designs and qualification test specifications were obtained for the purpose of this study. An example substructure is shown on the left side of Figure 84 – a volume that contains static metal spar-and-ribs structure with composite skin panels containing honeycomb filler. Figure 84 on the right shows automated inclusive filling of the envelope with a digital composite system. At very high resolutions for a given structure, digital materials can form apparently continuous shapes. Additionally, hierarchically scaled part types can allow for adjusting of resolution as necessary (see Figure 6).

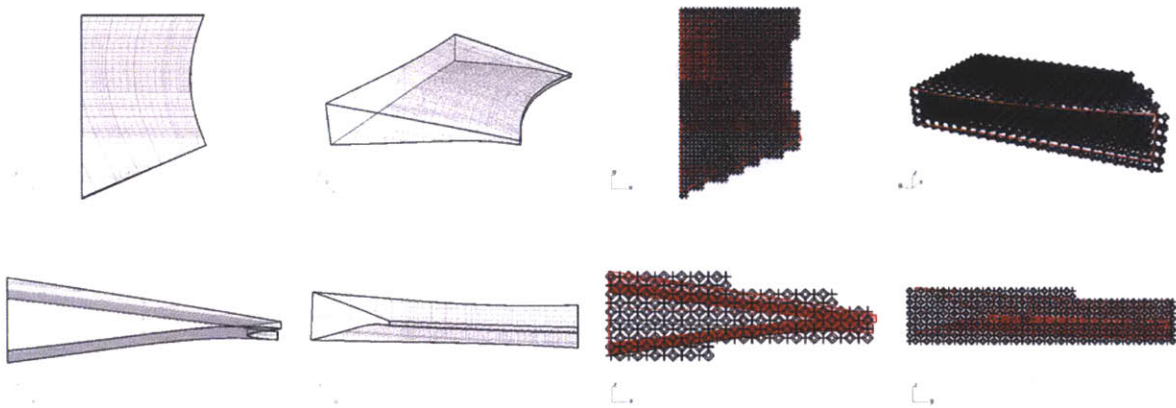


Figure 84 Structural Wedge Comparison Model

LC04 test interpreted as pressure map 08.10.2011  
according to Wing Deflection Data 03-02-11  
and 'Loads and EDIs' in Wing Mat'l Properties v00 04.14.2011



Figure 85 Generic Wing Box Relative Pressure Map

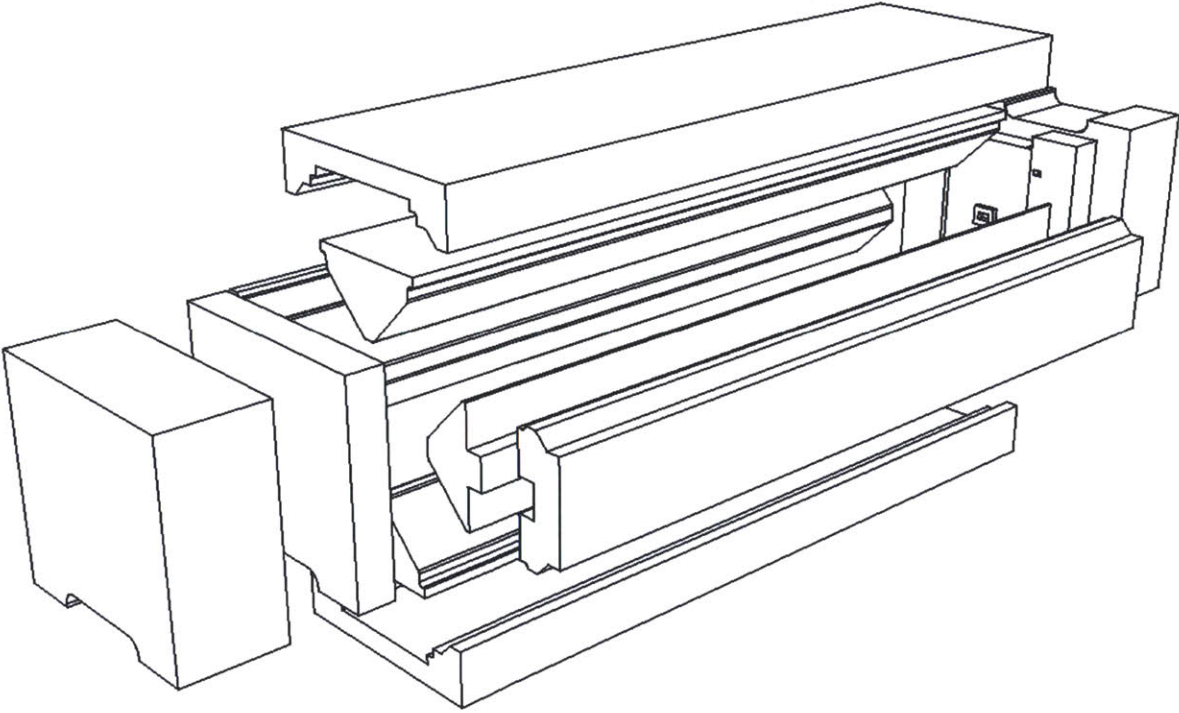
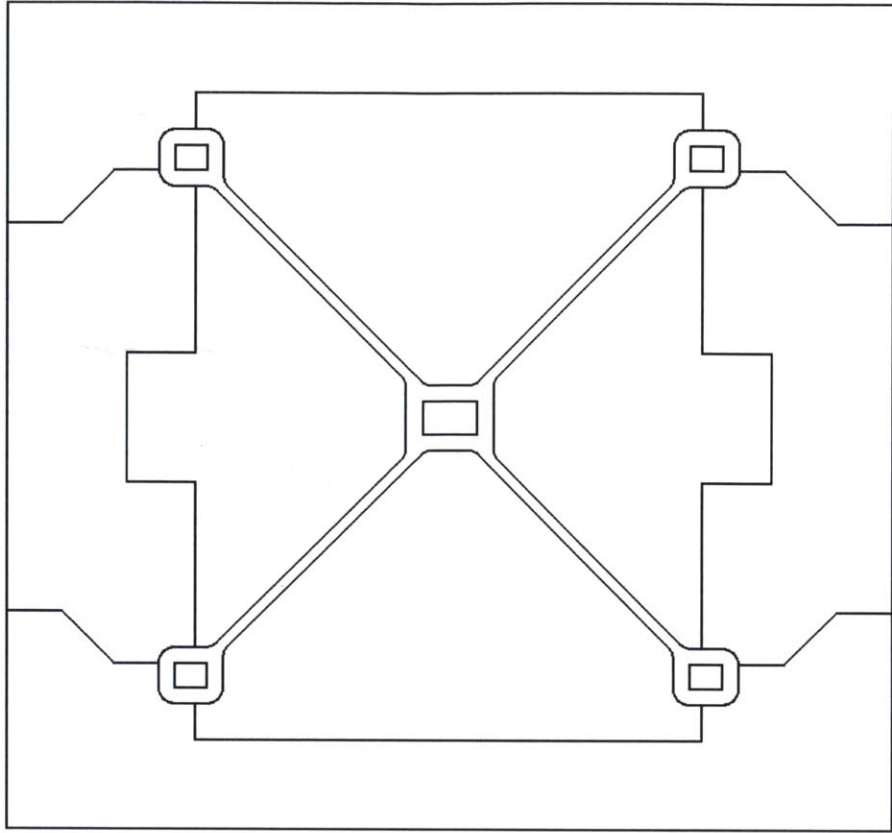
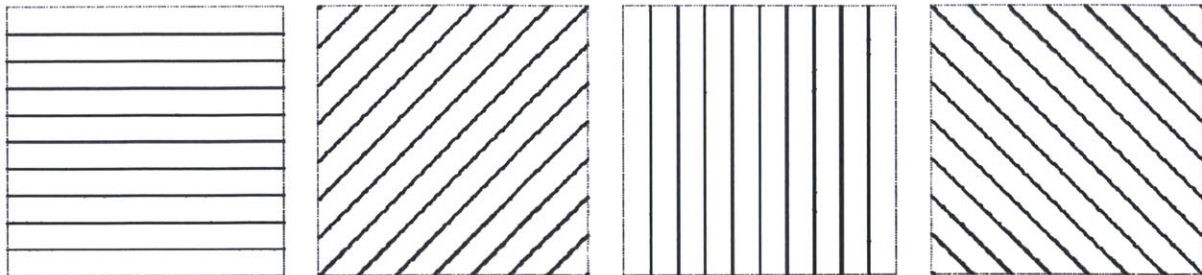


Figure 86 Multiplexed Winding Mold Diagram



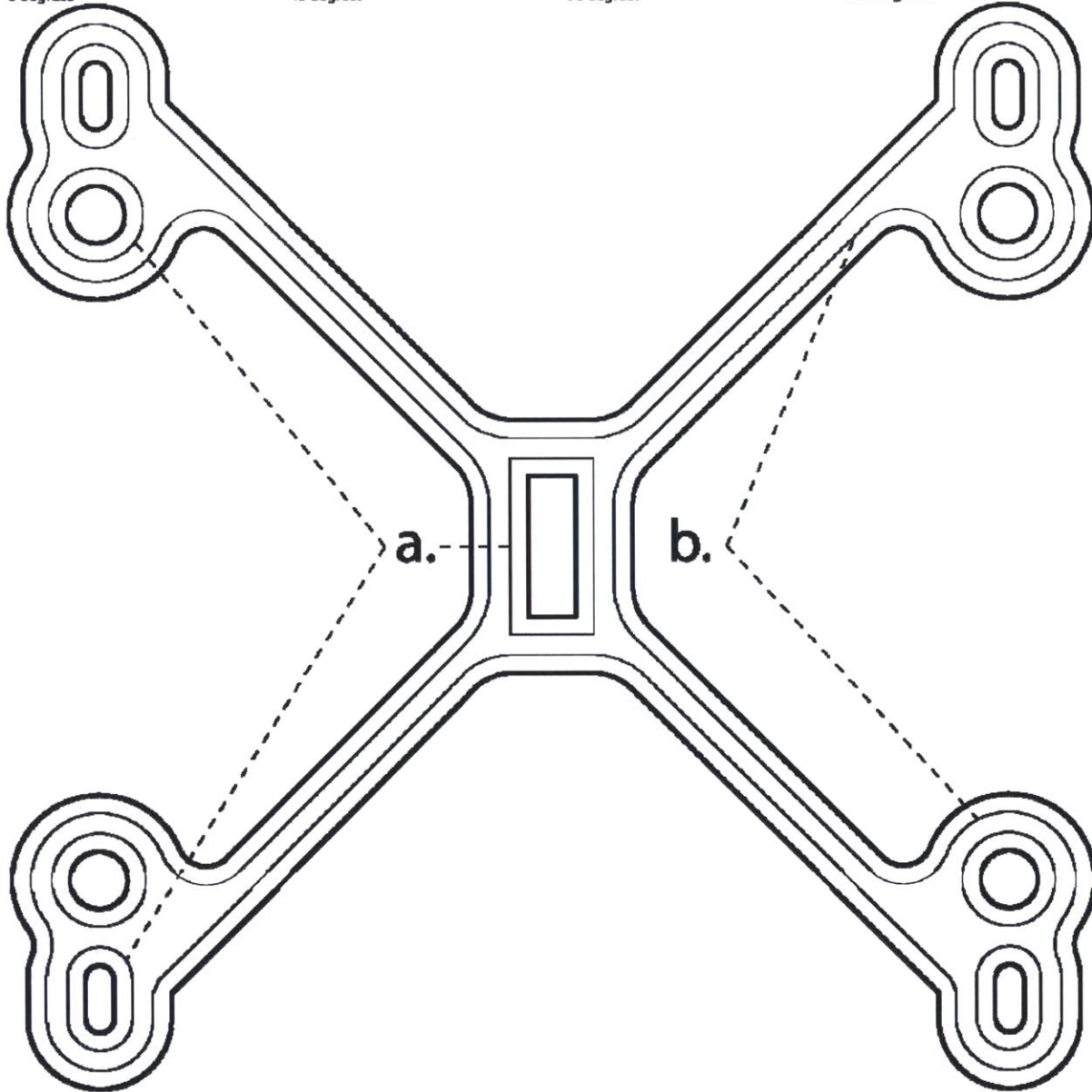


0 degrees

45 degrees

90 degrees

135 degrees



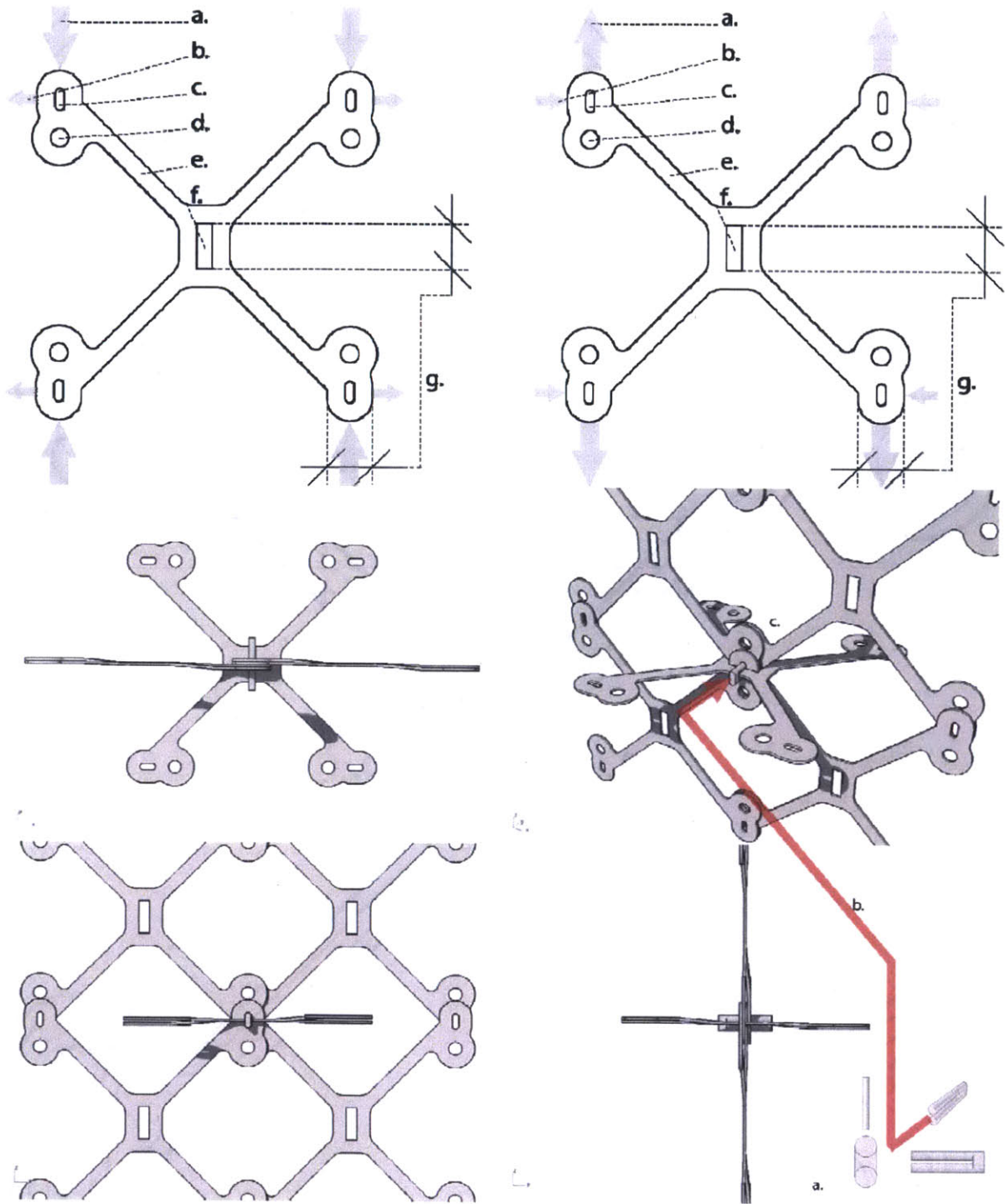


Figure 87 Assembly Process

Appendix E: Other Candidate Manufacturing Processes

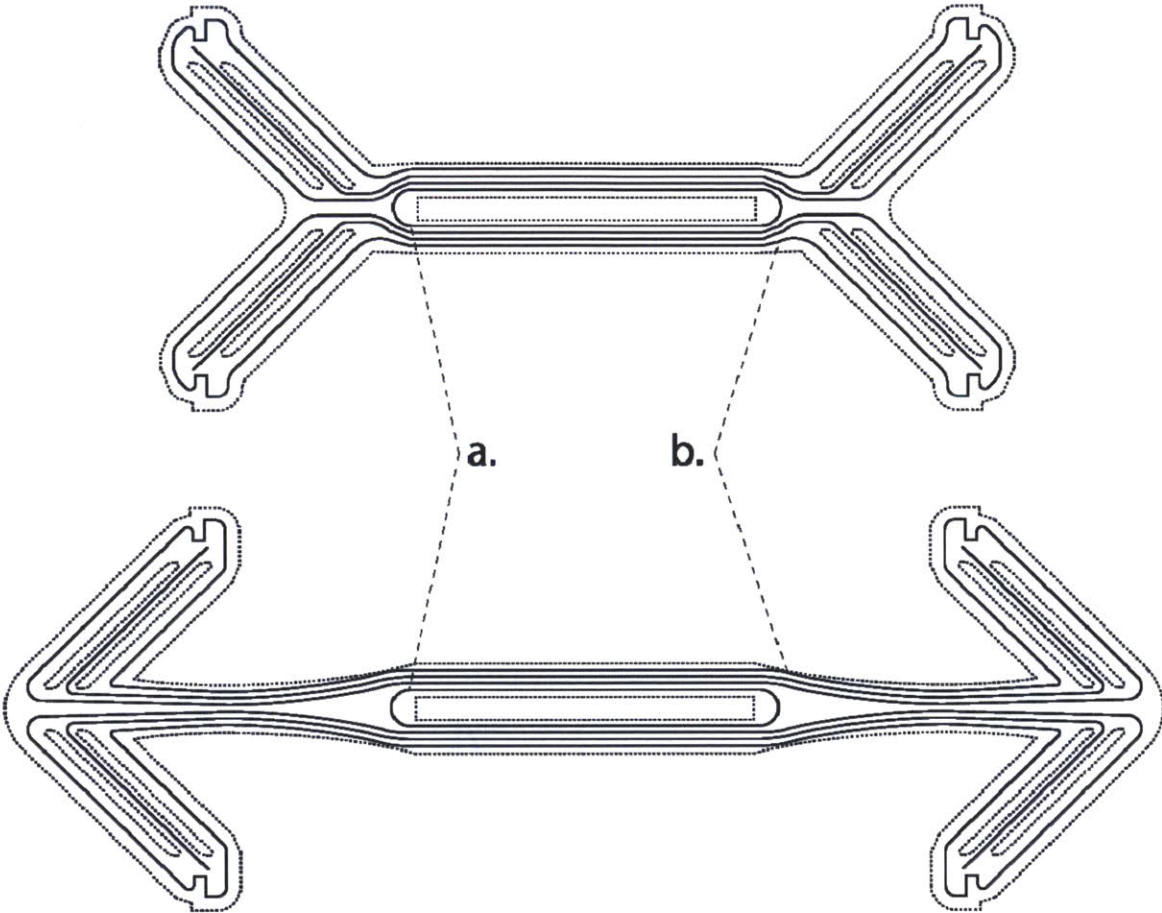


Figure 88 Fiber Layup within Components

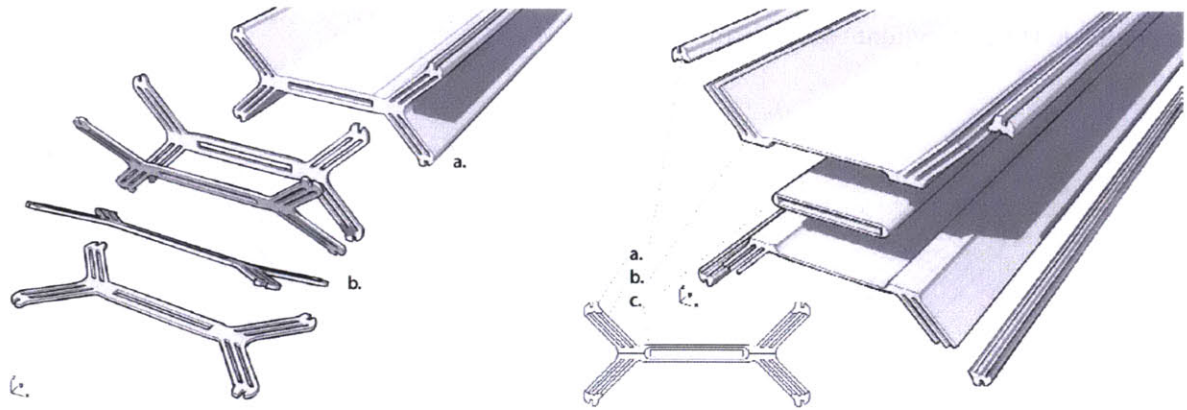


Figure 89 Sliced Pultrusion / Bonded Parts

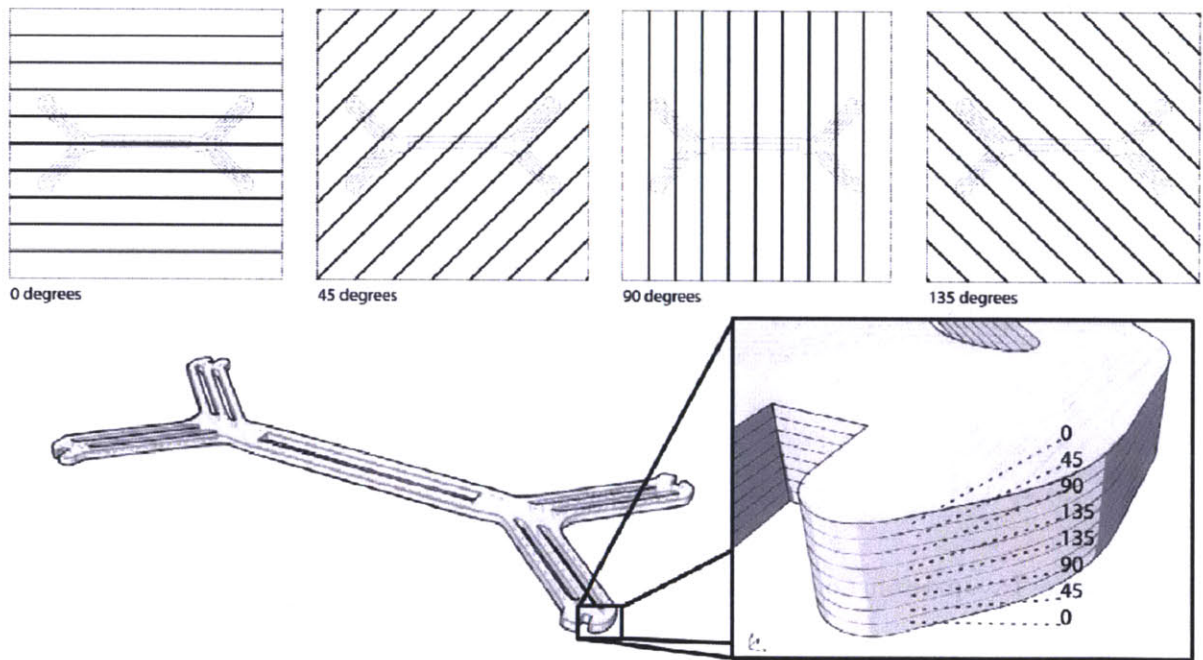


Figure 90 Fiber Layup within Pre-formed Laminate

## Appendix F – Strut Member Geometry – a study of asymmetric cross section design

The strut member portion of the a cuboct structure design is either axially loaded or loaded in groups that are oriented relative to the loading axis in such a fashion that a primary bending component (due to the simultaneous axial and transverse loads) only occurs in one plane. This plane will be referred to as the bending plane. The strut member therefore can be considered as a box with all three dimensions constrained by different sets of factors: length (l), thickness (t) orthogonal to the bending plane and the length, and width (w) within the bending plane and orthogonal to the thickness and length. We might optimize this geometry by considering the differences between the buckling out of the bending plane due to axial load, and the buckling within the bending plane due to simultaneous axial and transverse loads. With fixed end constraints, buckling out of the bending plane may be described as anti-symmetric buckling (Tymoshenko and Gere 1961), using the loading condition that results in maximum in-plane bending: for the cuboct structure, force F applied at an incident angle of  $\pi/8$  ( $F=F_{ext}/(\sqrt{2})$ ):

$$F=4\pi^2EI/l^2; F_{ext}=(\sqrt{2})8.18\pi^2EI_{OP}/l^2; I_{OP}=wt^3/12; F_{ext}=0.962\pi^2Ewt^3/l^2$$

$$F_{ext}=(\sqrt{2})4\pi^2EI_{OP}/l^2;$$

$$F_{ext}=(\sqrt{2})\pi^2Ewt^3/3l^2=0.47\pi^2Ewt^3/l^2$$

$$F_{ext}=(\sqrt{2})8.18\pi^2EI_{IN}/l^2; I_{IP}=tw^3/12; F_{ext}=0.68\pi^2Et w^3/l^2$$

For in plane bending due to the bending moment caused by the transverse loading component, we relate stress to the loading condition and dimensions of our beam (l, t, & w) with Euler Bernoulli theory.

$$\sigma=My/I; M=Fl/(\sqrt{2}); y=w/2; I_{IP}=tw^3/12$$

We can constrain this by the yield stress of the material:

$$\sigma_y=(6/(\sqrt{2}))(Fl/tw^2); l=((\sqrt{2})\sigma_y/6F)(tw^2); t=(6F/(\sqrt{2})\sigma_y)(l/w^2); w=\sqrt{((6F/(\sqrt{2})\sigma_y)(l/t))}$$

giving us optimal dimensions that should allow the loading condition that produces critical stress due to in plane bending to be equal to the loading condition that produces out of plane buckling:

$$\sigma_{bendIP}=F/(\sqrt{2})tw; F=(\sqrt{2})\sigma_ytw^2/6l; \sigma_{bendIP}=\sigma_yw/6l$$

$$\sigma_{\text{buckleOP}} = \sigma_{\text{buckleIP}} + \sigma_{\text{bendIP}}; ((\sqrt{2})\pi^2 E/3)(t^2/l^2) = ((\sqrt{2})\pi^2 E/3)(w^2/l^2) + \sigma_y w/6l$$

Note that this approximation does not take into account the additional bending expected due to simultaneous axial and transverse loading in the bending plane (which would add considerable complexity to the calculation), and therefore should be understood as an upper bound on aspect ratio of the strut member. Anyway, it is clear that the buckling terms dominate

Another design case study takes the following design constraints: a specific material with known modulus (E) and yield strength ( $\sigma_y$ ), that comes as sheet stock with thickness t, and a desired lattice pitch. To minimize mass density, we look to make  $w=t$ . Finding the maximum per-strut member load follows from Euler Bernoulli theory:

$$F_{\text{axial}} = (\sqrt{2}\sigma_y/6)(tw^2/l)$$

$$E_{\text{aluminum}} \approx 69 \text{ GPa}, \sigma_{y\text{aluminum}} \approx 400 \text{ MPa}, l = 1.8 \text{ cm (overall pitch of 2.54 cm)}, F_{\text{axial}} \approx 2.68 \text{ N}, t=w=0.8 \text{ mm}$$

$$E_{\text{carbon}} \approx 150 \text{ GPa}, \sigma_{y\text{carbon}} \approx 1.5 \text{ GPa}, l = 5.39 \text{ cm (overall pitch of 7.62 cm)}, F_{\text{axial}} \approx 3.36 \text{ N}, t=w=0.8 \text{ mm}$$

$$E_{\text{wood}} \approx 12 \text{ GPa}, \sigma_{y\text{wood}} = 40 \text{ MPa}, l = 10.78 \text{ cm (overall pitch of 15.24 cm)}, F_{\text{axial}} \approx 2.80 \text{ N}, t=w=3.175 \text{ mm}$$

$$AR = 20, 60, 30$$

## Appendix G – Atomic Theory of Digital Materials (a conjecture)

Considering a classical solid to be a periodic lattice of atoms, bulk material properties (such as elastic modulus and strength) may be derived from the interaction between each pair of atoms and knowledge about the packing lattice geometry.

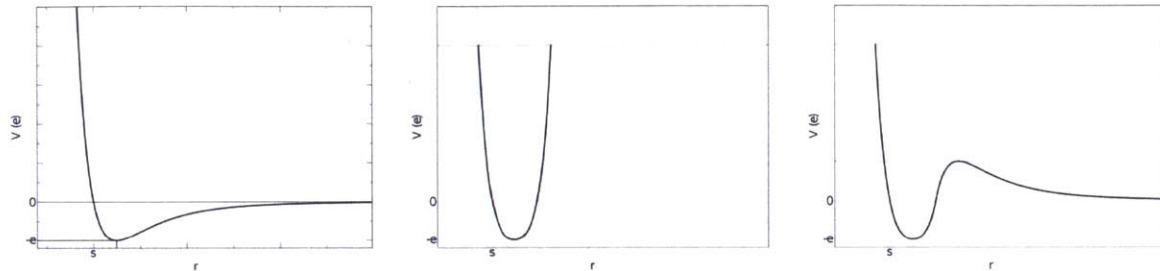


Figure 91 – Generalized Interaction Potential Diagrams

The graphs above describe a simplified model for actual atomic interaction in an elastic solid (left, Lennard-Jones potential) and hypothetical unit interaction (between-part) potential diagrams for digital materials with orthogonally pinned connections (middle) and preloaded snap-fit connections (right). The key attribute in any interaction potential model, for atoms in a bulk system, is the potential well. The potential limit line in the latter two models indicates the designed limits of secondary components (such as pins) or within-part strut members, respectively. The lower secondary limit in the snap-fit model indicates the designed limit of an in-band connection mechanism.

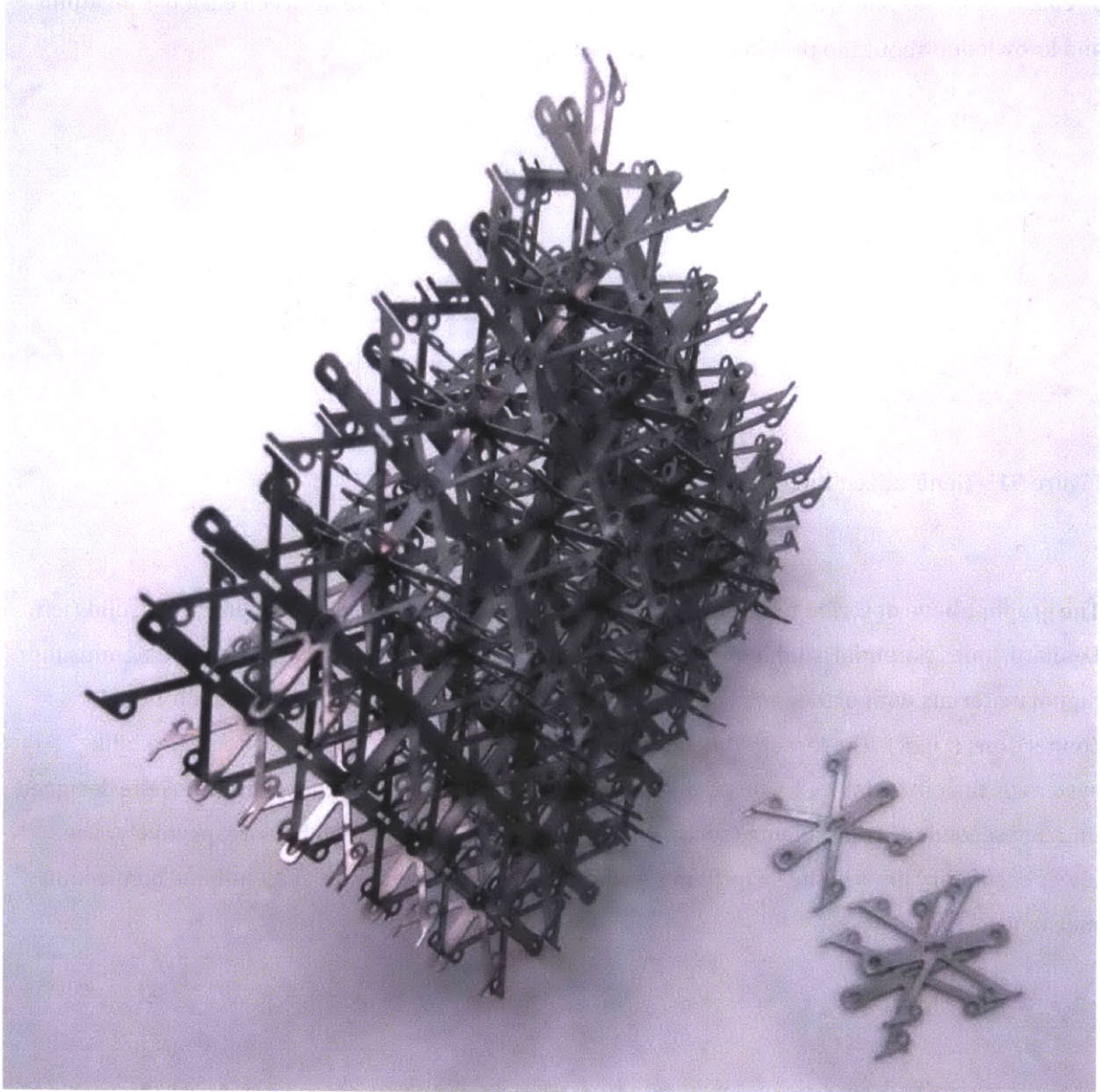


Figure 92 a scheme with only one part type (pins incorporated)

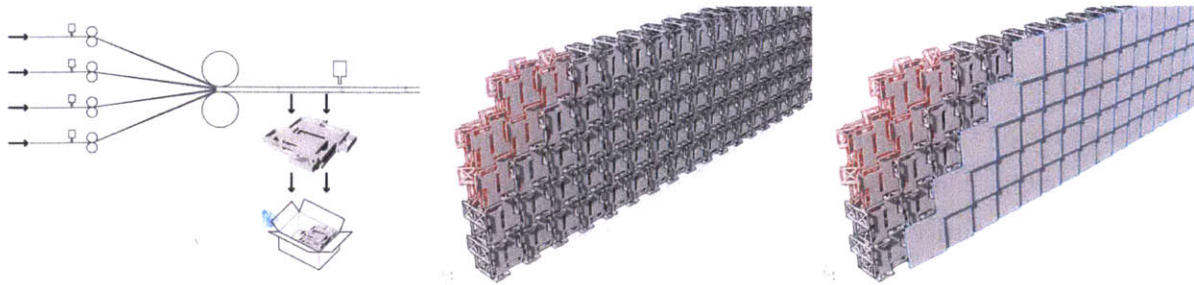


Figure 93 Roll to Roll Manufacturing of Pop-Up Cells

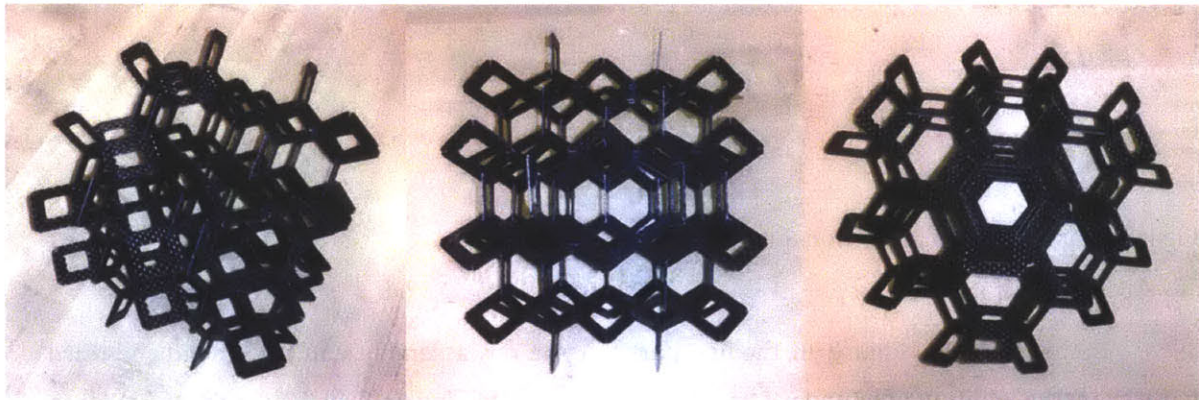


Figure 94 Kelvin Structure

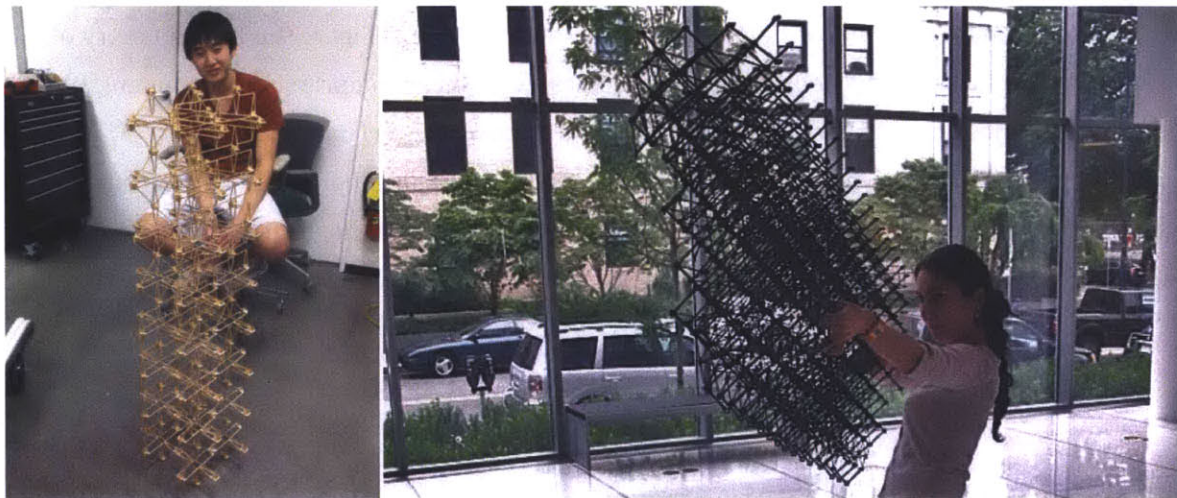


Figure 95 Today's Assemblers

## Appendix I – Directional Connection Schemes

To illustrate the principle of using part types with various mechanical properties, consider the three examples of digital material data types shown in Figure 96. These include one basic compression type and a paired (compatible) set of compression and tension types. The first is a basic orthotropic lattice system with diamond shaped parts and press-fit slotted interfaces (“Digital Composite A”).

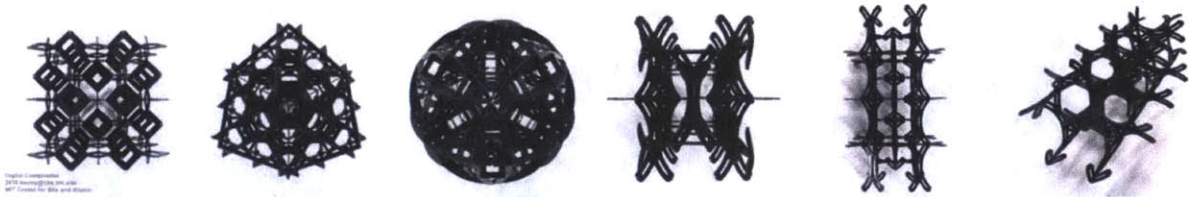


Figure 96 Directional Connection Structures (right)

In the left half of Figure 96, the first part shows a raw assembly, and the second and third parts show the addition of boundary types that aid in transferring uniform loading patterns onto the lattice. The other set shown includes a compression specific component (“Digital Composite B, push cam”) and a tension specific component (“Digital Composite C, pull cam”). These parts are shown, assembled together into a single structure, in the right half of Figure 96. The geometry of the load transfer mechanisms defines their function as a tension or compression component. When tension-loaded along the primary axis, given a normal force on the terminal ends (Figure 97, c), provided by through the keyhole (Figure 97, e) of its interlocked neighbor, the flexural arms (Figure 97, d) will provide a cam like action, transferring load to its orthogonal interlocked neighbors.

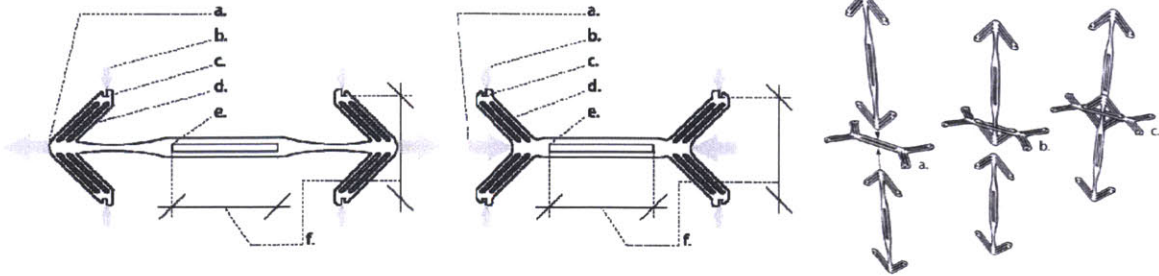


Figure 97 Directional Connection Schematic

Figure 98 shows sub-structures built from tension specific parts on the left, and compression specific parts on the right. Through mechanical property programming, as described above, the bulk properties of the Digital Composite material can progress from primarily compressive strength through tensegrity-like properties to primarily tensile strength. Related attributes (eg., Poisson ratio), can be programmed as easily.

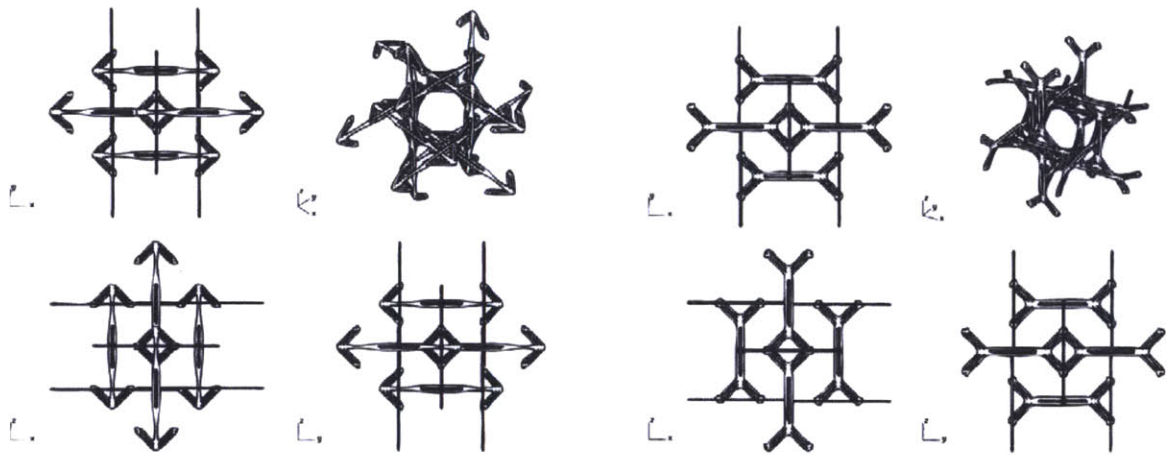


Figure 98 Directional Connection Cell Types (Tension, left; Compression, right)